

OPTIMIZATION OF SIGNAL-TO-NOISE RATIOS IN ANALYTICAL SPECTROMETRY:
THE EXTERNAL HEAVY ATOM EFFECT IN PULSED LASER
TIME RESOLVED PHOSPHORIMETRY

By

GLENN D. BOUTILIER

A DISSERTATION PRESENTED TO THE GRADUATE COUNCIL OF
THE UNIVERSITY OF FLORIDA
IN PARTIAL FULFILLMENT OF THE REQUIREMENTS FOR THE
DEGREE OF DOCTOR OF PHILOSOPHY

UNIVERSITY OF FLORIDA

1978

UNIVERSITY OF FLORIDA



3 1262 08552 5714

ACKNOWLEDGEMENTS

The author wishes to acknowledge the support of the American Chemical Society Analytical Division Summer Fellowship (1976) sponsored by the Society for Analytical Chemists of Pittsburgh and of a Chemistry Department Fellowship sponsored by the Procter and Gamble Company.

The author wishes to thank Art Grant, Chester Eastman, and Daley Birch of the machine shop for construction of many of the items required for this work. The author also gratefully acknowledges the aid of Professor Alkemade of Rijksuniversiteit Utrecht in preparing the work on signal-to-noise ratios. A special note of thanks for advice, support, and encouragement is extended to Professor James D. Winefordner and the members of the JDW research group.

TABLE OF CONTENTS

	<u>Page</u>
ACKNOWLEDGEMENTS.	ii
ABSTRACT.	v
CHAPTER	
I INTRODUCTION	1
II SIGNAL-TO-NOISE RATIOS IN ANALYTICAL SPECTROMETRY.	4
Noise and Signal-to-Noise Expressions.	4
Mathematical Treatment of Additive Noise	6
D.C. Measurement in the Presence of Background Shot Noise.	17
D.C. Measurement in the Presence of Background Flicker Noise	18
Other Measurement Systems in the Presence of Background Noise.	22
Mathematical Treatment of Multiplicative Noise	22
Assumptions	25
General Expression for the Relative Variance.	26
D.C. Measurement with a Current Meter for White Noise	33
D.C. Measurement with an Integrator for White Noise	35
D.C. Measurement with an Integrator for Flicker Noise	35
Signal-to-Noise Ratio Expressions in Emission and Luminescence Spectrometry.	37
Expressions for S/N for Single Channel Detectors.	37
Sample Modulation	41
Wavelength Modulation	42
Conclusions.	42
III MOLECULAR LUMINESCENCE RADIANCE EXPRESSIONS ASSUMING NARROW BAND EXCITATION	53
Assumptions.	53
Steady State Two Level Molecule.	55
Steady State Three Level Molecule.	62
Limiting Cases of Steady State Excitation.	69
Steady State Saturation Irradiance	71

	<u>Page</u>
Nonsteady State Two Level Molecule	72
Nonsteady State Three Level Molecule	73
Conclusions.	84
IV PULSED LASER TIME RESOLVED PHOSPHORIMETRY.	88
Introduction	88
External Heavy Atom Effect	91
Analytical Applications	91
Theory.	92
Experimental	94
Instrumentation	94
Instrumental Procedure.	115
Data Reduction.	117
Reagents.	118
Results and Discussion	119
External Heavy Atom Effect of Iodide, Silver, and Thallous Ions	119
Lifetimes and Limits of Detection for Several Drugs .	152
Comparison of Excitation Sources.	160
Conclusions.	170
APPENDIX COMPUTER PROGRAMS USED FOR LIFETIME CALCULATIONS . . .	172
LIST OF REFERENCES.	179
BIOGRAPHICAL SKETCH	186

Abstract of Dissertation Presented to the Graduate Council
of the University of Florida in Partial Fulfillment of the Requirements
for the Degree of Doctor of Philosophy

OPTIMIZATION OF SIGNAL-TO-NOISE RATIOS IN ANALYTICAL SPECTROMETRY:
THE EXTERNAL HEAVY ATOM EFFECT IN PULSED LASER
TIME RESOLVED PHOSPHORIMETRY

By

Glenn D. Boutilier

December 1978

Chairman: James D. Winefordner
Major Department: Chemistry

A treatment of noise and signal-to-noise ratios of paired readings is given for additive and multiplicative noise using the relation between the autocorrelation function and the spectral noise power. For additive noise the treatment is limited to cases where the background shows only either shot noise or flicker noise. In the case of multiplicative noise the treatment concerns cases of white noise or flicker noise causing signal fluctuations.

Radiance expressions are developed for molecular luminescence in terms of steady state and nonsteady state concentrations. The excitation source is approximated as a narrow line source since its bandwidth is assumed to be much narrower than the absorption profile. Limiting radiance expressions are given for both low (conventional) and high (laser) intensity sources. Saturation irradiances for the 2-level and 3-level molecular systems are also given.

A pulsed source time resolved phosphorimeter is described. A nitrogen laser and a flashlamp pumped dye laser are used as excitation sources and compared with respect to limits of detection for benzophenone,

quinine, and phenanthrene. The external heavy atom effect has been studied using iodide, silver, and thallous ions as external heavy atom perturbors in an ethanol and water solvent at 77 K. Phosphorescence lifetimes and relative intensities for carbazole, phenanthrene, quinine, 7,8-benzoflavone, and thiopropazate are given and the mechanism of the external heavy atom effect is discussed. Phosphorescence detection limits for several drugs are reported.

CHAPTER I

INTRODUCTION

The measurement of signals in optical spectrometry is influenced by the presence of spurious signals, or noise. Some types of noise may be eliminated by proper use of measuring equipment as in the case of pickup of 60 Hz from the alternating current (a.c.) electrical lines in the environment. Some types of noise are fundamental to a given experiment, and although they may not be entirely eliminated, it is often possible to minimize them. The quantity of fundamental importance in analytical spectrometry is the signal-to-noise (S/N) ratio.

Noise will be considered briefly from a fundamental point of view. The S/N ratios for cases where the signal is from the analyte and the noise due to the background (additive noise) and where the signal is from the analyte and the noise is a process which affects the magnitude of the signal (multiplicative noise) will be derived for several different measurement arrangements and optimization of S/N ratios will be discussed. General signal expressions in analytical spectrometry will be given along with S/N ratios for analytically important situations in emission and luminescence spectrometry. The generally useful S/N ratio expressions will be discussed with respect to analytical measurements.

Radiance expressions for atomic fluorescence excited by both high and low intensity sources have been given for both steady state (1-4) and nonsteady state (5) situations for two and three level atoms. The

intensity of saturation and excited state concentration expressions have been given for gaseous and liquid molecular systems (6-11). Despite the success of radiance expressions in predicting the variation in atomic fluorescence radiance with source spectral irradiance, no similar expressions have been developed for molecular luminescence spectrometry. Killinger et al. (12) have elegantly treated the molecular absorption of OH molecules in terms of the broadening processes (13) influencing the electronic absorption transition. This treatment was not concerned with steady state concentrations of levels or electronic molecular absorption in general.

In atomic fluorescence expressions, it is often possible to assume steady state conditions when using pulsed source excitation due to short lifetimes. In flames, the observed lifetime may be 10-fold or more smaller due to the concentration of quenchers in the flame. For molecules in flames, this is also often the case, and it may also apply to fluorescence in the condensed phase. It can not, however, apply to molecules which exhibit phosphorescence in rigid media due to the long lifetime of the triplet state compared to the pulse width of the excitation source. For this case, nonsteady state expressions will be given.

Phosphorescence is a luminescence process where radiation is emitted from the triplet state of an organic molecule. Time resolution in phosphorescence spectrometry makes use of the difference between the phosphorescence lifetime of a given molecule and the lifetimes of other sources of interference such as stray light, fluorescence, or phosphorescence from the solvent. Aaron and Winefordner (14) have reviewed the available techniques in phosphorimetry along with their analytical

applications. Two of these, the external heavy atom effect and the use of pulsed excitation sources will be studied here.

Pulsed sources offer several advantages over conventional sources in phosphorimetry (15). Higher peak source irradiance may be obtained and therefore increase the signal. Phosphors with shorter lifetimes may be measured due to the rapid termination of the pulsed source. The S/N ratio may be improved by using a gated detector with a pulsed source. The entire phosphorescence decay curve may be easily measured to check for exponential decay. The highest source irradiance available is from pulsed lasers. The construction of a pulsed source time resolved phosphorimeter using two different pulsed lasers as excitation sources will be described. This system will be applied to the measurement of phosphorescence lifetimes. Limits of detection for several drugs will also be reported and compared with results using conventional phosphorimetry.

The reported sensitivity of phosphorimetry has been increased by the external heavy atom effect using iodide ion (16,17), silver ion (18), and thallous ion (19) as external heavy atom perturbers. The effects of these heavy atom perturbers on the phosphorescence signals and lifetimes of carbazole, phenanthrene, quinine, 7,8-benzoflavone, and thiopropazate will be reported. Limits of detection using these heavy atom perturbers for these compounds and several drugs will be reported and compared with limits of detection without heavy atom perturbers.

CHAPTER II

SIGNAL-TO-NOISE RATIOS IN ANALYTICAL SPECTROMETRY

Noise and Signal-to-Noise Expressions

The quantum nature of radiation causes fluctuations for which the term shot noise is colloquial. Shot noise ultimately limits the maximum precision to which a signal can be measured to a statistically predictable level. In addition to the statistically predictable shot noise, additional scatter in the values of the measured signal occur due to excess low-frequency (e.l.f.) noise. The most common case of such noise has a noise power spectrum which is roughly inversely proportional to frequency and is termed flicker noise or $1/f$ noise. The cause of these noise sources may be found in the light sources, the absorbing medium, the detectors, and the electronic measurement systems used in optical spectrometry.

Calculations of shot noise in terms of standard deviations and noise power spectra generally do not present difficulties. Problems do arise when $1/f$ noise has to be taken into account, since the integral describing the standard deviation diverges. An adequate description can then be given when use is made of the auto-correlation function of the noise signals and when paired readings are considered; this treatment yields general expressions for the signal-to-noise (S/N) ratio. Inserting the specific time response and frequency response of the

measuring system and the specific noise power spectrum, one obtains S/N expressions in the various cases from which optimal values of the time constants can be derived.

The study of noise (20-24) forms part of the discussion of errors in analytical measurements. Errors may be divided into: (i) systematic errors (25) which may arise from the measuring procedure itself and from unwanted signals produced by background, stray light, detector offset, etc. which can be corrected for by various methods, including blank subtraction, signal modulation, careful calibration, etc.; and (ii) random errors or scatter which are a result of random variations with time of physical quantities or parameters that affect the signal reading, called noise.

The root mean square (r.m.s.)-value of a noise source and the signal-to-noise ratio are useful parameters to describe figures of merit of analytical procedures (26). These important analytical figures of merit are (i) the relative standard deviation which is the reciprocal of the signal-to-noise ratio; (ii) the analytical limit of detection which is the amount (or concentration) of analyte that can be detected with a certain confidence level by a given analytical procedure; (iii) the sensitivity of the analytical method, which corresponds to the slope of the analytical calibration curve. The limit of detection is defined by

$$C_L \text{ (or } q_L) \equiv \frac{\bar{X}_L - \bar{X}_{b1}}{S} = \frac{k\sigma_{b1}}{S} \quad (\text{II.1})$$

which ties together two of the analytical figures of merit, namely the limit of detection (concentration, C_L , or amount, q_L) and the sensitivity, S . The limit of detection is also related to the blank noise level, σ_{b1} , resulting from 16 measurements of the blank where \bar{X}_{b1} is

the average blank, σ_{bl} is the standard deviation of the blank, and k is a protection factor to give a desired confidence level (a value of $k = 3$ is recommended which gives a 99.67% confidence level).

Mathematical Treatment of Additive Noise

Several concepts are fundamental to the mathematical treatment of noise. Frequently, it is required to calculate the average of a function $g(X)$ where X is a random variable and a function of time, $X(t)$. This may be accomplished by using the probability density function, $f(X,t)$, of X which gives the probability that X has a value between X and $X + \Delta X$ at time t . If $f(X,t)$ is independent of time, $f(X,t) = f(X)$, then the variable X is said to be stationary. It is assumed that $f(X)$ is normalized so that $\int_{-\infty}^{\infty} f(X)dX = 1$. Ensemble averaging of a function $g(X)$ is defined as $\overline{g(X)} = \int g(X)f(X)dX$ where the bar means ensemble averaging.

The spectral noise power (noise power per unit frequency interval) in terms of current fluctuations for shot noise is given by

$$(S_i)_{sh}(f) \equiv S_0 = 2e \sum_j \overline{I_j} \quad (II.2)$$

where e is the elementary charge, C , and i_j is the j -th component in the current, A . The spectral noise power considered as a function of frequency, f , is called the noise spectrum. The units of S_i are A^2/s and bars denote average values.

Excess low-frequency noise has a noise power spectrum which increases towards low frequencies and has a frequency dependence often given by $f^{-\alpha}$ where α is close to unity (flicker noise). In spectrometry, $1/f$ noise is the most common and so will be the only one discussed in

detail. The frequency below which $1/f$ noise becomes important depends on the noise source and the signal level and can vary from less than 1 Hz to frequencies over 1000 Hz. This noise will be termed flicker noise throughout this manuscript despite the use of this term for a variety of other concepts. The cause of flicker noise is not well-known. Various models for $1/f$ noise in electronics have been developed (22) but most seem to have little relationship with spectrometric systems. The major sources of flicker noise involve drift of light sources, analyte production, and detection. The spectral noise power in terms of current fluctuations for flicker noise is given by

$$(S_i)_{f1}(f) = \sum_j \frac{K_{fj}^2}{f} \bar{i}_j^2 \quad (\text{II.3})$$

where f is the frequency, K_{fj}^2 is a constant with dimensions unity which describes the low-frequency stability of the noise source and \bar{i}_j is as defined previously. We note that the flicker noise power varies as \bar{i}_j^2 whereas the shot noise power varies as \bar{i}_j ; the r.m.s.-value of the flicker noise is thus proportional to the mean current (so called proportional noise).

Apart from the noise components mentioned there may occur peaks in the noise power spectrum which are, for example, due to oscillations in the flame-burner system, such as vortex formation in the gas flows and resonances in the tubings. They may extend to the audible frequency range and are then called whistle noise. The noise power in such peaks is also proportional to the square of the photocurrent, as in the case of e.l.f. noise.

When combining noises of different origins into a total noise expression, the method of addition must be carefully considered. For

example, if two noises with r.m.s.-values σ_a and σ_b exist together, the r.m.s.-value of the total noise, σ_T , is given by

$$\sigma_T = \sqrt{\sigma_a^2 + \sigma_b^2 + 2c\sigma_a\sigma_b} \quad (II.4a)$$

where c is a correlation coefficient; $|c|$ ranges between $|c| = 1$, in the case of complete statistical correlation, and $c = 0$ in the case that both noises are completely uncorrelated. Statistical correlation may exist when both noises have a common origin (e.g. fluctuations in the flame temperature).

Because noise is a sequence of unpredictable events, it is impossible to predict a future value based upon previous values. However, by means of probability theory, it is possible to state the chance that a certain process will be in a certain state at a certain time (20,22), yielding a distribution of probabilities for the possible states. A well-known distribution is the Poisson distribution. It is found when events occur independently, e.g. in time, then the variance of n events occurring in a time period of given length equals the mean value of n , found when the measurement is repeated a large number of times:

$$\text{var } n = \sigma_n^2 = \bar{n} \quad (II.4b)$$

where σ_n is the standard deviation of n .

In this chapter, the emphasis is on the S/N ratio of a measurement, which is the ratio of a signal to the standard deviation of the signal, as measured in the readings of a meter or an integrator.

In order to be able to compare the signal-to-noise ratio obtained with different types of noise and with different measuring procedures, and to find optimum values of the various characteristic times, one may

with advantage make use of the relation between the auto-correlation function and the spectral noise power involved.

The auto-correlation function of a continuously fluctuating signal $dx(t)$ is given by

$$\psi_x(\tau) \equiv \overline{dx(t)dx(t + \tau)} \quad (II.5)$$

where a bar denotes the average of a large number of values found at different times t for constant time difference τ . In the case of fluctuations, one generally makes $\overline{dx(t)} = 0$ by subtracting the average value from the signal. For a signal based on a purely statistical sequence of events (e.g. emission of photoelectrons in the case of a photocurrent in an ideal photomultiplier tube, upon which falls a constant light signal), $\psi_x(\tau)$ differs from zero only for $\tau = 0$, i.e., $\psi_x(\tau) = 0$ for $\tau \neq 0$. The values of $dx(t)$ at different times t are completely uncorrelated and the auto-correlation function is simply a delta-function at $\tau = 0$. This case is typical for shot noise. However, other noise sources may have a different character; in the case of e.l.f. noise, the values $dx(t)$ and $dx(t + \tau)$ do show a statistical correlation also for large τ , i.e., $\psi_x(\tau)$ differs from zero also for $\tau \neq 0$. Statistical correlation for $\tau \neq 0$ also occurs when shot noise is amplified and registered by an instrument that has a "memory," e.g. due to the incorporation of an RC-filter.

To obtain an expression of the noise in the frequency domain, use can be made of the Wiener-Khintchine theorem (22,27), which relates the auto-correlation function to the spectral noise power $S_x(f)$ through a Fourier transformation:

$$\begin{aligned}
 S_X(f) &= 4 \int_0^{\infty} \overline{dx(t) dx(t + \tau)} \cos(\omega\tau) d\tau \\
 &= 4 \int_0^{\infty} \psi_X(\tau) \cos(\omega\tau) d\tau
 \end{aligned}
 \tag{II.6}$$

and

$$\psi_X(\tau) = \int_0^{\infty} S_X(f) \cos(\omega\tau) df
 \tag{II.7}$$

with $\omega \equiv 2\pi f$.

The Fourier transform of a delta-function, which describes $\psi_X(\tau)$ for shot noise, is a constant. The transform shows that the shot noise power is evenly distributed over a large (ideally infinite) range of frequencies, because of which it is also called white noise.

When a noise signal is processed by a measuring system, its statistical properties will generally be changed. When a meter with time constant τ_c is used, this meter will, through its inertia, introduce a correlation-in-time which makes the auto-correlation function of the meter fluctuations due to the (originally) white noise differ from zero also for $\tau \neq 0$. It also changes the auto-correlation function of the e.l.f. noise; consequently, the related noise power spectra are also changed. When an integrating measuring system is used, an analogous effect occurs. For white noise, integrated over a time τ_i , a correlation will exist between the results of two integrations when they are taken less than τ_i seconds apart. When they are taken more than τ_i seconds apart, the results are again strictly uncorrelated. For e.l.f. noise, a similar reasoning holds, i.e., an extra correlation is introduced in the noise signal when the integrator readings are taken less than τ_i seconds apart; when the readings are taken more than τ_i seconds

apart, only the correlations in the original signal contribute to the correlation in the readings.

To relate the standard deviation of the signal, which is needed for the calculations of the signal-to-noise ratio, to the auto-correlation function and the spectral noise power, we follow the procedure outlined in reference (24).

When one works near the detection limit, which is set by the background fluctuations, one usually applies paired readings. The background, which has been admitted to the measuring system during a time long compared to the time constant of the system, is read just before the signal to be measured is admitted at $t = t_0$. Its value is subtracted from the signal-plus-background reading made τ_s seconds later; τ_s is called the sampling time. This difference, Δx , is taken to be the signal reading corrected for background where

$$\Delta x = x_{s+b}(t_0 + \tau_s) - x_b(t_0) \quad (\text{II.8})$$

Equation II.8 can be rewritten as

$$\Delta x = x_s(t_0 + \tau_s) + [dx_b(t_0 + \tau_s) - dx_b(t_0)] \quad (\text{II.9})$$

where $dx_b(t)$ is the statistical fluctuation in the meter deflection or integrator output due to the background alone. The signal-to-noise ratio (S/N) is then the signal reading, $x_s(t_0 + \tau_s)$, divided by the standard deviation $\sigma_{\Delta x}$, in the difference of the background fluctuations occurring τ_s seconds apart (see Figure 1). We assume the noise in the signal to be insignificant as compared to the background noise, and so

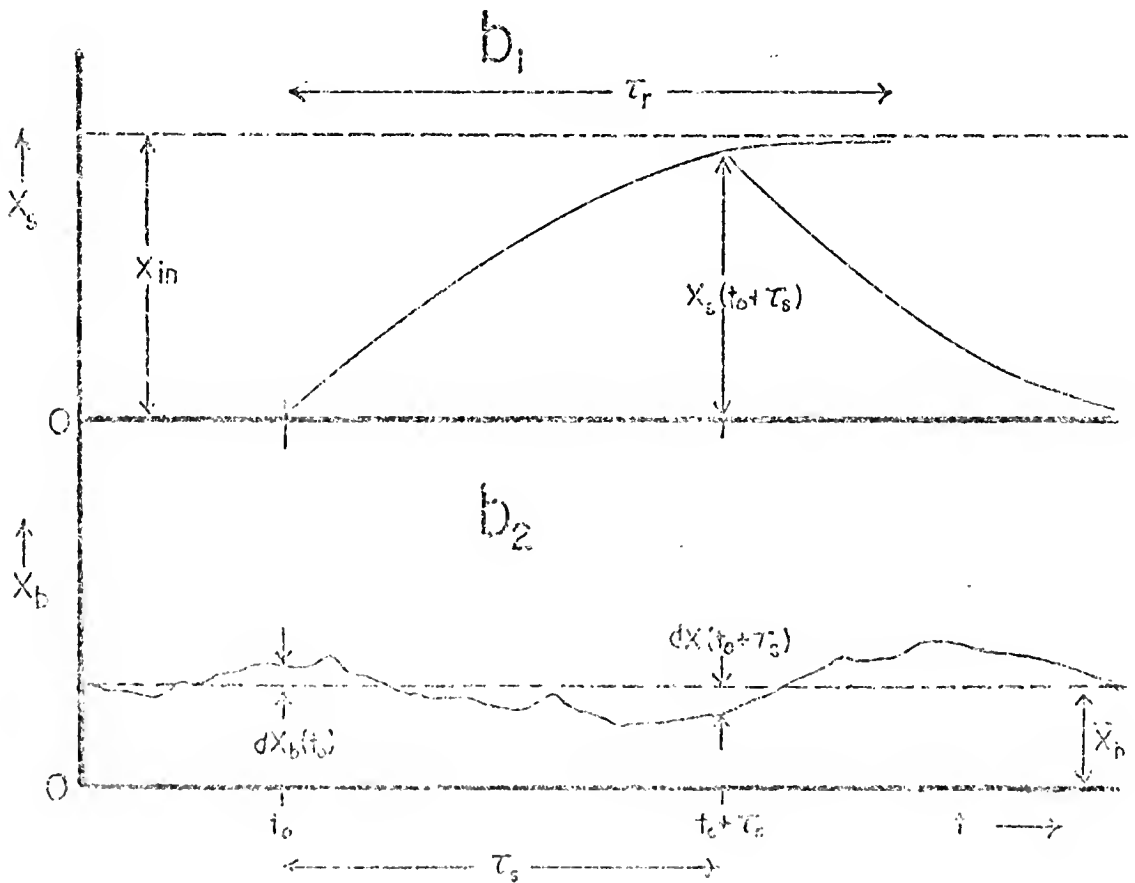
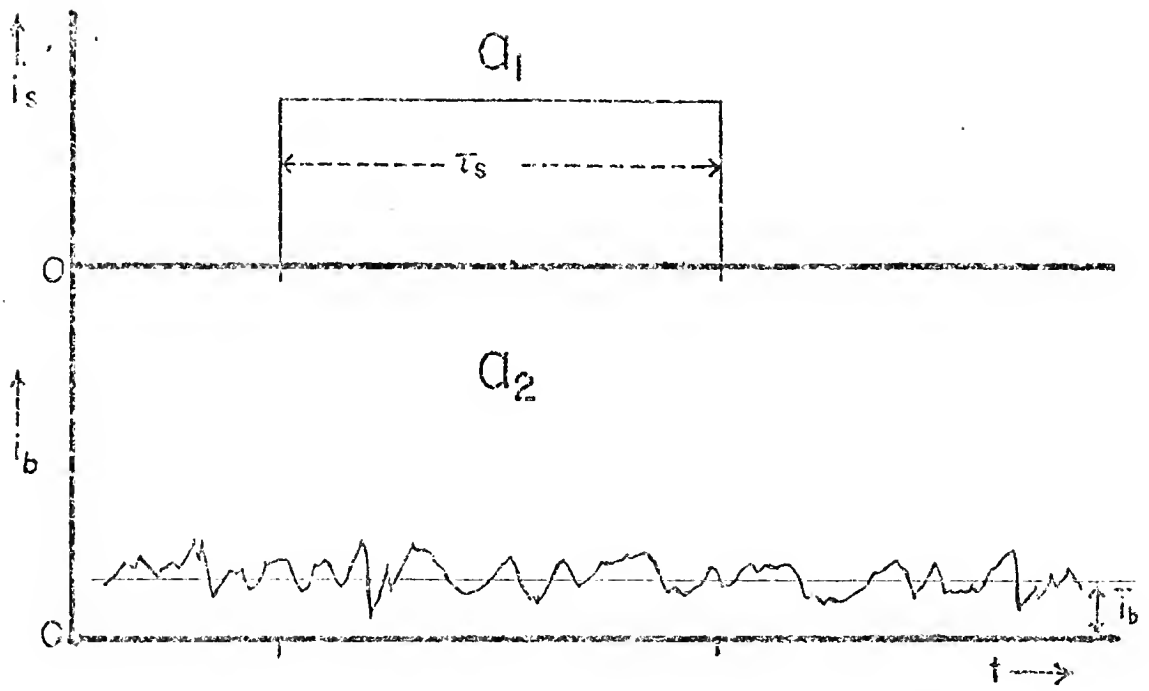
$$\frac{S}{N} = \frac{x_s(t_0 + \tau_s)}{\sigma_{\Delta x}} \quad (\text{II.10})$$

Figure 1. Representation of Signal and Noise Measured with a Meter

- a₁ Signal Photocurrent, i_s , vs Time and
- a₂ Fluctuating Background Photocurrent, i_b , vs Time.
- b₁ Meter Deflection for Signal, x_s , vs Time and
- b₂ Meter Deflection for Background, x_b , vs Time.

KEY TO SYMBOLS:

- i_s = signal primary photocurrent
- i_b = background primary photocurrent
- \bar{i}_b = average background photocurrent
- x_s = signal meter deflection
- x_b = background meter deflection
- \bar{x}_b = average background deflection
- t = time
- t_0 = sample producing signal introduced
- τ_s = sampling time
- τ_c = time constant of meter damped by RC-filter
- τ_r = response time of meter deflection
- $dx_b(t_0)$ = fluctuation in background deflection from \bar{x}_b at t_0
- $dx_b(t_0 + \tau_s)$ = fluctuation in background deflection from \bar{x}_b at $t_0 + \tau_s$



with

$$\sigma_{\Delta X} = \{[dx_b(t_0 + \tau_s) - dx_b(t_0)]^2\}^{1/2} \quad (II.11)$$

From Eq. II.11, the variance $\sigma_{\Delta X}^2$ can be straightforwardly expressed as

$$\sigma_{\Delta X}^2 = \overline{dx_b(t_0 + \tau_s)^2} + \overline{dx_b(t_0)^2} - 2\overline{dx_b(t_0 + \tau_s)dx_b(t_0)} \quad (II.12)$$

Because the background fluctuation is assumed to be stationary, each of the first two terms in the right-hand side of the latter equation is equal to σ_b^2 which is the time-independent variance of $dx_b(t)$. From the very definition of the auto-correlation function, $\sigma_{\Delta X}^2$ may be rewritten as

$$\sigma_{\Delta X}^2 = 2\sigma_b^2 - 2\overline{dx_b(t_0 + \tau_s)dx_b(t_0)} = 2[\psi_X(0) - \psi_X(\tau_s)] \quad (II.13)$$

where

$$\psi_X(0) = \overline{dx_b(t_0 + \tau_s)^2} = \overline{dx_b(t_0)^2} = \sigma_b^2$$

and

$$\psi_X(\tau_s) \equiv \overline{dx_b(t_0 + \tau_s)dx_b(t_0)}$$

To calculate $\sigma_{\Delta X}^2$, the auto-correlation function is expressed in terms of the spectral noise power $S_{i_b}(f)$ of the background current fluctuations and in the characteristics of the measuring system, using the Wiener-Khintchine theorem. Therefore, $\psi_X(\tau_s)$ may be expressed as

$$\psi_X(\tau_s) = \int_0^{\infty} S_X(f) \cos(2\pi f\tau_s) df \quad (II.14)$$

where

$$S_X(f) = S_{i_b}(f) |G(f)|^2 \quad (II.15)$$

and $G(f)$ is the frequency response of the (linear) measuring-readout

system. In other words, the spectral noise power of the meter fluctuations is the product of the spectral noise power of the background current fluctuations, S_{i_b} , and the squared absolute value of the frequency response of the measuring system, $|G(f)|^2$, including the amplification of the photomultiplier detector. Since noise power is a squared quantity, one needs here the square of the absolute value of the frequency response; phase-shifts and the associated complex form of the frequency response do not enter in the calculation of noise signals. Substituting Eq. II.15 into Eq. II.14 gives

$$\psi_x(\tau_s) = \int_0^{\infty} S_{i_b}(f) |G(f)|^2 \cos(2\pi f \tau_s) df \quad (II.16)$$

Using Eq. II.16, Eq. II.13 for $\sigma_{\Delta x}^2$ may be rewritten as

$$\sigma_{\Delta x}^2 = 2 \int_0^{\infty} S_{i_b}(f) |G(f)|^2 \{1 - \cos(2\pi f \tau_s)\} df \quad (II.17)$$

because $\cos(2\pi f \tau_s) = 1$ for $\tau_s = 0$; $\sigma_{\Delta x}^2$ is therefore a function of the sampling time τ_s and as $\tau_s \rightarrow 0$ both $\sigma_{\Delta x}^2$ and x_s approach zero. It should be noticed that the factor $1 - \cos 2\pi f \tau_s (= 2\sin^2 \pi f \tau_s)$ stems from the use of paired readings. The noise components having frequencies f for which $f \tau_s = 1, 2, 3$, etc. are completely rejected.

The signal deflection, $x_s(t_0 + \tau_s)$, due to a constant signal current i_s that is instantaneously applied to the input at time t_0 is

$$x_s(t_0 + \tau_s) = G i_s x(\tau_s) \quad (II.18)$$

where G is the d.c. response of the detector plus measuring system, and $x(\tau_s)$ is the normalized time response of the system used (meter or integrator), to a unit step function. Introducing the normalized

frequency response of the measuring system,

$$g(f) \equiv \frac{G(f)}{G(0)} \equiv \frac{G(f)}{G} \quad (\text{II.19})$$

Equation II.10 for the signal-to-noise ratio finally becomes

$$\frac{S}{N} = \frac{i_s x(\tau_s)}{\left[2 \int_0^{\infty} S_{i_b}(f) |g(f)|^2 \{1 - \cos(2\pi f \tau_s)\} df \right]^{1/2}} \quad (\text{II.20})$$

This equation is the general expression for the signal-to-noise ratio with dominant background noise in the case of paired readings with a d.c. measuring system (meter or integrator).

To optimize the S/N ratio for specific situations, we have to introduce in Eq. II.20:

- a. the background noise spectrum S_{i_b} (white noise or flicker noise);
- b. the time response $x(\tau_s)$ of the meter or the integrator used, and the associated normalized frequency response $g(f)$, and to determine the dependence of the S/N thus found on the sampling time τ_s and the other time parameters.

It is assumed that the photon irradiance to be measured has been converted to an electrical signal through the photocathode of a photomultiplier. All currents, i , refer to primary (or cathodic) currents or count rates, respectively. An anodic current, i_a , is related to the cathodic current, i_c , by

$$i_a = i_c G_{pm} \quad (\text{II.21})$$

where G_{pm} is the average gain of the photomultiplier. This expression

can be used if one wishes to convert final expressions for S/N to anodic currents.

D.C. Measurement in the Presence of Background Shot Noise

In this case, a constant signal current i_s is assumed to be applied to the input at $t = t_0$ whereas the background current i_b is assumed to be continuously present. The step response of a meter damped by an RC-filter (see Figure 1) or the normalized response of a meter when a constant d.c. current is suddenly applied at $t = t_0$, is

$$x(\tau_s) = 1 - \exp(-\tau_s/\tau_c) \quad (\text{for } \tau_s \geq 0) \quad (\text{II.22})$$

where the meter time constant $\tau_c = RC$. The response time of the meter is defined as

$$\tau_r = 2\pi\tau_c \quad (\text{II.23})$$

After a time τ_r , the meter has reached its final deflection within 0.2%. The squared absolute value of the normalized frequency response of such a meter is

$$|g(f)|^2 = \frac{1}{1 + (2\pi\tau_c f)^2} = \frac{1}{1 + (f\tau_r)^2} \quad (\text{II.24})$$

Inserting Eqs. II.22, II.23, and II.24 in Eq. II.20, with $S_{i_b}(f)$ for shot noise, one obtains

$$\frac{S}{N} = \frac{i_s \{1 - \exp(-2\pi\tau_s/\tau_r)\}}{\left\{ 2 \int_0^\infty \frac{S_0 \{1 - \cos(2\pi f\tau_s)\}}{1 + f^2\tau_r^2} df \right\}^{1/2}} \quad (\text{II.25})$$

The integral in Eq. II.25 can be evaluated by using

$$\int_0^{\infty} \frac{\sin^2 x}{\pi^2 + x^2} dx = \frac{1}{4} (1 - e^{-2\pi})$$

which yields

$$\frac{S}{N} = \frac{i_s \{1 - \exp(-2\pi\tau_s/\tau_r)\}^{1/2}}{(\pi S_0/\tau_r)^{1/2}} \quad (\text{II.26})$$

For fixed τ_r , the maximum value of S/N is reached for $\tau_s = \infty$ and is

$$\frac{S}{N} = \frac{i_s}{(\pi S_0/\tau_r)^{1/2}} = \frac{i_s}{(2\pi e i_b)^{1/2}} \tau_r^{1/2} \quad (\text{II.27})$$

Since the value is reached within 0.2% for $\tau_s = \tau_r$, the sampling time τ_s can be restricted to that value. A larger value of τ_s is only a waste of time; a smaller value yields a smaller S/N ratio. Equation II.27 shows that the S/N ratio is proportional to the square root of τ_r and thus improves with increasing response time τ_r , provided $\tau_s \lesssim \tau_r$.

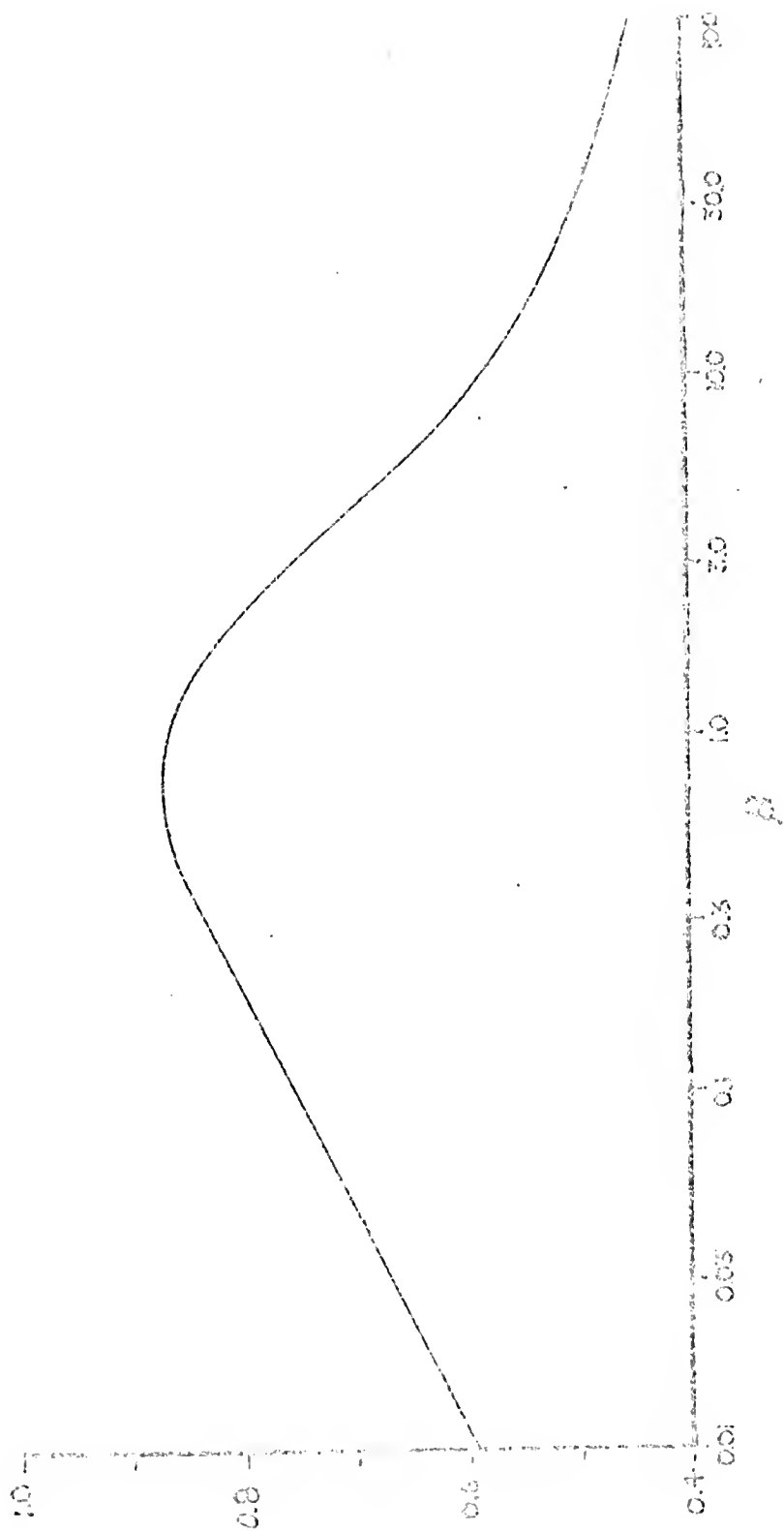
D.C. Measurements in the Presence of Background Flicker Noise

Substitution of the spectral noise $S_{i_b}(f) = K_f^2 i_b^2 / f$ into Eq. II.20 yields

$$\frac{S}{N} = \frac{i_s [1 - \exp(-2\pi\tau_s/\tau_r)]}{\{2K_f^2 i_b^2 \int_0^{\infty} \frac{1 - \cos(2\pi f\tau_s)}{f^2(1 + f^2\tau_r^2)} df\}^{1/2}} \quad (\text{II.28})$$

This expression is valid for any τ_s and τ_r , but can be evaluated only by numerical methods. It is possible to simplify this expression by introducing two new variables with dimension unity. Let β and z be defined as

Figure 2. Single Logarithmic Plot of the Function $f(\beta)$



$$\beta \equiv 2\pi\tau_s/\tau_r = \tau_s/\tau_c \quad (II.29)$$

$$z \equiv 2\pi f\tau_s \quad (II.30)$$

Substituting these new variables into Eq. II.28 leads to

$$\frac{S}{N} = \frac{i_s \{1 - \exp(-\beta)\}}{\{2K_f^2 i_b^2 \int_0^\infty \frac{1 - \cos z}{z(1 + z^2/\beta^2)} dz\}^{1/2}} \quad (II.31)$$

or

$$\frac{S}{N} = \frac{i_s}{(2K_f^2 i_b^2)^{1/2}} f(\beta) \quad (II.32)$$

where

$$f(\beta) = \frac{[1 - \exp(-\beta)]}{\left\{ \int_0^\infty \frac{1 - \cos z}{z(1 + z^2/\beta^2)} dz \right\}^{1/2}} \quad (II.33)$$

Numerical evaluation (24) of $f(\beta)$ gives a maximum of approximately 0.88 at β approximately equal to 0.8, i.e., $\tau_s \approx \tau_r/8$ or $\tau_s \approx 0.8 \tau_c$, and $f(\beta)$ falls to zero as β tends toward zero or infinity. A plot of $f(\beta)$ vs β is given in Figure 2.

The important point is thus that the maximum S/N for flicker noise is dependent only on the ratio τ_s/τ_r and not on τ_s and τ_r individually, and so there is no gain in S/N here when we make τ_r ($= 8\tau_s$) larger. Evidently in the flicker noise limited case, the increased smoothing effect of a longer time constant $\tau_r = 2\pi\tau_c$ is just offset by the increase in low-frequency noise from the equally longer sampling time τ_s , due to the $1/f$ -dependence of the flicker noise power spectrum. One can also show that for a noise power proportional to $f^{-\alpha}$ with $\alpha > 1$, the S/N ratio even decreases when τ_r (and τ_s) is increased.

The optimum S/N for background flicker noise is therefore

$$\frac{S}{N} = \frac{i_s}{\{2.6K_f^2 \bar{i}_b\}^{1/2}} = \frac{i_s}{2\xi_{dm} \bar{i}_b} \quad (II.34)$$

where $\xi_{dm} = 0.81 K_f$ is defined as the flicker factor for paired d.c. measurements.

Other Measurement Systems in the Presence of Background Noise

Many other measurement systems may be used in analytical spectrometry other than d.c. meter systems. Other d.c. systems possible are d.c. integration, photon counting with a rate meter, and photon counting with a digital counter (digital equivalent of integration). Modulated, or a.c., systems such as lock-in amplifiers or synchronous photon counting, may be used with meter (current or rate) and integration (counter) output. Detailed derivation of the S/N ratio expressions for background shot and flicker noise has been given (28), so only the final expressions for the S/N ratio will be given here. In the a.c. cases, it is assumed that the signal is modulated at frequency f_{mod} , while the background signal is not modulated. In Table I, the S/N ratios are given for the different measurement systems discussed for background flicker or background shot noise. In Table II, the flicker factors, ξ , are given for the different measurement approaches.

Mathematical Treatment of Multiplicative Noise

In the discussion of additive noise, it was assumed that fluctuations in the meter deflection due to a fluctuating background constituted a

Table I. Signal-to-Noise Ratio Expressions for Individual Shot and Flicker Noises and Several Measurement Systems

Measurement System	Shot Noise		Flicker Noise	
	d.c.	a.c.	d.c.	a.c.
Current Meter ($\tau_s = \tau_r$)	$\frac{i_s \sqrt{\tau_r}}{\sqrt{2\pi e \tau_b}}$	$\frac{F i_s \sqrt{\tau_r}}{\sqrt{2\pi e \tau_b}}$	$\frac{i_s}{2 \xi_{dm} \tau_b}$	$\frac{F i_s \sqrt{\tau_r}}{\sqrt{2} \xi_{am} \tau_b}$
Rate Meter ($\tau_s = \tau_r$)	$\frac{R_s \sqrt{\tau_r}}{\sqrt{2\pi R_b}}$	$\frac{F R_s \sqrt{\tau_r}}{\sqrt{2\pi R_b}}$	$\frac{R_s}{2 \xi_{dm} \bar{R}_b}$	$\frac{F R_s \sqrt{\tau_r}}{\sqrt{2} \xi_{am} \bar{R}_b}$
Current Integrator	$\frac{i_s \sqrt{\tau_i}}{\sqrt{2e \tau_b}}$	$\frac{F i_s \sqrt{\tau_i}}{\sqrt{2e \tau_b}}$	$\frac{i_s}{2 \xi_{di} \tau_b}$	$\frac{F i_s \sqrt{\tau_i}}{\sqrt{2} \xi_{ai} \tau_b}$
Digital Integrator	$\frac{R_s \sqrt{\tau_i}}{\sqrt{2\bar{R}_b}}$	$\frac{R_s \sqrt{\tau_i}}{\sqrt{2\bar{R}_b}}$	$\frac{R_s}{2 \xi_{di} \bar{R}_b}$	$\frac{F R_s \sqrt{\tau_i}}{\sqrt{2} \xi_{si} \bar{R}_b}$

Key to symbols: i_s , signal current; i_b , background current; R_s , signal count rate; R_b , background count rate; τ_r , response time; τ_i , integration time; ξ_{dm} , ξ_{am} , ξ_{di} , ξ_{ai} , ξ_{si} , defined in Table II; F is a factor close to 0.5 which depends on the modulation wave form.

Table II. Expressions for Flicker Factors, ξ , for Several Measurement Approaches

Measurement Device	d.c.	a.c.
Current Meter	$\xi_{dm} \equiv \sqrt{0.65 K_f^2} = 0.81 K_f$	$\xi_{am} \equiv K_f (\pi/2 f_{mod})^{1/2}$
Integrator	$\xi_{di} \equiv \sqrt{\ln 2 K_f^2} = 0.83 K_f$	$\xi_{ai} = K_f / (2 f_{mod})^{1/2}$
Synchronous Counter	---	$\xi_{si} = K_f (\ln 2 / f_{mod})^{1/2}$

stationary fluctuation process. The background current, i_b , was assumed to have been applied to the meter for a long time before a reading was taken. In the case of multiplicative noise, noise is introduced simultaneously with a signal due to the analyte. If one applies paired measurements such as the measurement of a reference (standard) followed by measurement of an analyte signal, the very nature of the noise source considered makes it impossible to ignore the noise in one of the measurements. Since these signals are read after a sampling time τ_s which may be shorter than the response time, τ_r , a stationary state of the meter deflection may neither be reached for the average signal nor for the fluctuations inherent to the signal. It is necessary to deal with the transient response of the meter to fluctuations.

Assumptions

The assumptions used in this model of multiplicative noise are (see Figure 3):

- (i) The input analytical signal, $i_s(t)$, and reference signal, $i_r(t)$, are noise-free;
- (ii) the time dependence of the input signal is a step function,
 $i_s(t) = i_s$ for $T < t < T + \tau_s$,
 $i_r(t) = i_r$ for $0 < t < \tau_s$, and
 $i_s(t) = i_r(t) = 0$ for t outside the given intervals;
- (iii) at $t = 0$ and $t = T$, the meter deflection caused by the preceding signal has decayed ($T \gtrsim \tau_s$) or been reset to zero;
- (iv) no additive noises are present;

- (v) i_s is proportional to the analyte sample concentration (C_s) and i_r is proportional to a reference parameter (C_r) which may be a calibration standard, excitation source intensity in luminescence spectrometry, etc;
- (vi) a "multiplication factor," $G(t)$, is a stationary, Gaussian noise process which produces multiplicative noise and is given by $G(t) = \bar{G} + dG(t)$;
- (vii) after "multiplication," the input signal $i(t)$ is transformed into the multiplied signal $A(t)$ where $A(t) = G(t)i(t)$;
- (viii) the meter deflection $x(t)$ and $A(t)$ are related by

$$A(t) = \frac{dx}{dt} + \frac{x}{\tau_c} \quad (\text{II.35})$$

- (ix) the estimate of the analyte concentration, C_s , is given by

$$C_s = \frac{x_s(T + \tau_s)}{x_r(\tau_s)} C_r \quad (\text{II.36})$$

Several points should be carefully noted. The noise in the multiplicative factor, $G(t)$, is itself a stationary noise process, but $x(t)$ is not a stationary noise process. The reference signal, i_r , and the reference parameter, C_r , have been defined in a completely general way. The most common case in analytical spectrometry is that the reference is a standard of known analyte concentration. It is possible that other references may be used, such as an internal standard.

General Expression for the Relative Variance

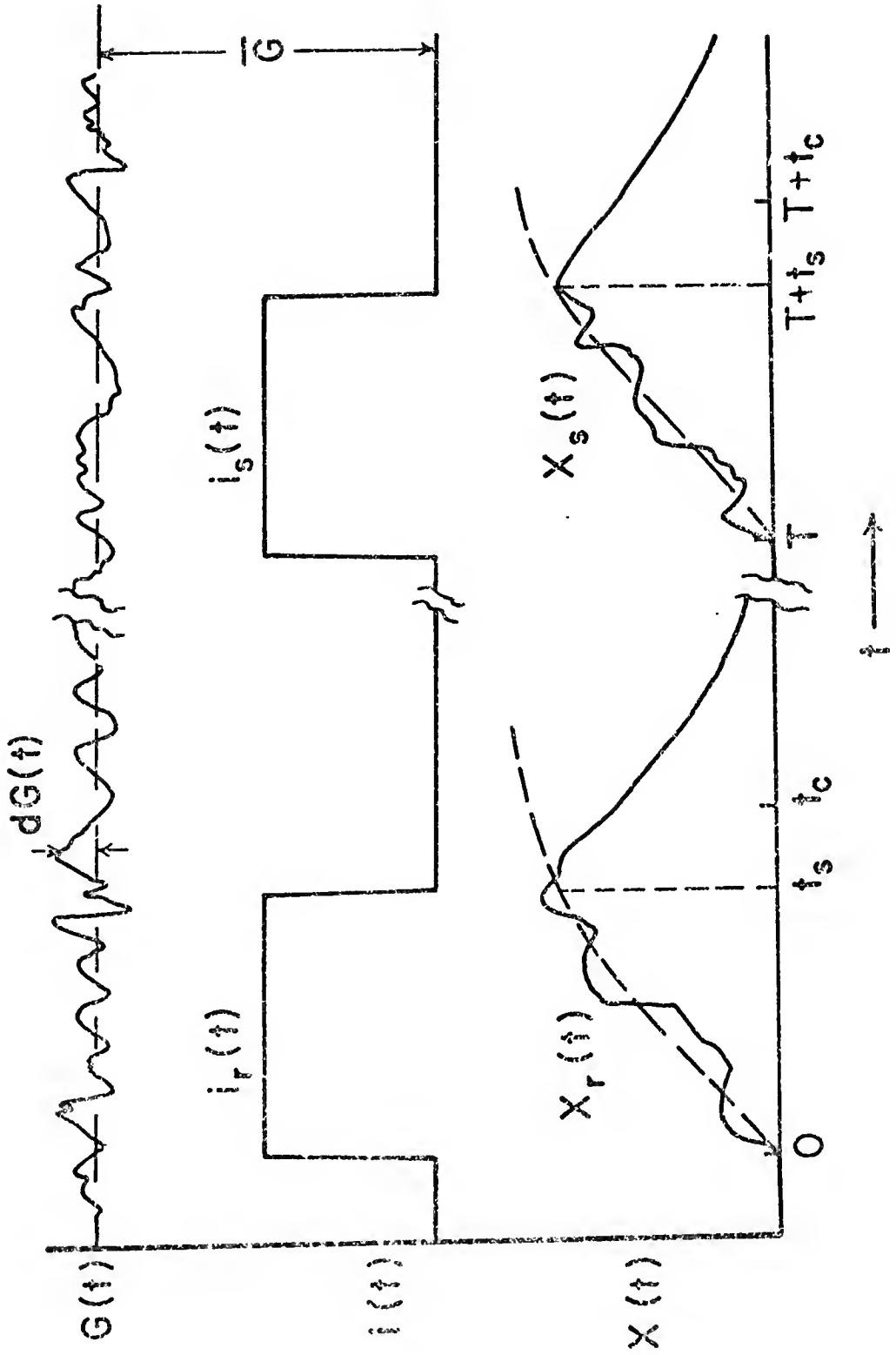
From Eq. II.36, the differential of C_s may be written as

$$\frac{dC_s}{C_s} = \frac{dx_s(T + \tau_s)}{x_s(T + \tau_s)} - \frac{dx_r(\tau_s)}{x_r(\tau_s)} \quad (\text{II.37})$$

Figure 3. Representation of Analyte Signal and Reference Signal Measured with a Meter

KEY TO SYMBOLS:

$x(t)$ = meter deflection
 $x_r(t)$ = meter deflection due to reference signal
 $x_s(t)$ = meter deflection due to analyte signal
 $i(t)$ = current
 $i_r(t)$ = reference current
 $i_s(t)$ = analyte current
 t = time
 τ_s = sampling time
 τ_c = time constant of meter damped by RC-filter
 τ_f = time analyte signal is input to meter
 $G(t)$ = multiplicative noise factor
 \bar{G} = average multiplicative noise factor
 $dG(t)$ = deviation of $G(t)$ from \bar{G}



and the variance of C_s , $\sigma_{C_s}^2$, is given by

$$\sigma_{C_s}^2 = \left[\frac{dx_s(T + \tau_s)}{x_s(T + \tau_s)} - \frac{dx_r(\tau_s)}{x_r(\tau_s)} \right]^2 C_s^2 \quad (II.38)$$

The relative variance of C_s may be written as

$$\frac{\sigma_{C_s}^2}{C_s^2} = 2 \left[\frac{dx_r(\tau_s)^2}{x_r(\tau_s)^2} - \frac{dx_r(\tau)dx_s(T + \tau_s)}{x_s(T + \tau_s)x_r(\tau)} \right] \quad (II.39)$$

where use has been made of the fact that $\overline{(dx_s/x_s)^2} = \overline{(dx_r/x_r)^2}$. The S/N ratio is given by C_s/σ_s . We wish to find how the S/N ratio depends on τ_s , τ_c , and T for given statistical properties of $dG(t)$ and what the optimum measurement conditions are.

From the definition of $A(t)$ and $G(t)$ and integration of Eq. II.35, the expression for $\overline{x(\tau)}$ is

$$\overline{x(\tau_s)} = i\tau_c \overline{G}[1 - \exp(-\tau_s/\tau_c)] \quad (II.40)$$

For general expressions, the subscripts s and r will be dropped. For $A(t)$, an arbitrary function of t for $t > 0$ and zero for $t < 0$, the general solution of Eq. II.35 is

$$x(\tau_s) = x(0)\exp(-\tau_s/\tau_c) + \exp(-\tau_s/\tau_c) \int_0^{\tau_s} \exp(u/\tau_c) A(u) du \quad (II.41)$$

where u is a dummy integration variable (23). Treating the meter deflection from the reference signal, $x_r(\tau_s)$, and using the definitions of $A(t)$ and $G(t)$ with $x(0) = 0$, it follows from Eq. II.41 that

$$x_r(\tau_s) = i\tau_c \overline{G}[1 - \exp(-\tau_s/\tau_c)] + i\tau_c \exp(-\tau_s/\tau_c) \int_0^{\tau_s} \exp(u/\tau_c) dG(u) du \quad (II.42)$$

or (see Eq. II.40)

$$x_r(\tau_s) = \overline{x_r(\tau_s)} + dx_r(\tau_s) \quad (\text{II.43})$$

and $dx_r(\tau_s)$ is given by

$$dx_r(\tau_s) = i_r \exp(-\tau_s/\tau_c) \int_0^{\tau_s} \exp(u/\tau_c) dG(u) du \quad (\text{II.44})$$

From the previous evaluation of $x_r(\tau_s)$, the expression for the meter deflection due to the analyte signal is $x_s(T + \tau_s) = \overline{x_s(T + \tau_s)} + dx_s(T + \tau_s)$, where

$$\overline{x_s(T + \tau_s)} = i_s \tau_c \overline{G[1 - \exp(-\tau_s/\tau_c)]} \quad (\text{II.45})$$

and

$$dx_s(T + \tau_s) = i_s \exp(-\tau_s/\tau_c) \int_T^{T+\tau_s} \exp[(v - T)/\tau_c] dG(v) dv \quad (\text{II.46})$$

where v is a dummy variable for integration.

To find the expression for $\overline{dx_r(\tau_s) dx_s(T + \tau_s)}$, Eq. II.44 and Eq. II.46 are multiplied and ensemble averaged. It is found that

$$\begin{aligned} \overline{dx_r(\tau_s) dx_s(T + \tau_s)} &= i_r i_s \exp(-2\tau_s/\tau_c) \cdot \\ &\cdot \overline{\int_0^{\tau_s} du \int_T^{T+\tau_s} \exp[(u + v - T)/\tau_c] dG(u) dG(v) dv} \end{aligned} \quad (\text{II.47})$$

The ensemble average over a double integral may be replaced by a double integral over an ensemble average. Equation II.47 can be rewritten as

$$\begin{aligned} \overline{dx_r(\tau_s) dx_s(T + \tau_s)} &= i_r i_s \exp(-2\tau_s/\tau_c) \cdot \\ &\cdot \int_0^{\tau_s} du \int_T^{T+\tau_s} dv \exp[(u + v - T)/\tau_c] \overline{dG(u) dG(v)} \end{aligned} \quad (\text{II.48})$$

Because $dG(t)$ has been defined as a stationary noise process, it is possible to define the time-independent auto-correlation function of $dG(t)$ by

$$\psi_G(s) = \overline{dG(t)dG(t+s)} \quad (II.49)$$

The term $\overline{dG(u)dG(v)}$ is therefore equal to $\psi_G(v-u)$. Rearranging Eq. II.48 and replacing the integration over v by $y = v-u$ for given u results in

$$\begin{aligned} \overline{dx_r(\tau_s)dx_s(T+\tau_s)} &= i_r i_s \exp(-2\tau_s/\tau_c) \cdot \\ &\cdot \int_0^{\tau_s} du \exp[(2u-T)/\tau_c] \int_{T-u}^{T-u+\tau_s} \exp(y/\tau_c) \psi_G(y) dy \end{aligned} \quad (II.50)$$

This is the general expression for $\overline{dx_r(\tau_s)dx_s(T+\tau_s)}$.

In an entirely analogous fashion to that in which the expression for $\overline{dx_r(\tau_s)dx_s(T+\tau_s)}$ was obtained, the expression for $\overline{dx_r(\tau)^2}$ is found to be

$$\begin{aligned} \overline{dx_r(\tau_s)^2} &= i_r^2 \exp(-2\tau_s/\tau_c) \cdot \\ &\cdot \int_0^{\tau_s} du \exp(2u/\tau_c) \int_{-u}^{-u+\tau_s} \exp(s/\tau_c) \psi_G(s) ds \end{aligned} \quad (II.51)$$

where $s = u' - u$ for constant u .

Substituting Eqs. II.40, II.50, and II.51 into Eq. II.39, the expression for the relative variance of C_s is

$$\begin{aligned} \frac{\sigma_{C_s}^2}{C_s^2} &= \frac{2\exp(-2\tau_s/\tau_c)}{\tau_c^2 G^2 [1 - \exp(-\tau_s/\tau_c)]^2} \left\{ \int_0^{\tau_s} du \exp(2u/\tau_c) \int_{-u}^{-u+\tau_s} \exp(s/\tau_c) \psi_G(s) ds + \right. \\ &\quad \left. - \int_0^{\tau_s} du \exp[(2u-T)/\tau_c] \int_{T-u}^{T-u+\tau_s} dy \exp(y/\tau_c) \psi_G(y) \right\} \end{aligned} \quad (II.52)$$

The integral over u may be factored out, the integration variable y replaced by $s = y - T$, and the integrals over s combined. This results in

$$\frac{\sigma_{C_S}^2}{C_S^2} = \frac{2\exp(-2\tau_S/\tau_C) \int_0^{\tau_S} du \exp(2u/\tau_C)}{\tau_C^2 G^2 [1 - \exp(-\tau_S/\tau_C)]^2} \cdot \left\{ \int_{-u}^{-u+\tau_S} ds \exp(s/\tau_C) [\psi_G(s) - \psi_G(s + T)] \right\} \quad (II.53)$$

From Eq. II.14, the Wiener-Khinchine theorem,

$$\psi_G(s) - \psi_G(s + T) = 2 \int_0^{\infty} S_G(f) \sin \pi f (2s + T) \sin \pi f T df \quad (II.54)$$

Substituting Eq. II.54 into II.53, gives the final, general expression for the relative variance of C_S , which is Eq. II.55.

$$\frac{\sigma_{C_S}^2}{C_S^2} = \frac{4\exp(-2\tau_S/\tau_C) \int_0^{\tau_S} du \exp(2u/\tau_C)}{\tau_C^2 G^2 [1 - \exp(-\tau_S/\tau_C)]^2} \cdot \int_{-u}^{-u+\tau_S} ds \exp(s/\tau_C) \cdot \int_0^{\infty} S_G(f) \sin \pi f (2s + T) \sin \pi f T df \quad (II.55)$$

The integral over u is defined over the range $0 \leq u \leq \tau_S \leq T$, and the integral over s is defined over the range $-u \leq s \leq -u + \tau$.

Up until this point, the derivation of the expression for the relative variance of C_S was general for $S_G(f)$, τ_S , τ_C , and T subject to the constraints of the assumptions. The divergency of flicker noise as $f \rightarrow 0$ is neutralized by the two sine functions of frequency, f , in

Eq. II.55. For mathematical evaluation, the order of integration in Eq. II.55 may be reversed. As is usually the case, it is complex to evaluate.

D.C. Measurement with a Current Meter for White Noise

A case of interest is the case of a white noise spectrum. It is possible to define a correlation time, τ_G , of noise $dG(t)$ by

$$\tau_G = \frac{\int_0^\infty \psi_G(s) ds}{\psi_G(0)} \quad (\text{II.56})$$

where $\psi_G(0) = \overline{dG(t)^2}$. Because $\psi_G(s)$ differs from zero only for $|s| \lesssim \tau_G$, while $\tau_G \leq \tau_s, \tau_c$, and T , for this case, $S_G(f)$ is a constant over the relative frequency range, but falls off at $2\pi f \gtrsim \tau_G^{-1}$. Starting from Eq. II.53, $\psi_G(s + T) = 0$ because $(s + T) \gg \tau_G$. Because $\psi_G(s)$ exists only for $s \lesssim 0$, the integral over s can be approximated by $\int_{-\infty}^{+\infty} \psi_G(s) ds$. It is a valid approximation as $0 \leq u < \tau_s$; s is within the integration limits of $-u$ and $-u + \tau_s$. From Eq. II.56, the definition of $\psi_G(s)$, and the approximation of the integral over s , Eq. II.53 becomes

$$\frac{\sigma_{C_s}^2}{C_s^2} = \frac{2 \exp(-2\tau_s/\tau_c) \int_0^\tau \exp(2u/\tau_c) du \overline{dG^2} \tau_G}{\tau_c^2 \overline{G^2} [1 - \exp(-\tau_s/\tau_c)]^2} \quad (\text{II.57})$$

Making the substitution $z = 2u/\tau_c$ and evaluating Eq. II.57 gives

$$\frac{\sigma_{C_s}^2}{C_s^2} \approx \frac{2 \overline{dG^2} \tau_G [1 - \exp(-2\tau_s/\tau_c)]}{\overline{G^2} \tau_c [1 - \exp(-\tau_s/\tau_c)]^2} \quad (\text{II.58})$$

From the definition, $\overline{dG^2} = \psi_G(0)$, the inverse Wiener-Khinchine theorem,

and Eq. II.56 (see Eq. II.6)

$$\overline{dG^2} = S_G(0)/4\tau_G \quad (\text{II.59})$$

Substituting Eq. II.59 into Eq. II.58 yields

$$\frac{\sigma_C^2}{C_S^2} \approx \frac{S_G(0)[1 - \exp(-2\tau_S/\tau_C)]}{2\overline{G^2}\tau_C[1 - \exp(-\tau_S/\tau_C)]^2} \quad (\text{II.60})$$

The S/N ratio is therefore

$$\frac{S}{N} \approx \frac{\overline{G}\sqrt{2\tau_C} [1 - \exp(-\tau_S/\tau_C)]}{\sqrt{S_G(0)}[1 - \exp(-2\tau_S/\tau_C)]} \quad (\text{II.61})$$

The S/N ratio is found to be independent of T, or in other words, the S/N ratio is unaffected by the time between measurement of the reference signal and the analyte signal. The S/N ratio is maximum when $\tau_S \rightarrow \infty$. In practical measurements, the maximum S/N ratio is obtained when $\tau_S = 2\pi\tau_C$ where $2\pi\tau_C$ has been defined as the response time, τ_r , in Eq. II.24. In terms of the response time, the maximum signal-to-noise is given by

$$\frac{S}{N} \max = \frac{\overline{G} \sqrt{\tau_r}}{\sqrt{S_G(0)}\pi} \quad (\text{II.62})$$

If this equation is compared with Eq. II.27 for the case of background shot noise, it is seen that the S/N ratio increases in both with $\sqrt{\tau_r}$. It should be noted that the expression for shot noise may not be substituted here for $S_G(0)$ because shot noise is not a multiplicative noise. All that can be specified is that for the white noise case $S_G(0)$ is constant. The S/N ratio will also increase as $\sqrt{S_G(0)}$ decreases.

D.C. Measurement with an Integrator for White Noise

The case of an integrator may be derived from Eq. II.61 by taking the limit as $\tau_c \rightarrow \infty$ for an integration time $\tau_i = \tau_s$ (28). The result for the case of white noise is given by

$$\frac{S}{N} \approx \frac{\bar{G} \sqrt{\tau_i}}{\sqrt{S_G(0)}} \quad (\text{II.63})$$

This shows an improvement in S/N ratio over a d.c. meter by a factor of $\sqrt{\pi}$ assuming $\tau_i = \tau_r$.

D.C. Measurement with an Integrator for Flicker Noise

It is necessary to assume that $\tau_i < \tau_c$, as was the case for the integrator in the case of white noise. Starting from Eq. II.55, setting $S_G(f) = K_f^2/f$ for flicker noise, and approximating $\exp(2u/\tau_c)$, $\exp(-2\tau_s/\tau_c)$, and $\exp(s/\tau_c)$ by unity give

$$\begin{aligned} \frac{\sigma_{C_S}^2}{C_S^2} = \frac{4K_f^2}{\bar{G}^2} \left\{ \frac{1}{2} \left(\frac{T}{\tau_i} - 1 \right)^2 \ln(T - \tau_i) + \frac{1}{2} \left(\frac{T}{\tau_i} + 1 \right)^2 \ln(T + \tau_i) - \right. \\ \left. \left(\frac{T}{\tau_i} \right)^2 \ln T - \ln \tau_i \right\} \end{aligned} \quad (\text{II.64})$$

With a fixed integration time τ_i , the minimum value of T is given by $T_{\min} = \tau_i$ (see assumptions). Solving for the S/N ratio gives

$$\frac{S}{N} (T = \tau_i) = \frac{\bar{G}}{2K_f \sqrt{\ln 4}} \quad (\text{II.65})$$

If T is increased relative to τ_i , for the limit of $T \gg \tau_i$, the

signal-to-noise ratio becomes

$$\frac{S}{N} (T \gg \tau_i) = \frac{\bar{G}}{2K_f \sqrt{2 + \ln(T/\tau_i)}} \quad (\text{II.66})$$

As T increases, the S/N ratio decreases. For a fixed total measurement time, the optimum S/N will be achieved by making n measurements of reference and standard with $T = \tau_i$ and averaging the results, which increases the S/N ratio by a factor of \sqrt{n} . This conclusion has been reached by Snelleman (29) and Léger et al. (30) for the case of additive flicker noise. In practice, there is a fundamental limit to the amount of improvement that may be achieved by this procedure. In the model for multiplicative noise, only multiplicative noise sources have been treated. All signals in analytical spectrometry will have shot noise, and if the integration time becomes short enough, the shot noise may become the dominant noise source. In this case, there will be no improvement in S/N ratio as n is increased. For the case of multiplicative white noise, there will be no difference between making one set of paired measurements of sample and reference or n sets during the total measurement time. The general conclusion is that the optimum signal-to-noise ratio will be achieved when the sample and reference pair are measured as rapidly as possible during the measurement time.

It is not possible to evaluate the case of a current meter for arbitrary τ_c , τ_s , and T without numerical integration. If one assumes $T \gg \tau_r$, then the noise can be treated as "quasi-stationary." In this case, the conclusions for background flicker noise should apply. Again, it is optimal to make several measurements and average the results, which is the same conclusion reached for integration.

Signal-to-Noise Ratio Expressions in Emission and
Luminescence Spectrometry

Expressions for S/N for Single Channel Detectors

It should be emphasized that in the previous discussion only one noise source was considered in calculating the signal-to-noise ratios. However, when making measurements in analytical spectrometry, more than one noise source occurs and so must be considered whatever measurement system is being utilized for the signal measurement. In this section, only emission (atomic and molecular) and luminescence (atomic and molecular) spectrometry will be explicitly considered. No attempt will be made here to give general expressions for absorption (atomic and molecular) spectrometry, although the expressions for emission and luminescence spectrometry can be applied, with some changes, to absorption spectrometry, which is somewhat more complex due to the necessity of making ratio measurements and the nonlinearity of absorbance with analyte concentration. The noises occurring in emission and luminescence spectrometry will be explicitly discussed and evaluated in this section, particularly with regard to how the noises combine to give the total noise in the measurement.

In general, shot noises are simple to consider since they add quadratically, i.e., no correlation between these noises. Flicker noises are much more complicated to handle because they may be dependent, independent, or a combination of dependency and independency. Although high frequency proportional noises are similar in complexity to flicker noises, they can be omitted in the following treatment because such noises can be minimized by proper selection of the frequency of the

measurement system. In the following treatment, flicker noises will be assumed to be completely dependent or completely independent (no correlation coefficients) according to the best experimental evidence available to the authors (31-33). Although the most general expressions should contain flicker noises with correlation coefficients, such expressions would be exceedingly complex and of little use since correlation coefficients for flicker noises are rarely available. It was necessary in the present treatment to assume the linear addition of analyte emission or luminescence flicker noises to the related "background" flicker noises (background emission in emission spectrometry and source related background, such as scatter and luminescence background in luminescence spectrometry); this addition is not exact because analyte flicker occurs only during the sample and not the blank. Nevertheless, the expressions to be given should be good estimates of S/N for actual experimental situations. Finally, tables of expressions and evaluations of parameters will be utilized where feasible to simplify the expressions and evaluations of the expressions. The S/N expressions to be given will contain various parameters, such as total measurement time and counting rates, which are evaluated according to the analytical system under study, flicker factors which are evaluated according to the analytical system under study and the measurement method, and constant terms characteristic of the measurement method.

General S/N expressions (digital case only) for atomic or molecular emission spectrometry and for atomic or molecular luminescence spectrometry, are given in Table III. All terms are defined at the end of the table. The power terms, p , q , r , u , and w , are also evaluated in Table III for the cases of CW (continuous excitation-continuous emission

or luminescence and continuous measurement), AM (amplitude modulation of emitting radiation in emission spectrometry or of exciting source in luminescence spectrometry), WM (wavelength modulation of optical system to produce an a.c. current for the analyte), SM (sample-blank modulation, i.e., repetitive measurement of sample and blank), AM + WM (double modulation where the optical system is slowly wavelength modulated while rapidly amplitude modulating the signal as described above), and AM + SM (double modulation where the sample and blank are repetitively and slowly introduced while the amplitude is rapidly modulated as described above). Other double modulation approaches, as WM + SM, and triple modulation, as AM + WM + SM, result in little gain in analytical figures of merit and are more complex and so will not be discussed here.

Modulation methods are only useful in minimizing flicker noises (any noise source which is present during both halves of the modulation is reduced since ξ is given by the appropriate AC-expression, i.e., ξ_{ai} for the synchronous counter, rather than by the d.c. integrator expression, ξ_{di} ($\xi_{di} > \xi_{ai}$)).

In Table IV, the appropriate flicker factor, ξ_{di} or ξ_{ai} for the d.c. integrator or digital synchronous counter, respectively, is noted. In Table V, evaluation of the duty factors for the various measurement modes and for the various duty factors in the general noise expressions defined in Table III (at end of table) are given. The duty factor is generally defined as the fractional on time for any given process by any type of measurement mode.

The expressions in Table III with the definition and evaluation of terms in Tables III, IV, and V describe all measurement modes in emission and luminescence spectrometry except for those cases where the emission

source in emission spectrometry or the excitation source in luminescence spectrometry is pulsed and the detector-electronics system is gated with or without time delay between the termination of excitation and the initiation of measurement (31). In Table VI, expressions for duty factors to describe source pulsing-detector gating are given with definition of terms. The duty factors, D_{EM} and D_{LM} replace the values of 1/2 or 1 in Table V for CW, AM, WM, SM, AM + WM, and AM + SM measurement modes. The CW mode for source pulsing-detector gating implies that a blank is determined in order to correct for background, interferent, and dark counts in emission and for background, interferent, scatter, and dark counts in luminescence. The AM mode for source pulsing-detector gating implies that a blank is determined as above for the CW mode but also in between source pulses for a time period of t_g , s, dark counts are observed in emission spectrometry and dark counts, analyte emission, and background emission are observed in luminescence spectrometry. The other modes have not been used for analytical emission and luminescence spectrometry but would involve the following: WM mode means that every other pulse is "on" wavelength and alternate pulses are "off" wavelength in either emission or luminescence spectrometry--again a blank must be "run"; SM mode means that one or more pulses occur for the sample and one or more (the same number as for the sample) occur for the blank and then the process is repeated for either emission or luminescence spectrometry--in this case, in luminescence spectrometry, a separate source of measurement must be "run" to determine the emission signal; double modulation methods, AM + WM and AM + SM are of interest only for luminescence spectrometry and involve a combination of the above modes. Therefore, to obtain the appropriate S/N expression, one takes the

appropriate expression from Table I with noise terms described by the expressions at the end of the table; the flicker factors are those listed in Table II. The duty factors, except for D_{EM} , D_{LM} , and D_{GD} are those in Table V, and the ones for D_{EM} , D_{LM} , and D_{GD} are given in Table III.

Sample Modulation

Sample modulation, SM, was discussed in the previous section. However, this rather unique approach to analysis (34,35) requires some specific comments. In SM, the sample and blank are repetitively measured for n equal time periods each, and so unmodulated flicker noise sources, e.g., flame background in atomic fluorescence flame spectrometry, continuum scatter or molecular band interferences in atomic fluorescence flame spectrometry, etc., will be reduced as the modulation frequency, f_{mod} , increases and the measurement system's noise bandwidth, Δf , decreases, i.e., the flicker factor, ϵ_{ai} is related to $\Delta f/f_{mod}$ by

$$\epsilon_{ai} \propto \sqrt{\frac{\Delta f}{f_{mod}}} = \sqrt{\frac{1}{2nt_0}} = \sqrt{\frac{1}{n}} \quad (II.67)$$

where t_0 is the observation time of sample or blank per cycle and n is the number of sample-blank cycles. As the number of sample-blank cycles, n , increases ϵ_{ai} decreases inversely with \sqrt{n} . There is a practical limit to f_{mod} and therefore to $\Delta f/f_{mod}$, namely, the time to mechanically change from sample to blank with no memory effects, and so $f_{mod} \gtrsim 10$ Hz, which may not be as effective in removing noise as WM modulation which requires twice the number of measurements. In addition in SM, an

"ideal" blank, (contains everything in the sample except the analyte) must be prepared and used.

Wavelength Modulation

In WM, all flicker noise sources which are present "on" and "off" the analyte measurement wavelength are reduced, i.e., $\xi_{ai} < \xi_{di}$. If the samples and standards are identical in all respects, except for the analyte, then WM corrects the signal level for unmodulated signal components and reduces flicker noises due to these sources. Because WM can involve the mechanical movement of a small refractor plate or mirror in the optical train of a spectrometer, it is possible to obtain higher modulation frequencies, e.g., ≈ 100 Hz, than in SM (but lower than in AM); therefore, because $\xi_{ai} \propto \sqrt{\Delta f / f_{\text{mod}}}$ as in Eq. (II.67), ξ_{ai} can be made smaller than for the corresponding noise in SM. Of course, in luminescence spectrometry, any analyte emission signals must be corrected for by a separate "source off" measurement unless the sum of emission plus fluorescence is desired. If line interferences are present, WM may result in an erroneous analyte signal, whereas in SM, assuming the line interferent is present in sample and blank, the analyte signal level will be correct but the noise is still degraded.

Conclusions

The major conclusions which can be drawn from the treatment of signal-to-noise ratios are

- (i) For the cases of white noise, whether additive or multiplicative, the S/N ratio increases as the square root of the

response time, τ_r , or the integration time, τ_i , for current meters and integrators respectively;

- (ii) For background shot noise limited cases, modulation techniques will give S/N ratios $\sqrt{2}$ times poorer. Sample modulation is an exception, because it is necessary to measure the blank regardless;
- (iii) For the cases of white noise, whether additive or multiplicative, the S/N ratio is independent of the rate at which sample and background or sample and reference are measured;
- (iv) For the cases of flicker noise, whether additive or multiplicative, the S/N ratio is approximately independent of response time or integration time;
- (v) For the cases of flicker noise, whether additive or multiplicative, the S/N will decrease with increasing sampling time relative to a fixed response time. It is optimum to make the integration or response time as short as is practical and repeat the pair of measurements n times;
- (vi) The case of multiple sampling during the measurement time for background flicker noise cases is essentially the same as using an a.c. system where the signal is modulated and the noise is not modulated;
- (vii) If both the signal and background noise are modulated in a background flicker noise case, no increase in S/N ratio results;
- (viii) In a background flicker noise case when using an a.c. system, it is optimum to make $\Delta f/f_{\text{mod}}$ as small as possible (either with small Δf or large f_{mod});

- (ix) The optimum system in the case of multiplicative flicker noise is to measure sample and reference simultaneously. The best reference in most cases is a calibration standard, but it is often impossible to measure a signal and a standard simultaneously. In some situations, an internal standard, excitation source intensity, etc., measurement may be made simultaneously and will improve the S/N if the source of multiplicative noise affects both in the same way and is the limiting source of noise. An example is that taking the ratio of the signal to the excitation source intensity in luminescence spectrometry will not improve the S/N ratio if the major source of multiplicative noise is connected with the sample introduction system.

Table III. General Signal-to-Noise Ratio Expressions for Emission and Luminescence Spectrometry with Definition of Terms

$$\frac{S}{N}_E = \frac{S_E}{\sqrt{N_{ES}^2 + N_{BS}^2 + N_{I_eS}^2 + N_{DS}^2 + (N_{EF} + 2^q N_{I_eF} + 2^q N_{BF})^2 + (2^w N_{DF})^2 + (2^w N_A)^2}}$$

Measurement Mode	q	w
CW	1	1
AM	1/2	1/2
WM	1/2	1/2
SM	0	1/2

$$\frac{S}{N}_L = \frac{S_L}{\left[N_{LS}^2 + N_{ES}^2 + N_{I_fS}^2 + N_{SS}^2 + N_{BS}^2 + N_{DS}^2 + (N_{LF} + 2^u N_{I_fF} + 2^r N_{SF})^2 + 2^p (N_{EF} + 2^q N_{BF})^2 + (2^w N_{DF})^2 + (2^w N_A)^2 \right]^{1/2}}$$

Measurement Mode	p	q	r	u	w
CW	1	1	1	1	1
AM	0	1/2	1	1	1/2
WM	1	1/2	{ 1/2 (continuum) 1 (line)	1/2	1/2
SM	1	0	0	0	1/2
AM + WM	0	0	{ 1/2 (continuum) 1 (line)	1	1/2
AM + SM	1	0	0	0	0

Table III. (continued)

Definition of Terms

- N_{ES} = analyte emission shot noise = $\sqrt{\frac{1}{2} D_{EM} D_{WM} R_E t_m}$, counts
 N_{BS} = background emission shot noise = $\sqrt{D_{EM} D_O R_B t_m}$, counts
 $N_{I_e S}$ = interferent (in matrix emission) shot noise = $\sqrt{D_{EM} R_{I_e} t_m}$, counts
 N_{DS} = detector dark shot noise = $\sqrt{D_{GD} R_D t_m}$, counts
 N_{LS} = analyte luminescence shot noise = $\sqrt{\frac{1}{2} D_{LM} D_{WM} D_O R_L t_m}$, counts
 N_{SS} = scatter (source) shot noise = $\sqrt{D_{LM} D_{\text{LM}} D_O R_S t_m}$, counts
 $N_{I_f S}$ = interferent (in sample/blank) luminescence shot noise = $\sqrt{D_{LM} D_O R_{I_f} t_m}$, counts
 $2^w N_A$ = amplifier readout noise (generally negligible in S/N measurements), counts
 N_{EF} = analyte emission flicker noise = $\frac{1}{2} \epsilon_{EF} D_{EM} D_{WM} D_O R_E t_m$, counts
 $2^q N_{BF}$ = background emission flicker noise = $2^q \epsilon_{BF} D_{DM} D_{SB} D_O R_B t_m$, counts
 $2^q N_{I_e F}$ = interferent (in emission flicker noise = $2^q \epsilon_{I_e F} D_{EM} R_{I_e} t_m$, counts
 $2^w N_{DF}$ = detector dark flicker noise = $2^w \epsilon_{DF} D_{GD} R_D t_m$, counts
 $2^r N_{SF}$ = scatter (source) flicker noise = $2^r \epsilon_{SF} D_{\text{LM}} D_{LM} D_{SB} D_O R_S t_m$, counts
 $2^u N_{I_f F}$ = interferent (in sample/blank) luminescence flicker noise = $2^u \epsilon_{I_f F} D_{LM} D_O R_{I_f} t_m$, counts
 N_{LF} = analyte luminescence flicker noise = $\frac{1}{2} \epsilon_L D_{LM} D_{SB} D_O R_L t_m$, counts
 S_E = analyte emission signal = $\frac{1}{2} D_{EM} D_{WM} R_E t_m$, counts
 S_L = analyte luminescence signal = $\frac{1}{2} D_{LM} D_{WM} D_O R_L t_m$, counts
 t_m = measurement time for one spectral component, s (see Figure 3 and text)
 D_{LM} = amplitude modulation factor for luminescence spectrometry, dimensionless

Table III. (continued)

Definition of Terms (continued)

D_{EM} = emission modulation factor for emission spectrometry, dimensionless

D_{SB} = sample-blank factor, fraction of time sample is "on," dimensionless

D_{WM} = wavelength modulation factor, dimensionless

D_{LM} = wavelength modulation factor for narrow line, dimensionless

D_0 = factor for correction for emission in luminescence spectrometry, fraction of time emission or luminescence (equal times) is measured, dimensionless

D_{GD} = gated detector factor to account for fraction of time detector is gated "on," dimensionless

R_E = photoelectron counting rate of analyte emission, s^{-1}

R_B = photoelectron counting rate of background emission, s^{-1}

R_{I_e} = photoelectron counting rate of interferent in emission spectrometry, assumed to be in both blank and sample, s^{-1}

R_S = photoelectron counting rate of source scatter in luminescence spectrometry, s^{-1}

R_{I_f} = photoelectron counting rate of interferent luminescence in luminescence spectrometry, assumed to be in sample and blank, s^{-1}

R_D = detector dark counting rate of detector, s^{-1}

R_L = photoelectron counting rate of analyte luminescence, s^{-1}

ξ_{EF} = flicker factor for analyte emission flicker, dimensionless

$\xi_{I_e F}$ = flicker factor for emission interferent flicker factor, dimensionless

Table III. (continued)

Definition of Terms (continued)

ξ_{BF} = flicker factor for background emission flicker factor,
dimensionless

ξ_{SF} = flicker factor for source scatter (in luminescence spectrometry)
flicker factor, dimensionless

ξ_{I_fF} = flicker factor for luminescence interferent (in luminescence
spectrometry) flicker factor, dimensionless

ξ_{DF} = detector flicker factor, dimensionless

ξ_{LF} = flicker factor for analyte luminescence, dimensionless

Table IV. Evaluation of Flicker Factors in Emission and Luminescence Spectrometry

EMISSION*				
Measurement Mode	ξ_{EF}	ξ_{BF}	$\xi_{I_e F}$	ξ_{DF}
CW	DC	DC	DC	DC
AM	DC	DC	DC	AC
WM	DC	AC	AC	AC
SM	DC	AC	AC	AC

LUMINESCENCE*						
Measurement Mode	ξ_{LF}	ξ_{EF}	ξ_{BF}	$\xi_{I_f F}$	ξ_{SF}	ξ_{DF}
CW	DC	DC	DC	DC	DC	DC
AM	DC	AC	AC	DC	DC	AC
WM	DC	DC	AC	AC	AC	AC
SM	DC	DC	AC	AC	AC	AC
AM + WM	DC	AC	AC	AC	AC	AC
AM + SM	DC	AC	AC	AC	AC	AC

*The flicker factors are either given by the d.c. integrator case or the a.c. Synchronous Counter Case in Table II.

Table V. Evaluation of Duty Factors in Emission and Luminescence Spectrometry

EMISSION*			
Measurement Mode	D_{EM}^1	D_{WM}	D_{GD}^2
CW [#]	1	1	1
AM [#]	$1/2(1)^{\#}$	1	1
WM	1	1/2	1
SM	1	1	1

LUMINESCENCE*

Measurement Mode	D_{LM}	D_{WM}	D_{SB}	D_{LM}^3	D_0	D_{GD}^2
CW [#]	1	1	1/2	1	1/2	1
AM [#]	$1/2(1)^{\#}$	1	1/2	1	1	1
WM	1	1/2	1/2	$1/2 \text{ (line)}^{\dagger}$ $1 \text{ (cont)}^{\dagger}$	1/2	1
SM	1	1	1	1	1/2	1
AM + WM	1/2	1/2	1/2	$1/2 \text{ (line)}^{\dagger}$ $1 \text{ (cont)}^{\dagger}$	1/2	1
AM + WM	1/2	1	1	1	1	1

Notes:

* $D_{EM} = 1/2$ if the emission is modulated in emission spectrometry

$D_{EM} = 1$ if the emission is not modulated in emission spectrometry

$D_{WM} = 1/2$ if wavelength modulation is used and 1 if it is not used

$D_{LM} = 1/2$ if the source of excitation in luminescence spectrometry is modulated

Table V. (continued)

Notes (continued):

$D_{LM} = 1$ if the source of excitation in luminescence spectrometry is not modulated

$D_{SB} = 1/2$ for paired sample-blank measurements

$D_{SB} = 1$ for sample modulation

$D_{GD} = 1$ if the detector is "on" during the entire measurement

$D_{GD} < 1$ if the detector is gated

$D_{LM} = 1$ if the exciting source in atomic fluorescence spectrometry is a continuum source

$D_{LM} = 1/2$ if the exciting source in luminescence spectrometry is a line source

$D_0 = 1$ if the analyte emission in luminescence spectrometry is automatically compensated for as in AM

$D_0 = 1/2$ if a separate "source off" measurement must be made in luminescence spectrometry to compensate for analyte emission as in CW, WM, and SM cases

[#]Only these two measurement modes are of importance for image device detectors with image detectors, all duty factors are as shown except for the case of background emission shot and flicker noise in the AM mode where D_{EM} and D_{LM} are both as shown in parentheses.

[†]Line means a line interferent; cont means a continuum interferent.

Table VI. Duty Factors for Pulsed Source-Gated Detector Cases

Pulsed Source-Gated Detector^a--No Time Resolution (No Delay Between Pulsing and Detection)

$$d_{AM} \text{ or } d_{EM} = \frac{\{t_g - \tau_i [1 - e^{-t_g/\tau_i}]\}}{t_g [1 - e^{-1/f\tau_i}]}$$

$$d_{GD} = t_g/t_g$$

Pulsed Source-Gated Detector^a--With Time Resolution (Delay of t_d , s Between Pulsing and Detection)

$$d_{AM} \text{ or } d_{EM} = \frac{\tau_i [1 - e^{-t_p/\tau_i}] [1 - e^{-t_g/\tau_i}] e^{-t_d/\tau_i}}{t_g [1 - e^{-1/f\tau_i}]}$$

$$d_{GD} = t_g/t_g$$

Definition of Terms

t_p = pulse width of source (assuming rectangular pulse), s

t_g = gate width of detector (assuming rectangular gate), s

t_d = delay time between end of excitation and beginning of measurement

f = repetition rate of source (gate), Hz

τ_i = lifetime of radiative process, i, s

^aThe duty factors, d_{AM} or d_{EM} , become d_{GD} in the event the radiative process, i, is not pulsed. These expressions apply to an averager; one must replace t_g in the denominator by $1/f$ for an integrator.

CHAPTER III
MOLECULAR LUMINESCENCE RADIANCE EXPRESSIONS ASSUMING
NARROW BAND EXCITATION

Assumptions

In the derivations to follow, it will be assumed:

- (i) that all molecules are in the condensed phase at room temperature or lower;
- (ii) that all molecules are in the zeroth vibrational level of the ground electronic state prior to excitation;
- (iii) that thermal excitation of the upper electronic states is negligible;
- (iv) that the source of excitation is a narrow line, i.e., the source linewidth is much narrower than the absorption bandwidth;
- (v) that only one vibrational level in the upper electronic state is excited;
- (vi) that all luminescence transitions originate from the zeroth vibrational level of the excited electronic state;
- (vii) that self-absorption is negligible;
- (viii) that prefilter and postfilter effects are negligible;
- (ix) that photochemical reactions do not occur;
- (x) that only homogeneous broadening occurs.

The expression for the single line excitation rate for induced absorption used is given by (36)

$$\frac{E(\nu_{\ell,\mu})}{c} \int B_{\ell,\mu} \alpha_{\ell}(\nu, \nu_0) G(\nu, \nu_0) d\nu \quad (\text{III.1})$$

and the single line de-excitation rate for stimulated emission is given by

$$-\frac{E(\nu_{\ell,\mu})}{c} \int B_{\mu,\ell} \alpha_{\mu}(\nu, \nu_0) G(\nu, \nu_0) d\nu \quad (\text{III.2})$$

where $E(\nu_{\ell,\mu})$ is the integrated source irradiance, W m^{-2} , c is the velocity of light, ms^{-1} , $B_{\ell,\mu}$ and $B_{\mu,\ell}$ are the Einstein coefficients for absorption and stimulated emission respectively, $\text{J}^{-1} \text{m}^3 \text{Hz s}^{-1}$, $\alpha_{\ell}(\nu, \nu_0)$ and $\alpha_{\mu}(\nu, \nu_0)$ are the normalized spectral profiles of the lower and upper levels respectively, Hz^{-1} , and $G(\nu, \nu_0)$ is the normalized spectral profile of the excitation source. For molecules in the condensed phase, free rotation is not possible. The rotational levels have therefore lost their meaning and the sharp rotational lines of gas phase spectra merge into regions of continuous absorption. The vibrational bands may be further broadened by intermolecular forces from the solvent molecules (37). If the only broadening present is assumed to be homogeneous broadening, then the normalized spectral profiles are given by

$$\alpha_{\ell}(\nu, \nu_0) = \alpha_{\mu}(\nu, \nu_0) = \alpha(\nu, \nu_0) = \frac{1}{\pi} \left[\frac{\delta\nu/2}{(\nu - \nu_0)^2 + (\delta\nu/2)^2} \right] \quad (\text{III.3})$$

where $\delta\nu$ is the absorption bandwidth and ν_0 is the center frequency. If the excitation source profile $G(\nu, \nu_0)$ is much narrower than the normalized absorption spectral profile and the source is operating at the line center, ν_0 , then

$$\alpha(\nu, \nu_0) = \frac{2}{\pi \delta\nu} \quad (\text{III.4})$$

The excitation and de-excitation rate therefore become, respectively,

$$B_{\mu, \ell} \left(\frac{2E}{\pi C \delta \nu} \right) = B_{\mu, \ell} \rho \quad (\text{III.5})$$

and

$$B_{\ell, \mu} \left(\frac{2E}{\pi C \delta \nu} \right) = B_{\ell, \mu} \rho \quad (\text{III.6})$$

where ρ is the spectral radiant energy density, $\text{J m}^{-3} \text{Hz}^{-1}$, and $E = E(\nu_{\ell, \mu})$.

For a gas phase molecule, even a laser may not necessarily have a narrower profile than the absorption profile of individual rotational lines. For this reason, it will be necessary to convolute the absorption profile, which is generally best represented by a Voigt profile, with the spectral profile of the excitation source. Since the source may also overlap several rotational lines, a summation over all the transitions is required. The absorption rate is then given by

$$\sum_i \frac{E(\nu_{\ell, \mu})}{c} \int B_{\ell, \mu} \alpha_{\ell, i}(\nu, \nu_0) G(\nu, \nu_0) d\nu \quad (\text{III.7})$$

and the de-excitation rate for stimulated emission by an analogous term. Integrals of this form for a Gaussian laser profile and a Voigt line profile have been given by Sharp and Goldwasser (36).

Steady State Two Level Molecule

This is a case often valid for condensed phase molecules where primarily two electronic energy levels are involved in both the radiative and nonradiative excitation processes. An example would be a highly fluorescent molecule with little intersystem crossing.

The energy efficiency for such a process is given by

$$Y_{p21} = \frac{\sum_i A_{20,1i} \nu_{20,1i}}{\nu_{2j,10} (\sum_i A_{20,1i} + k_{21})} \quad (\text{III.8})$$

and the quantum efficiency

$$Y_{21} = \frac{\sum_i A_{20,1i}}{\sum_i A_{20,1i} + k_{21}} \quad (\text{III.9})$$

where

$A_{20,1i}$ = Einstein transition probability for emission (luminescence transition from the zeroth vibrational level of the radiatively-excited, 2, electronic state to the i th vibrational level of the lower, 1, electronic state), s^{-1} ;

k_{21} = nonradiative first order de-excitation rate constant for same transition given in definition of $A_{20,1i}$, s^{-1} ;

$\nu_{20,1i}$ = frequency of luminescence transition, Hz;

$\nu_{2j,10}$ = frequency of excitation transition (absorption transition from zeroth vibrational level of ground, 1, electronic state to j th vibrational level of upper, 2, electronic state), Hz.

The integrated absorption coefficient for the radiative excitation process, $k_{\nu_{2j,10}}$, is given (38) by

$$\int_0^{\infty} k_{\nu_{2j,10}} d\nu = \left(\frac{h\nu_{10,2j}}{c} \right) B_{10,2j} n_1 \left[1 - \frac{g_1 n_2}{g_2 n_1} \right] \quad (\text{III.10})$$

where

$h\nu_{10,2j}$ = energy of absorption transition, J;

c = speed of light, ms^{-1} ;

$B_{10,2j}$ = Einstein coefficient of induced absorption, $\text{m}^3 \text{J}^{-1} \text{s}^{-2}$;

g_k = statistical weight of electronic state, k ;

n_k = concentration of electronic state, k , m^{-3} .

The Einstein coefficients are related to each other (38,39) by

$$A_{20,1i} = \left(\frac{8\pi h \nu_{20,1i}^3}{c^3} \right) B_{20,1i} \quad (\text{III.11})$$

where

$B_{20,1i}$ = Einstein coefficient of induced emission, $\text{m}^3 \text{J}^{-1} \text{s}^{-2}$;

n = refractive index of environment (medium), dimensionless.

The Einstein coefficients of induced emission and induced absorption are related to the electric dipole line strength by

$$B_{20,1i} = \left(\frac{2\pi^2}{3\epsilon_0 h^2} \right) \left(\frac{1}{g_2} \right) S_{20,1i} = \left(\frac{2\pi^2}{3\epsilon_0 h^2} \right) \left(\frac{1}{g_2} \right) (R_{21}^{e1})^2 |\langle \theta_{20}(Q) | \theta_{1i}(Q) \rangle|^2 \quad (\text{III.12})$$

$$B_{10,2j} = \left(\frac{2\pi^2}{3\epsilon_0 h^2} \right) \left(\frac{1}{g_1} \right) S_{10,2j} = \left(\frac{2\pi^2}{3\epsilon_0 h^2} \right) \left(\frac{1}{g_1} \right) (R_{21}^{e1})^2 |\langle \theta_{10}(Q) | \theta_{2j}(Q) \rangle|^2 \quad (\text{III.13})$$

where

$S_{20,1i}, S_{10,2j}$ = electric dipole line strength, $\text{C}^2 \text{m}^2$;

ϵ_0 = permittivity of vacuum, $8.854 \times 10^{-12} \text{C}^2 (\text{Nm}^2)^{-1}$;

h = Planck's constant, $6.626 \times 10^{-34} \text{J s}^{-1}$;

$(R_{21}^{e1})^2$ = pure electronic transition moment, $\text{C}^2 \text{m}^2$;

$|\langle \theta(Q) | \theta(Q) \rangle|$ = vibrational overlap integral (Franck-Condon factor)
between vibrational levels in two electronic states

involved in the absorption and luminescence processes (Q is vibrational coordinate); the Born-Oppenheimer approximation is assumed to apply here;

$\theta(Q)$ = vibrational wave function which is a parametric function in Q, the nuclear coordinate, dimensionless.

The concentration ratio of state 2 to state 1, n_2/n_1 , is given by

$$\frac{n_2}{n_1} = \frac{B_{10,2j} \frac{2E(\nu_{10,2j})}{\pi C \delta \nu}}{\sum_i A_{20,1i} + B_{2j,10} \frac{2E(\nu_{10,2j})}{\pi C \delta \nu} + k_{21}} \quad (\text{III.14})$$

for steady state conditions and for the condition of negligible thermal excitation ($k_{12} \approx 0$). In Eq. III.14, $E(\nu_{10,2j})$ is the source irradiance (integrated spectral irradiance) of the exciting line and $\delta \nu$ is the half-width of the absorption band undergoing the transition, e.g., for a gaseous molecule, as OH (12); the absorption bands will be of the order of 0.1 cm^{-1} , whereas for a molecule in the liquid state, all rotational and often even most of the vibrational structure of the electronic band is lost resulting in a broad band, such as $\delta \nu \gtrsim 10 \text{ nm}$. Equation III.14 can be rewritten in terms of the quantum efficiency (see Eq. II.9).

$$\frac{n_2}{n_1} = \frac{B_{10,2j} \frac{2E(\nu_{10,2j})}{\pi C \delta \nu}}{\frac{\sum_i A_{20,1i}}{\gamma_{21}} + B_{2j,10} \frac{2E(\nu_{10,2j})}{\pi C \delta \nu}} \quad (\text{III.15})$$

By utilizing the definitions of the A's and B's (see Eqs. III.11-III.13)

$$\sum_i A_{20,1i} = A_{2j,10} \frac{(\sum_i |\langle \theta_{20}(Q) | \theta_{1i}(Q) \rangle|^2 v_{20,1i}^3)}{|\langle \theta_{2j}(Q) | \theta_{10}(Q) \rangle|^2 v_{2j,10}^3} \quad (III.16)$$

where $A_{2j,10}$, the electronic-vibrational transition probability at the absorption frequency, is

$$A_{2j,10} = \left(\frac{16\pi^3 n^3}{3\epsilon_0 hc^3 g_2} \right) |R_{21}^{el}|^2 v_{2j,10}^3 |\langle \theta_{2j}(Q) | \theta_{10}(Q) \rangle|^2 \quad (III.17)$$

where all terms have been previously defined. If we now use the following substitutions for simplicity

$$V_{20,1i} = |\langle \theta_{20}(Q) | \theta_{1i}(Q) \rangle|^2 = |\langle \theta_{1i}(Q) | \theta_{20}(Q) \rangle|^2$$

$$V_{2j,10} = |\langle \theta_{2j}(Q) | \theta_{10}(Q) \rangle|^2 = |\langle \theta_{10}(Q) | \theta_{2j}(Q) \rangle|^2$$

$$A_{21} = A_{2j,10}$$

$$B_{21} = B_{2j,10}$$

$$B_{12} = B_{10,2j}$$

$$E = E(v_{10,2j})$$

then

$$\frac{n_2}{n_1} = \frac{\frac{2B_{12}V_{2j,10}E}{\pi c A_{21}^{\delta v}} \sum_i V_{20,1i} v_{20,1i}^3}{1 + \frac{2B_{21}V_{2j,10}E}{\pi c A_{21}^{\delta v}} \sum_i V_{20,1i} v_{20,1i}^3} \quad (III.18)$$

Simplifying Eq. III.18 by use of the relationships between B_{12} and B_{21} ($B_{21}g_2 = B_{21}g_1$) and dividing numerator and denominator by $V_{2j,10}$ gives

$$\frac{g_1 n_2}{g_2 n_1} = \frac{\left(\frac{2EY_{21}B_{21}}{\pi c A_{21} \delta \nu} \right) \left(\frac{\nu_{2j,10}^3}{\sum_i V_{20,1i} \nu_{20,1i}^3} \right)}{\frac{1}{V_{2j,10}} + \left(\frac{2EY_{21}B_{21}}{\pi c A_{21} \delta \nu} \right) \left(\frac{\nu_{2j,10}^3}{\sum_i V_{20,1i} \nu_{20,1i}^3} \right)} \quad (\text{III.19})$$

According to Strickler and Berg (39),

$$\frac{\sum_i V_{20,1i} \nu_{20,1i}^3}{\sum_i V_{20,1i}} = \frac{\int F(\nu) d\nu}{\int F(\nu) \nu^{-3} d\nu} = \langle \nu_L^{-3} \rangle_{AV}^{-1} \quad (\text{III.20})$$

where $F(\nu)$ is the luminescence profile function and $\langle \nu_L^{-3} \rangle_{AV}^{-1}$ is the reciprocal of the average value of ν_L^{-3} in the luminescence spectrum.

Because $\sum_i V_{20,1i} = 1$, i.e., orthonormal complete set, Eq. III.19 can be rewritten as

$$\frac{g_1 n_2}{g_2 n_1} = \frac{\left(\frac{2EY_{21}B_{21}}{\pi c A_{21} \delta \nu} \right) \nu_{2j,10}^3 \langle \nu_L^{-3} \rangle_{AV}}{\frac{1}{V_{2j,10}} + \left(\frac{2EY_{21}B_{21}}{\pi c A_{21} \delta \nu} \right) \nu_{2j,10}^3 \langle \nu_L^{-3} \rangle_{AV}} \quad (\text{III.21})$$

If as in atomic fluorescence (4), E_v^* , a modified saturation spectral irradiance, i.e., E_v^* is related to E_v^S , is defined as

$$E_{v12}^* = \frac{c A_{21}}{B_{21} Y_{21}} \quad (\text{III.22a})$$

and if $\xi_{2j,10}$ is defined as

$$\xi_{2j,10} = \nu_{2j,10}^3 \langle \nu_L^{-3} \rangle_{AV} V_{2j,10} \quad (\text{III.22b})$$

then

$$\frac{g_1 n_2}{g_2 n_1} = \frac{\frac{2E}{\pi \delta \nu}}{\frac{E_{v12}^*}{\xi_{2j,10}} + \frac{2E}{\pi \delta \nu}} \quad (\text{III.23})$$

The fluorescence radiance expression (4,40) for a two level system is given by

$$B_F = \left(\frac{\ell}{4\pi}\right) Y_{p21} \left(\frac{2E}{\pi \delta \nu}\right) n_1 \left(\frac{h\nu_{2j,10}}{c}\right) B_{12} \left[1 - \frac{g_1 n_2}{g_2 n_1}\right] \quad (\text{III.24})$$

where ℓ is the fluorescence path length in the direction of the detector. Substituting into Eq. III.24 for the ratio $g_1 n_2 / g_2 n_1$ from Eq. III.23 and for n_1 in terms of n_2 from Eq. III.23 gives

$$B_F = \left(\frac{\ell}{4\pi}\right) Y_{p21} E_{v12}^* \left(\frac{h\nu}{c}\right) \left(\frac{B_{12} g_1 n_2}{g_2 \xi_{2j,10}}\right) \quad (\text{III.25})$$

By evaluation of $\sum_i A_{20,1i}$ (combining Eqs. III.16 and III.20)

$$\sum_i A_{20,1i} = \frac{A_{2j,10}}{\xi_{2j,10}} \quad (\text{III.26})$$

and by substituting for Y_{p21} in terms of Y_{21} (Eq. III.8) and for E_{v12}^* (Eq. III.22a) into Eq. III.25, B_F becomes

$$B_F = \left(\frac{\ell}{4\pi}\right) n_2 \sum_i A_{20,1i} h\nu_{20,1i} \quad (\text{III.27})$$

which is the expected expression based upon previous derivations for atomic fluorescence (4,41). However, it is interesting to stress that B_F is independent of the vibrational overlap integrals.

Evaluating n_2 in terms of n_T , where $n_T = n_1 + n_2 \cong$ total concentration of molecules in all electronic states gives

$$B_F = \left(\frac{\rho}{4\pi}\right) \sum_i A_{20,1i} h\nu_{20,1i} \left(\frac{2E}{\pi\delta\nu}\right) \left\{ \frac{n_T}{\left(1 + \frac{g_1}{g_2}\right) \left(\frac{2E}{\pi\delta\nu}\right) + \frac{g_1}{g_2} \frac{E_{j,10}^*}{\epsilon_{2j,10}}} \right\} \quad (\text{III.28})$$

which has exactly the same form as the 2-level atom fluorescence radiance (1-4).

Steady State Three Level Molecule

Molecules in the condensed phase (solids mainly) as well as some molecules in the gas phase (depending upon pressure) must be treated as at least a 3-level system, e.g., a ground singlet, 1, a first excited singlet, 3, and a first excited triplet, 2. The same approach as in the previous section will be carried out.

Assuming the upper level, 3 (1st excited singlet) is being radiatively excited and assuming the nonradiational excitation rate constants, k_{12} and k_{13} and the radiational rate constant A_{32} are negligibly small (here only the electronic states are listed in the subscript, not the vibrational levels), then the ratio of concentrations for state 3 to state 1, n_3/n_1 , is

$$\frac{n_3}{n_1} = \frac{\frac{2B_{10,3j}E}{\pi c \delta\nu} \left(\sum_i A_{20,1i} + k_{23} + k_{21} \right)}{\left[\frac{2B_{3j,10}E}{\pi c \delta\nu} + \sum_i A_{30,1i} + k_{31} + k_{32} \right] \left[\sum_i A_{20,1i} + k_{23} + k_{21} \right] - k_{23}k_{32}} \quad (\text{III.29})$$

where all terms have the same definitions given previously except the levels involved may differ and $E = E(\nu_{3j,10})$.

The definition of the power, Y_p , and quantum, Y , efficiencies for electronic transitions $3 \rightarrow 1$ according to Lipsett (42) and Förster (43) are

$$Y_{p31} = \frac{\sum_i A_{30,1i} \nu_{30,1i}}{\left[\sum_i A_{30,1i} + k_{31} + k_{32} - \frac{k_{23}k_{32}}{\sum_i A_{20,1i} + k_{21} + k_{23}} \right] \nu_{ex}} \quad (\text{III.30})$$

$$Y_{31} = \frac{\sum_i A_{30,1i}}{\sum_i A_{30,1i} + k_{31} + k_{32} - \frac{k_{23}k_{32}}{\sum_i A_{20,1i} + k_{21} + k_{23}}} \quad (\text{III.31})$$

where ν_{ex} is the excitation frequency with appropriate subscripts. For the $2 \rightarrow 1$ transition excited by radiationless transitions from level 3, the power and quantum efficiencies are given by

$$Y_{p21} = x_{32} Y_{p21} \quad (\text{III.32})$$

$$Y_{21} = x_{32} Y_{21} \quad (\text{III.33})$$

where x_{32} is the crossing fraction (also termed quantum yield of inter-system crossing or triplet yield) and is given by

$$x_{32} = \frac{k_{32}}{\sum_i A_{30,1i} + k_{31} + k_{32} - \frac{k_{23}k_{32}}{\sum_i A_{20,1i} + k_{21} + k_{23}}} \quad (\text{III.34})$$

where y_{p21} is the radiative power efficiency and y_{21} the radiative efficiency, given respectively by

$$y_{p21} = \frac{\sum_i A_{20,1i} \nu_{20,1i}}{\left[\sum_i A_{20,1i} + k_{21} + k_{23} \right] \nu_{ex}} \quad (\text{III.35})$$

and

$$y_{21} = \frac{\sum_i A_{20,1i}}{\sum_i A_{20,1i} + k_{21} + k_{23}} \quad (\text{III.36})$$

for $2 \rightarrow 1$ luminescence excited indirectly. Combining Eqs. III.29 and III.31 gives

$$\frac{n_3}{n_1} = \frac{\frac{2g_3 B_{3j,10} E Y_{31}}{g_1 \pi c \delta \nu \sum_i A_{30,1i}}}{\frac{2B_{3j,10} E Y_{31}}{\pi c \delta \nu \sum_i A_{30,1i}} + 1} \quad (\text{III.37})$$

Substituting for $\sum_i A_{30,1i}$ from Eq. III.16 (replace 2 by 3 in all terms) and making substitutions of $B_{13} = B_{10,3j}$ and $B_{31} = B_{3j,10}$, and $A_{31} = A_{3j,10}$

$$\frac{n_3}{n_1} = \frac{\frac{2g_3 B_{31} Y_{31} E V_{3j,10} \nu_{3j,10}^3}{g_1 \pi c A_{31} \delta \nu \sum_i V_{30,1i} \nu_{30,1i}^3}}{1 + \left(\frac{2B_{31} Y_{31} E V_{3j,10} \nu_{3j,10}^3}{\pi c A_{31} \delta \nu (\sum_i V_{30,1i} \nu_{30,1i}^3)} \right)} \quad (\text{III.38})$$

Using the Strickler and Berg (39) approach (see Eq. III.20) and the definition of $E_{\nu_{13}}^*$ and $\xi_{3j,10}$ as

$$E_{\nu_{13}}^* = \frac{c A_{31}}{B_{31} Y_{31}} \quad (\text{III.39a})$$

$$\xi_{3j,10} = \nu_{3j,10}^3 \langle \nu_L^{-3} \rangle_{AV} V_{3j,10} \quad (\text{III.39b})$$

then n_3/n_1 is given by

$$\frac{n_3}{n_1} = \frac{\left(\frac{g_3}{g_1}\right) \frac{2E}{\pi \delta \nu}}{\frac{2E}{\pi \delta \nu} + \frac{E_{\nu 13}^*}{\xi_{3j,10}}} \quad (\text{III.40})$$

The fluorescence radiance for the $3 \rightarrow 1$ fluorescence transition is given (4,40) by

$$B_F = \left(\frac{\ell}{4\pi}\right) Y_{p_{31}} \left(\frac{2E}{\pi \delta \nu}\right) n_1 \left(\frac{h\nu_{10,3j}}{c}\right) B_{10,3j} \left[1 - \frac{g_1 n_3}{g_3 n_1}\right] \quad (\text{III.41})$$

Substituting for n_1 in terms of n_3 and for n_3/n_1 from Eq. III.40 gives

$$B_F = \left(\frac{\ell}{4\pi}\right) n_3 \sum_i A_{30,1i} h\nu_{30,1i} \quad (\text{III.42})$$

which is identical in form to the expression for the 2-level case (Eq. III.27). Substituting for n_3 in terms of n_T ($n_T \cong n_1 + n_2 + n_3$) can be done using Eq. III.40 for n_3/n_1 and Eq. III.32 below for n_2/n_1

$$\frac{n_2}{n_1} = \left(\frac{k_{32}}{\sum_i A_{20,1i} + k_{21} + k_{23}} \right) \frac{n_3}{n_1} \quad (\text{III.43})$$

and so

$$n_3 = \frac{n_T}{1 + \frac{\frac{2E}{\pi \delta \nu} + \frac{E_{\nu 13}^*}{\xi_{3j,10}}}{\left(\frac{g_3}{g_1}\right) \left(\frac{2E}{\pi \delta \nu}\right)} + \frac{k_{32}}{\sum_i A_{20,1i} + k_{21} + k_{23}}} \quad (\text{III.44})$$

and

$$B_{F_{3 \rightarrow 1}} = \left(\frac{\ell}{4\pi} \right) \sum_i A_{30,1i} h\nu_{30,1i} \cdot \left\{ \frac{n_T}{1 + \frac{\frac{2E}{\pi\delta\nu} + \frac{E_{\nu 13}^*}{\xi_{3j,10}}}{\left(\frac{g_3}{g_1}\right) \left(\frac{2E}{\pi\delta\nu}\right)} + \frac{k_{32}}{\sum_i A_{20,1i} + k_{21} + k_{23}}} \right\} \quad (\text{III.45})$$

where the subscript on B_F indicates the emission process (above) and the absorption process (below).

The radiance for the $2 \rightarrow 1$ phosphorescence transition (assuming conventional $1 \rightarrow 3$ excitation) is given (4,40) by

$$B_{P_{2 \rightarrow 1}} = \left(\frac{\ell}{4\pi} \right) Y_{p_{21}} \left(\frac{h\nu_{10,3j}}{c} \right) B_{10,3j} n_1 \left[1 - \frac{g_1 n_3}{g_3 n_1} \right] \left(\frac{2E}{\pi\delta\nu} \right) \quad (\text{III.46})$$

where $Y_{p_{21}}$ is the quantum efficiency for luminescence from level 2 while exciting level 3. Substituting $Y_{p_{21}}$ (Eq. III.32) and n_1 and n_3/n_1 (Eq. III.40) gives the expected relationship for $1 \rightarrow 3$ excitation

$$B_{P_{2 \rightarrow 1}} = \left(\frac{\ell}{4\pi} \right) n_2 \sum_i A_{20,1i} h\nu_{20,1i} \quad (\text{III.47})$$

and substituting for n_2 in terms of n_T gives

$$B_{P_{2 \rightarrow 1}} = \left(\frac{\ell}{4\pi} \right) \sum_i A_{20,1i} h\nu_{20,1i} \cdot \left\{ \frac{n_T}{1 + \left[\frac{\sum_i A_{20,1i} + k_{21} + k_{23}}{k_{32}} \right] \left[1 + \frac{\frac{2E}{\pi\delta\nu} + \frac{E_{\nu 13}^*}{\xi_{3j,10}}}{\left(\frac{g_3}{g_1}\right) \left(\frac{2E}{\pi\delta\nu}\right)} \right]} \right\} \quad (\text{III.48})$$

The final case of potential interest is radiative excitation of state 2 directly from state 1. In this case, B_p is given by

$$B_{P_{2 \rightarrow 1}} = \left(\frac{\ell}{4\pi}\right) Y_{p_{21}} \left(\frac{h\nu_{10,2j}}{c}\right) B_{10,2j} n_1 \left[1 - \frac{g_1 n_2}{g_2 n_1}\right] \left(\frac{2E}{\pi \delta \nu}\right) \quad (\text{III.49})$$

where $E = E(\nu_{10,2j})$. The ratios n_2/n_1 and n_3/n_1 for this excitation case (2 becomes 3 and 3 becomes 2 in Eq. III.40) are

$$\frac{n_2}{n_1} = \frac{\left(\frac{g_2}{g_1}\right) \frac{2E}{\pi \delta \nu}}{\frac{2E}{\pi \delta \nu} + \frac{E_{\nu_{12}}^*}{\xi_{2j,10}}} \quad (\text{III.50})$$

and

$$\frac{n_3}{n_1} = \left(\frac{k_{23}}{\sum_i A_{30,1i} + k_{31} + k_{32}} \right) \frac{n_2}{n_1} \quad (\text{III.51})$$

Substituting for n_2/n_1 (Eq. III.50), for n_1 (Eq. III.51) and for $Y_{p_{21}}$ (Eq. III.32) gives

$$B_{P_{2 \rightarrow 1}} = \left(\frac{\ell}{4\pi}\right) n_2 \sum_i A_{20,1i} h\nu_{20,1i} \quad (\text{III.52})$$

and substituting for n_2 in terms of n_T ($n_T \cong n_1 + n_2 + n_3$ using Eqs. III.50 and III.51)

$$B_{P_{2 \rightarrow 1}} = \left(\frac{\ell}{4\pi} \right) \sum_i A_{20,1i} \nu_{20,1i} \cdot \left\{ \frac{n_T}{1 + \frac{\frac{2E}{\pi \delta \nu} + \frac{E_{\nu 12}^*}{\xi_{2j,10}}}{\left(\frac{g_2}{g_1} \right) \left(\frac{2E}{\pi \delta \nu} \right)} + \frac{k_{23}}{\sum_i A_{30,1i} + k_{31} + k_{32}}} \right\} \quad (\text{III.53})$$

A rather trivial case involves excitation of state 2 from state 1, intersystem crossing 2 to 3, and fluorescence from 3 to 1. This case is a form of fluorescence. The radiance expression for B_F is

$$B_{F_{3 \rightarrow 1}} = \left(\frac{\ell}{4\pi} \right) \sum_i A_{30,1i} h\nu_{30,1i} \cdot \left\{ \frac{n_T}{\left(1 + \frac{\sum_i A_{30,1i} + k_{31} + k_{32}}{k_{23}} \right) \left(1 + \frac{\frac{2E}{\pi \delta \nu} + \frac{E_{\nu 12}^*}{\xi_{2j,10}}}{\left(\frac{g_2}{g_1} \right) \left(\frac{2E}{\pi \delta \nu} \right)} \right)} \right\} \quad (\text{III.54})$$

A nontrivial but analytically unimportant case is E-type delayed fluorescence, DF, where excitation of 3 from 1 occurs followed by intersystem crossing 3 to 2, reverse intersystem crossing 2 to 3, and, finally, delayed fluorescence from 3 to 1. The quantum efficiency and power efficiency for this process is

$$Y_{p_{31}} = x_{32} \kappa_{23} y_{p_{31}} \quad (\text{III.55})$$

where x_{32} is given by Eq. III.34, and κ_{23} and $y_{p_{31}}$ are given (42) by

$$\kappa_{32} = \frac{k_{23}}{\sum_i A_{20,1i} + k_{21} + k_{23}} \quad (\text{III.56})$$

and

$$y_{p_{31}} = \frac{\sum_i A_{30,1i} \nu_{30,1i}}{(\sum_i A_{30,1i} + k_{31} + k_{32}) \nu_{3j,10}} \quad (\text{III.57})$$

Substituting for $y_{p_{31}}$ into Eq. III.41 and for n_1 and n_3/n_1 as previously for the case of $1 \rightarrow 3$ excitation and $3 \rightarrow 1$ fluorescence, gives

$$B_{DF} = \left(\frac{\ell}{4\pi} \right) \left\{ \frac{k_{23} k_{32}}{[\sum_i A_{30,1i} + k_{31} + k_{32}][\sum_i A_{20,1i} + k_{21} + k_{23}]} \right\} \sum_i A_{30,1i} h\nu_{30,1i} \cdot$$

$$\left\{ \frac{\frac{g_3}{g_1} \frac{2E}{\pi \delta \nu} n_T}{\left[1 + \frac{g_3}{g_1} + \frac{g_3}{g_1} \left(\frac{k_{32}}{\sum_i A_{20,1i} + k_{21} + k_{23}} \right) \right] \left(\frac{2E}{\pi \delta \nu} \right) + \frac{E_{\nu_{13}}^*}{\xi_{3j,10}}} \right\} \quad (\text{III.58})$$

where $E = E(\nu_{10,3j})$.

Limiting Cases of Steady State Excitation

In all cases given, high implies that $E(\nu) \gg E_{\nu}^* \delta \nu \pi / 2 \xi$ and low implies that $E(\nu) \ll E_{\nu}^* \delta \nu \pi / 2 \xi$. Limiting expressions are given for cases of analytical utility.

For a two level molecule, if the source irradiance is low, then B_F (see Eq. III.28) becomes

$$B_{F_{2 \rightarrow 1}}^{(lo)} = \left(\frac{\ell}{4\pi} \right) \sum_i A_{20,1i} h\nu_{20,1i} \left(\frac{g_2}{g_1} \right) n_T \left\{ \frac{2E(\nu_{10,2j}) \xi_{2j,10}}{E_{\nu_{12}}^* \pi \delta \nu} \right\} \quad (\text{III.59})$$

and if the irradiance is high, then B_F (see Eq. III.28) becomes

$$B_{F_{2 \rightarrow 1}}^{(hi)} = \left(\frac{\ell}{4\pi} \right) \sum_i A_{20,1i} h\nu_{20,1i} \left(\frac{n_T}{1 + \frac{g_1}{g_2}} \right) \quad (\text{III.60})$$

For a three level molecule assuming $1 \rightarrow 3$ excitation and $3 \rightarrow 1$ fluorescence, if the source irradiance is low, then B_F (see Eq. III.45) becomes

$$B_{F(10)} = \left(\frac{\ell}{4\pi}\right) \sum_i A_{30,1i} h\nu_{30,1i} \left(\frac{g_3}{g_1}\right) n_T \left(\frac{2E(\nu_{10,3j}) \epsilon_{3j,10}}{E_{\nu_{13}}^* \pi \delta \nu} \right) \quad (\text{III.61})$$

and if the source irradiance is high (see Eq. III.45), B_F becomes

$$B_{F(hi)} = \left(\frac{\ell}{4\pi}\right) \sum_i A_{30,1i} h\nu_{30,1i} \left(\frac{n_T}{1 + \frac{g_1}{g_3} + \frac{k_{32}}{\sum_i A_{20,1i} + k_{21} + k_{23}}} \right) \quad (\text{III.62})$$

For a three level molecule, assuming $1 \rightarrow 3$ excitation and $2 \rightarrow 1$ phosphorescence, if the source irradiance is low, then B_P (see Eq. III.48) becomes

$$B_{P(10)} = \left(\frac{\ell}{4\pi}\right) \sum_i A_{20,1i} h\nu_{20,1i} \left(\frac{g_3}{g_1}\right) \left(\frac{n_T k_{32}}{\sum_i A_{20,1i} + k_{21} + k_{23}} \right) \left(\frac{2E(\nu_{10,3j}) \epsilon_{3j,10}}{E_{\nu_{13}}^* \pi \delta \nu} \right) \quad (\text{III.63})$$

and if the source irradiance is high (see Eq. III.48), the B_P becomes

$$B_{P(hi)} = \left(\frac{\ell}{4\pi}\right) \sum_i A_{20,1i} h\nu_{20,1i} \left(\frac{n_T k_{32}}{\sum_i A_{20,1i} + k_{21} + k_{23}} \right) \left(\frac{1}{1 + \frac{g_1}{g_3} + \frac{k_{32}}{\sum_i A_{20,1i} + k_{21} + k_{23}}} \right) \quad (\text{III.64})$$

For a three level molecule assuming $1 \rightarrow 2$ excitation and $2 \rightarrow 1$ phosphorescence, if the source irradiance is low, then B_P (see Eq. III.53) becomes

$$B_p(10) = \left(\frac{\ell}{4\pi}\right) \sum_i A_{20,1i} h\nu_{20,1i} \left(\frac{g_2}{g_1}\right) n_T \left(\frac{2E(\nu_{10,2j}) \epsilon_{2j,10}}{E_{\nu_{12}}^* \pi \delta \nu} \right) \quad (III.65)$$

and if the source irradiance is high, then B_p (see Eq. III.53) becomes

$$B_p(hi) = \left(\frac{\ell}{4\pi}\right) \sum_i A_{20,1i} h\nu_{20,1i} \left(\frac{n_T}{1 + \frac{g_1}{g_2} + \frac{k_{23}}{\sum_i A_{30,1i} + k_{31} + k_{32}}} \right) \quad (III.66)$$

Steady State Saturation Irradiance

The saturation irradiance is that source irradiance resulting in a luminescence radiance equal to 50% of the maximum possible value. For a 2-level molecule, it is given by

$$E^S(\nu_{10,2j}) = \left(\frac{g_1}{g_1 + g_2} \right) \left(\frac{E_{\nu_{12}}^* \pi \delta \nu}{2\nu_{2j,10}^3 \langle \nu_L^{-3} \rangle_{AV} \nu_{2j,10}} \right) \quad (III.67)$$

For a 3-level molecule (1 → 3 excitation), it is given by

$$E^S(\nu_{10,3j}) = \frac{\left(\frac{g_1}{g_3} \right) \left(\frac{E_{\nu_{13}}^*}{\nu_{3j,10}} \right) \left(\frac{\pi \delta \nu}{2\nu_{3j,10}^3 \langle \nu_L^{-3} \rangle_{AV}} \right)}{1 + \frac{g_1}{g_3} + \frac{k_{32}}{\sum_i A_{20,1i} + k_{21} + k_{23}}} \quad (III.68)$$

For a 3-level molecule (1 → 2 excitation), it is given by

$$E^S(\nu_{10,2j}) = \frac{\left(\frac{g_1}{g_2} \right) \left(\frac{E_{\nu_{12}}^*}{\nu_{2j,10}} \right) \left(\frac{\pi \delta \nu}{2\nu_{2j,10}^3 \langle \nu_L^{-3} \rangle_{AV}} \right)}{1 + \frac{g_1}{g_2} + \frac{k_{23}}{\sum_i A_{30,1i} + k_{31} + k_{32}}} \quad (III.69)$$

However, Eq. III.69 can be simplified further since the final term in the denominator will generally be negligible and so reverts to the 2 level expression in Eq. III.67.

For a typical organic molecule at 298°C, $E_{v_{12}}^* \sim 1.8 \times 10^{-6} \text{ W cm}^{-2} \text{ Hz}^{-1}$ ($6 \times 10^6 \text{ W cm}^{-2} \text{ nm}^{-1}$) (assuming $Y_{21} = 1$ and $\lambda_{21} = 300 \text{ nm}$) or $E_{v_{12}}^* \sim 1.8 \times 10^{-5} \text{ W cm}^{-2} \text{ Hz}^{-1}$ ($6 \times 10^7 \text{ W cm}^{-2} \text{ nm}^{-1}$) (assuming $Y_{21} = 0.1$ and $\lambda_{21} = 300 \text{ nm}$). Assuming $v_{2j,10}^3 < v_L^{-3} > A v_{2j,10}^3 \sim 1$, $g_1 = g_2 = 1$ and $\delta v \cong 10^{10} \text{ Hz}$ (gaseous molecule) or $\delta v \cong 10^{14} \text{ Hz}$ (molecule in liquid solution), then $E^S(v_{10,2j}) \sim 10 \text{ kW/cm}^2$ for the gaseous molecule and $E^S(v_{10,2j}) \sim 10^5 \text{ kW/cm}^2$ for the molecule in the liquid state assuming $Y_{21} = 1$ and $\lambda_{21} = 300 \text{ nm}$. For a 3-level molecule, $E^S(v_{10,3j})$ will be smaller than $E^S(v_{10,2j})$ by a factor $k_{32} / \sum_i A_{20,1i} + k_{21} + k_{23}$ which will be $\sim 10^5 - 10^7$ for most molecules (44,45).

Nonsteady State Two Level Molecule

If the duration of an excitation source pulse is comparable to or shorter than the excited state lifetime, then the steady state approach does not hold. The nonsteady state treatment of two level atoms has been given by de Olivares (5). It is only necessary to slightly modify the expressions she has given for atoms, so no detailed solution will be given.

From Eq. II.28, it is possible to define a steady state concentration of n_2 , n_{2ss} . This is given by

$$n_{2ss} = \frac{n_T}{\left(1 + \frac{g_1}{g_2}\right) c \rho_{10,2j} + \frac{g_1}{g_2} \frac{E_{v_{12}}^*}{\xi_{2j,10}}} \quad (\text{III.70})$$

where the spectral radiant energy density, ρ , has been used. For a rectangular excitation pulse, $\rho(t) = \rho_0$ for $0 \leq t \leq t_0$ and $\rho(t) = 0$ for $t > t_0$ where t_0 is the pulse width, s. The concentration of n_2 as a function of time, $n_2(t)$, for $0 \leq t \leq t_0$ is

$$n_2(t) = n_{2ss}[1 - \exp(-(a + b\rho_0)t)] \quad (\text{III.71})$$

where

$$a = \frac{A_{21}}{\xi_{2j,10}} + k_{21} \quad (\text{III.72})$$

and

$$b = B_{12} + B_{21} \quad (\text{III.73})$$

For low irradiance cases, the growth of n_2 population is controlled by the luminescence lifetime, a^{-1} . As the irradiance exceeds the saturation irradiance, the growth of n_2 population is more rapid. If the pulse width is long compared to the lifetime, the steady state concentration of n_2 is reached.

Nonsteady State Three Level Molecule

The solutions for a three level atom under nonsteady state conditions have been given assuming thermal equilibrium between the two upper levels (5). This situation will not apply to molecules, as the relative populations to the two upper levels is also dependent on the intersystem crossing rate constant. Collisions are not required for population of the triplet from the singlet. Starting from the rate equations assuming excitation of level 3 from level 1,

$$\frac{dn_3}{dt} = -(B_{31}\rho_{13}(t) + \frac{A_{31}}{\xi_{3j,10}} + k_{31} + k_{32})n_3 + (B_{13}\rho_{13}(t) + k_{12})n_1 + k_{23}n_2 \quad (\text{III.74})$$

and

$$\frac{dn_2}{dt} = -(\sum_i A_{20,1i} + k_{21} + k_{23})n_2 + k_{32}n_3 + k_{12}n_1 \quad (\text{III.75})$$

It will be assumed that thermal population of levels 2 and 3 is negligible at room temperature or lower, making $k_{12} = k_{13} = 0$. It will also be assumed that intersystem crossing from level 2 to level 3 is negligible, making $k_{23} = 0$. The following terms are defined to simplify Eqs. III.74 and III.75.

$$a_3 = \frac{A_{31}}{\xi_{3j,10}} + k_{31} + k_{32} \quad (\text{III.76})$$

$$a_2 = \sum_i A_{20,1i} + k_{21} \quad (\text{III.77})$$

$$b_3 = B_{31}\rho_{13}(t) + B_{13}\rho_{13}(t) \quad (\text{III.78})$$

$$B = B_{13}\rho_{13}(t) \quad (\text{III.79})$$

Using D to denote the differential operator, Eqs. III.74 and III.75 may be written as III.80 and III.81, respectively, after substituting

$$n_1 = n_T - n_2 - n_3.$$

$$(D + b_3 + a_3)n_3 + Bn_2 = Bn_T \quad (\text{III.80})$$

$$-n_3 + \frac{D + a_2}{k_{32}} n_2 = 0 \quad (\text{III.81})$$

Eliminating the n_3 term from Eq. III.80 by multiplying $(D + b_3 + a_3)$ times Eq. III.81 and adding the result to Eq. III.80 gives

$$(D + b_3 + a_3)(D + a_2)n_2 + Bk_{32}n_2 = Bk_{32} \quad (\text{III.82})$$

The solution to the homogeneous differential equation of the form of Eq. III.82 for $\rho_{13} = \rho_0$ for $0 \leq t \leq t_0$ is

$$n_2(t) = C_1 \exp(-\alpha_2 t) + C_2 \exp(-\alpha_3 t) + C_0 \quad (\text{III.83})$$

where

$$\alpha_2 = \frac{X - \sqrt{X^2 - 4Y}}{2} \quad (\text{III.84})$$

$$\alpha_3 = \frac{X + \sqrt{X^2 - 4Y}}{2} \quad (\text{III.85})$$

and

$$X = b_3 + a_3 + a_2 \quad (\text{III.86})$$

$$Y = (b_3 + a_3)a_2 + Bk_{32} \quad (\text{III.87})$$

The particular solution of the nonhomogeneous equation gives C_0 as

$$C_0 = \left(\frac{k_{32}}{a_2}\right) \frac{n_T}{\frac{k_{32}}{a_2} + \frac{a_3 + b_3}{B}} \quad (\text{III.88})$$

Using the solution for $n_2(t)$, the solution for $n_3(t)$ may be found using Eq. III.81. The arbitrary constants C_1 and C_2 are evaluated from the boundary conditions $n_2(0) = 0$ and $n_3(0) = 0$. This gives the final expressions for $n_2(t)$ and $n_3(t)$ as

$$n_2(t) = n_{2ss} \left[\frac{-\alpha_3}{\sqrt{X^2 - 4Y}} \exp(-\alpha_2 t) + \frac{\alpha_2}{\sqrt{X^2 - 4Y}} \exp(-\alpha_3 t) + 1 \right] \quad (\text{III.89})$$

$$n_3(t) = n_{3ss} \left[\frac{\alpha_3(\alpha_2 - a_2)}{a_2 \sqrt{\chi^2 - 4\gamma}} \exp(-\alpha_2 t) + \frac{\alpha_2(a_2 - \alpha_3)}{a_2 \sqrt{\chi^2 - 4\gamma}} \exp(-\alpha_3 t) + 1 \right] \quad (\text{III.90})$$

where n_{3ss} is given by Eq. III.44 and n_{2ss} is given by

$$n_{2ss} = \frac{k_{32} n_{3ss}}{\sum_i A_{20,1i} + k_{21}} \quad (\text{III.91})$$

At low source irradiance, $\alpha_2 \approx a_2$ and $\alpha_3 \approx a_3$, where a_2 is the reciprocal of the level 2 lifetime (phosphorescence) and a_3 is the reciprocal of the level 3 lifetime (fluorescence) which is the conventional low irradiance case (40).

In order to better understand the expressions for $n_2(t)$ and $n_3(t)$, calculations using literature values (44-46) for transition probabilities and rate constants were performed and plotted for three limiting cases. Benzophenone represents the case of a molecule with a poor fluorescence quantum efficiency ($\sim 10^{-4}$) and a large phosphorescence quantum efficiency (~ 0.9). Fluorene represents the case of a molecule with a moderate fluorescence quantum efficiency (~ 0.45) and a moderate phosphorescence quantum efficiency (~ 0.36). Rhodamine 6G represents the case of a high fluorescence quantum efficiency (~ 1) and a small phosphorescence quantum efficiency ($\sim 10^{-3}$). Results of calculations of $\log(n_2/n_T)$ and $\log(n_3/n_T)$ versus $\log(t)$ are plotted for benzophenone, fluorene, and rhodamine 6G and shown in Figures 4, 5, and 6, respectively. In all cases, the value of n_2/n_T approaches the steady state value of n_2/n_T more slowly after n_3/n_T reaches its steady state value. As the source irradiance increases above the steady state saturation irradiance, the time required to attain steady state decreases. If the source irradiance

is less than or equal to the steady state saturation irradiance, the value of n_3/n_T increases until it reaches a value predicted by the 3-level steady state model. If the source irradiance exceeds the steady state saturation irradiance, the value of n_3/n_T will also exceed the 3-level steady state saturation value of n_3/n_T until n_2/n_T saturates. Until the concentration of level 2 approaches steady state, levels 1 and 3 are acting in a fashion similar to the 2-level model. The 2-level model predicts a saturation irradiance approximately 10^5 times higher than the 3-level model for rhodamine 6G, and it is observed in Figure 6 that at 10^6 E^S , the concentration of level 3 is close to saturation. For benzophenone and fluorene, the 2-level saturation irradiance is greater than 10^7 times the 3-level saturation irradiance, so no saturation of level 3 is observed. It should also be noted that for the pulse widths of available lasers ($\sim 1 \mu\text{s}$ for flashlamp pumped dye lasers and $\sim 10 \text{ ns}$ for nitrogen laser systems), it is not possible to saturate level 2 (triplet) of most molecules in a single pulse without focusing to a very small area. For lifetimes longer than the time between pulses, the effect of short pulse width is partially offset because the triplet population does not decay to zero between pulses. This will decrease the required irradiance by approximately the factor $1 - \exp(-1/f\tau_p)$, where f is the source repetition rate and τ_p is the triplet lifetime (see Table VI).

Returning to the terms in Eqs. III.89 and III.90, the coefficients of the exponential terms may be discussed. The factor $-\alpha_3/\sqrt{x^2 - 4Y}$ in Eq. III.89 is approximately -1 and the factor $\alpha_2/\sqrt{x^2 - 4Y}$ is approximately the ratio of the fluorescence rise time to the phosphorescence rise time. As the source irradiance increases above the

Figure 4. Temporal Behavior of Levels 2 and 3 for Benzophenone

Values of E increase in same manner for n_3/n_T as given for n_2/n_T . Values used in calculations are

$$\begin{aligned} A_{31} &= 1.0 \times 10^6 \text{ s}^{-1}; \\ k_{31} &= 1.0 \times 10^7 \text{ s}^{-1}; \\ k_{32} &= 1.0 \times 10^{10} \text{ s}^{-1}; \\ A_{21} &= 1.8 \times 10^2 \text{ s}^{-1}; \\ k_{21} &= 1.8 \times 10^1 \text{ s}^{-1}; \\ \xi_{3j}, I_0 &= 1.0 \times 10^{-3}; \\ \lambda &= 337.1 \text{ nm}; \\ \delta\nu_{\text{abs}} &= 2.6 \times 10^{13} \text{ Hz}; \\ E_s &= 6.8 \times 10^8 \text{ W m}^{-2} \end{aligned}$$

Values for A_{31} , k_{31} , k_{32} , A_{21} , and k_{21} taken from Turro (45).

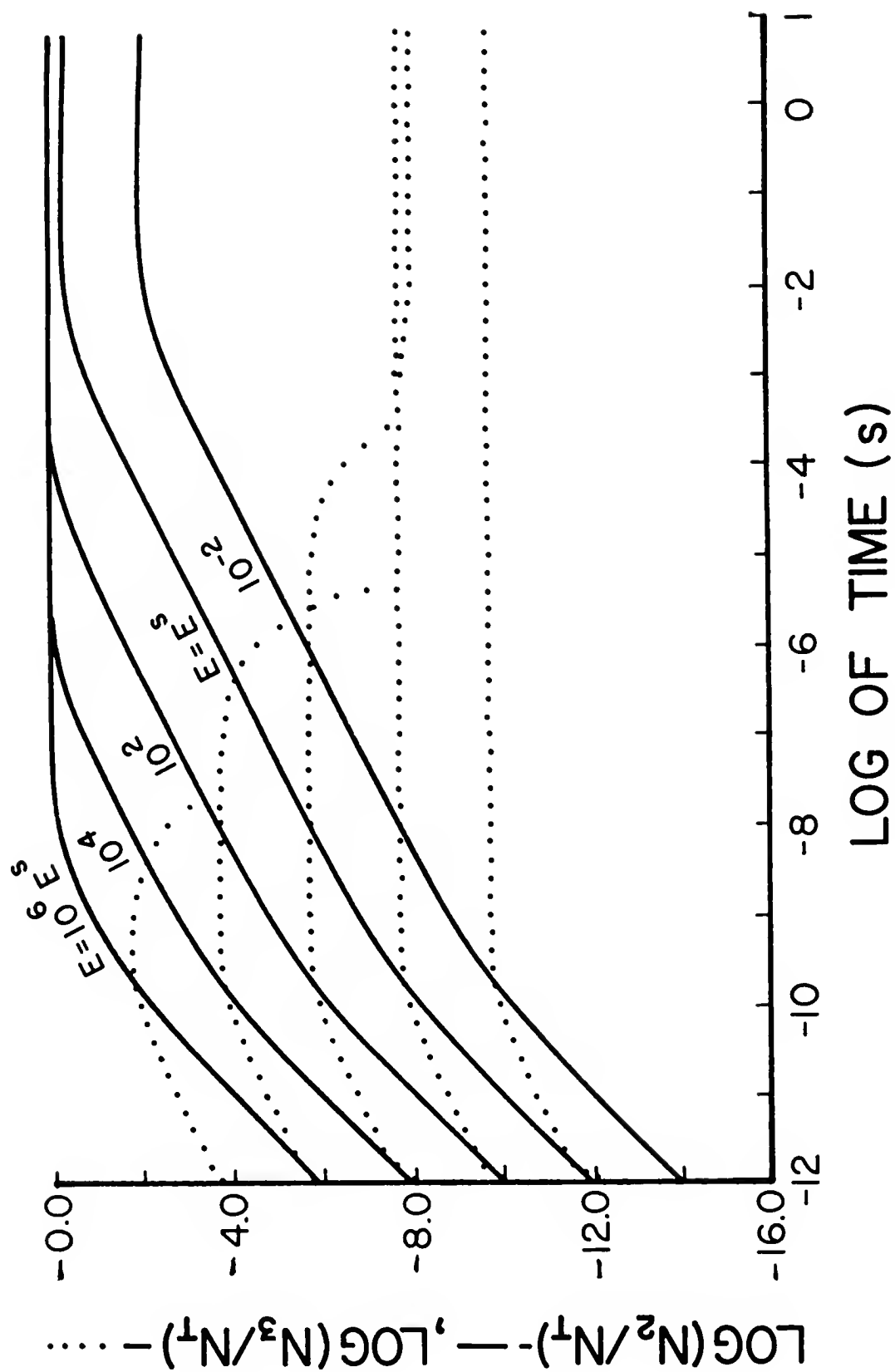


Figure 5. Temporal Behavior of Levels 2 and 3 for Fluorene

Values of E increase in same manner for n_3/n_T as given for n_2/n_T . Values used in calculations are

$$\begin{aligned} A_{31} &= 5.4 \times 10^7 \text{ s}^{-1}; \\ k_{31} &= 2.2 \times 10^7 \text{ s}^{-1}; \\ k_{32} &= 4.5 \times 10^7 \text{ s}^{-1}; \\ A_{21} &= 2.0 \times 10^{-1} \text{ s}^{-1}; \\ k_{21} &= 4.0 \times 10^{-3} \text{ s}^{-1}; \\ \epsilon_{3j}, I_0 &= 1.0 \times 10^{-1}; \\ \lambda &= 250 \text{ nm}; \\ \delta \nu_{\text{abs}} &= 2.6 \times 10^{13} \text{ Hz}; \\ E^s &= 8.6 \times 10^2 \text{ W m}^{-2} \end{aligned}$$

Values for A_{31} , k_{31} , k_{32} , A_{21} , and k_{21} taken from Becker (44).

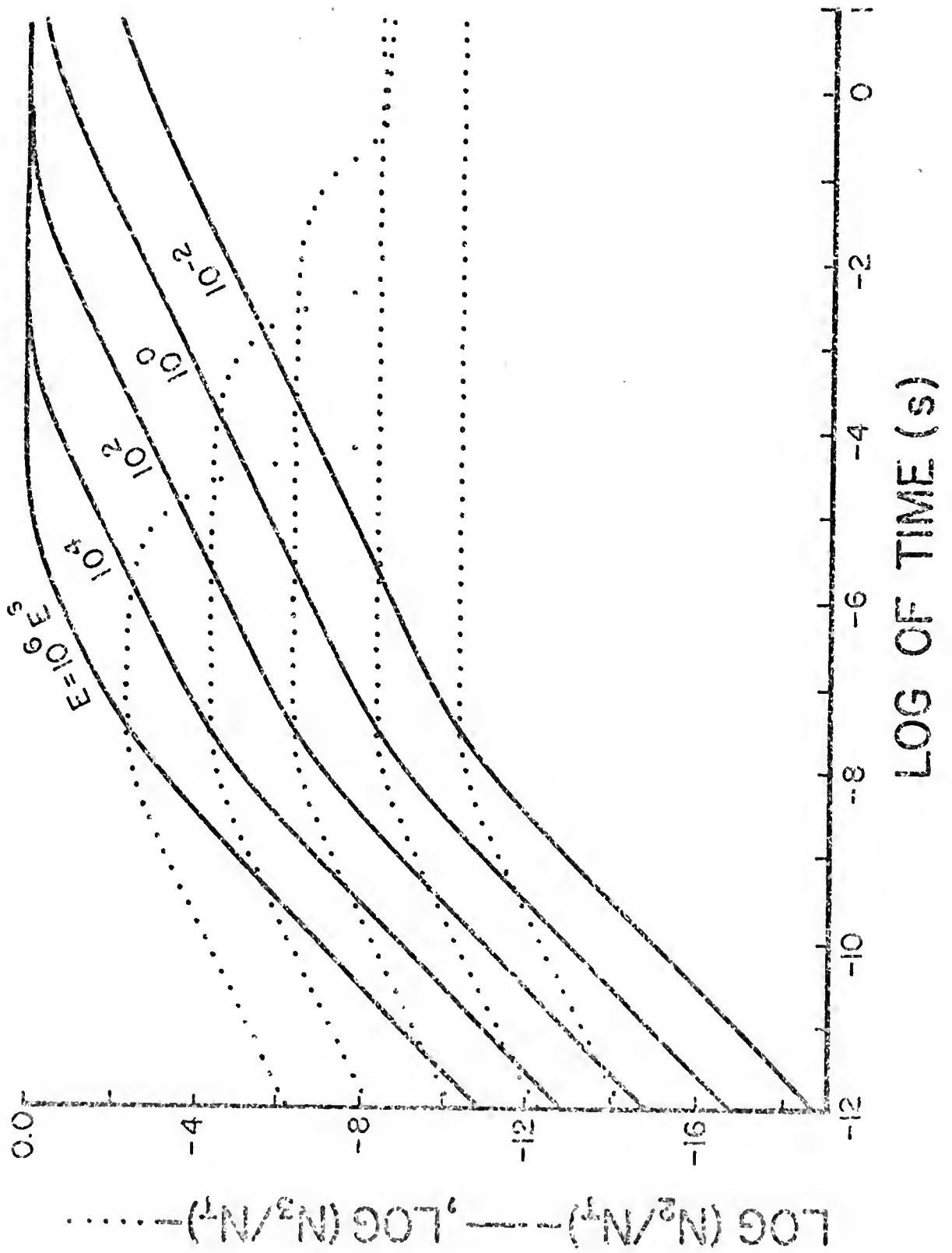
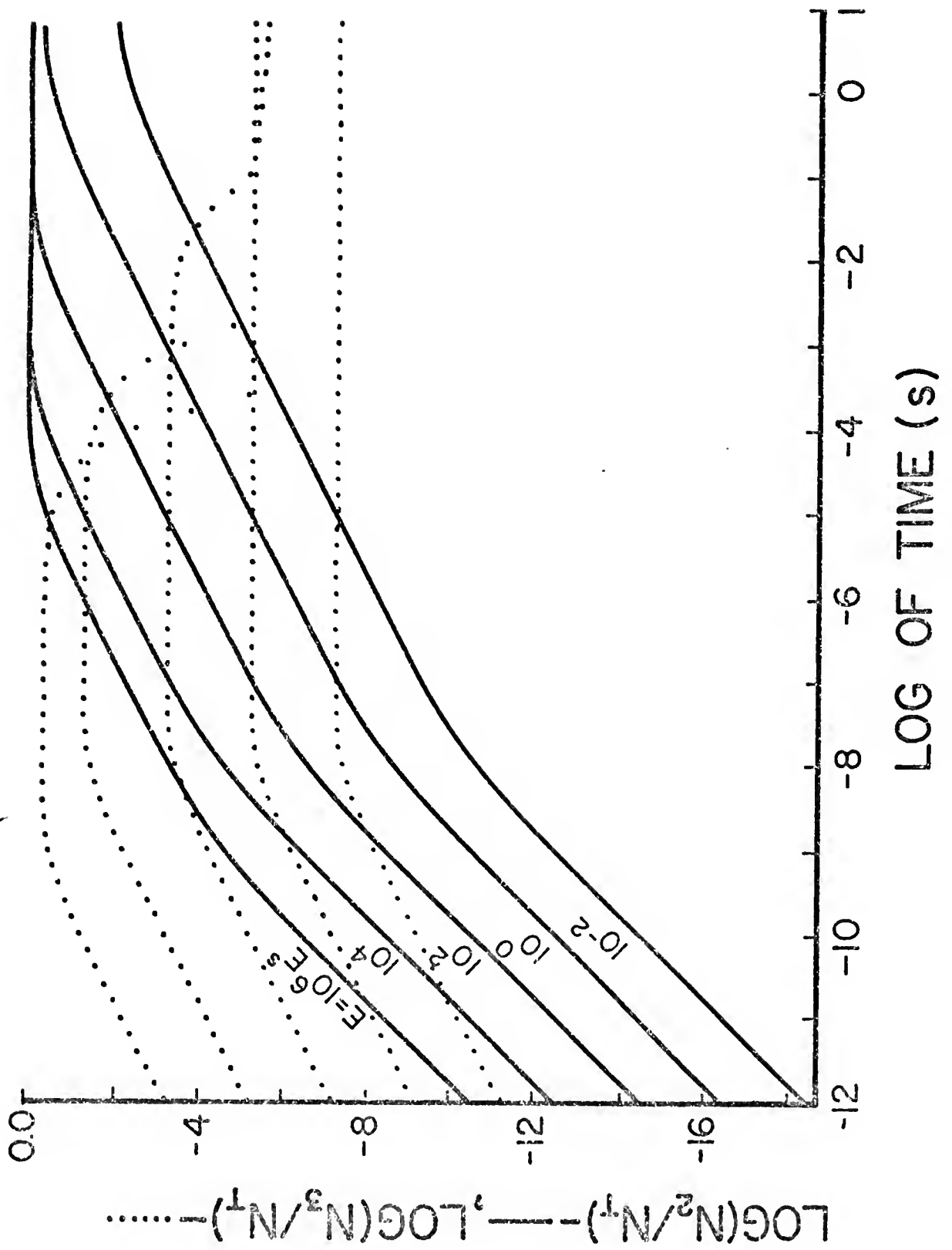


Figure 6. Temporal Behavior of Levels 2 and 3 for Rhodamine 6G

Values of E increase in same manner for n_3/n_T as given for n_2/n_T . Values used in calculations are

$$\begin{aligned} A_{31} &= 1.2 \times 10^8 \text{ s}^{-1}; \\ k_{31} &= 1.0 \times 10^5 \text{ s}^{-1}; \\ k_{32} &= 1.1 \times 10^5 \text{ s}^{-1}; \\ A_{21} &= 5.0 \times 10^{-1} \text{ s}^{-1}; \\ k_{21} &= 8.0 \times 10^{-2} \text{ s}^{-1}; \\ \xi_{3j,10} &= 5.0 \times 10^{-2}; \\ \lambda &= 514 \text{ nm}; \\ \delta v_{\text{abs}} &= 2.6 \times 10^{13}; \\ E_S &= 1.0 \times 10^5 \text{ W m}^{-2} \end{aligned}$$

Values for A_{31} , k_{31} , k_{32} , A_{21} , and k_{21} taken from reference (46).



saturation irradiance, phosphorescence rise time decreases. When the n_3 concentration reaches steady state, the rise time ratio term contribution approaches zero as it is multiplied by $\exp(-\alpha_3 t)$. The terms $\alpha_3(\alpha_2 - a_2)/(a_2\sqrt{x^2 - 4Y})$ and $\alpha_2(a_2 - \alpha_3)/(a_2\sqrt{x^2 - 4Y})$ in Eq. III.90 are close to the same value and opposite in sign; this value is the ratio of the excitation irradiance to the steady state saturation irradiance, E/E^S . As time increases, the term $\exp(-\alpha_3 t)$ decreases the absolute magnitude of the negative term and the concentration of n_3 increases to the value allowed by the positive coefficient of $\exp(-\alpha_2 t)$. As $\exp(-\alpha_2 t)$ decreases (time approaching the lifetime of level 2), the value decreases, and the steady state concentration of level 3 is reached.

Thus far, only the relative populations of the levels have been discussed. The expression for the luminescence radiance may be obtained by substituting Eq. III.89 for n_2 in Eq. III.47 and substituting Eq. III.90 for n_3 in Eq. III.43.

Conclusions

The major conclusions which can be made from the previous expressions are

- (i) the radiance expressions for molecular fluorescence are similar to those for atomic fluorescence (2-4), and reduce to the case of atoms if the term ξ is equal to unity;
- (ii) for low source irradiances, the luminescence radiance depends directly upon the source irradiance and the quantum efficiency;

- (iii) for high source irradiances, the luminescence radiance is independent of the source irradiance and the quantum efficiency;
- (iv) for all cases, the fluorescence radiance depends directly upon the total concentration of analyte, n_T ;
- (v) for all cases, the fluorescence radiance depends directly upon the transition (emission) probability for the measured process;
- (vi) for the 2-level case under saturation conditions, the total concentration, n_T , can be determined by absolute measurement of the steady state B_F -value, by knowledge of $A_{20,1i}$, g_1 , g_2 , and by measurement of the cell path length in the direction of the detector;
- (vii) the product $v^3_{<v_L^{-3}>_{AV}}$ term, occurring implicitly in the factor in all radiance expressions will be not greatly different from unity;
- (viii) the V-term occurring implicitly in the ξ -factor in all general radiance expressions, accounts for the overlap of vibrational levels during the excitation transitions as well as for the fractional portion of the electronic absorption band being excited, e.g., with a gaseous molecule, one could excite only one of the vibrational levels of the excited electronic state and so only a fraction of the absorption band is excited (actually this factor could be separated out of V and designated $\Delta f/f$ where f is the oscillator strength of electronic transition and Δf is the oscillator strength portion attributed to the excitation transition);

- (ix) the saturation irradiance, E^S , for a 3-level molecule at room temperature is 10^5 to 10^7 less than for a 2-level atom or molecule at any temperature or for a 3-level atom or molecule at high, e.g., flame, temperatures; because of the greater half-widths of molecules, saturation can be achieved either by a high spectral irradiance over a narrow line width or a low spectral irradiance over the broad absorption line width assuming the same effective irradiance (within the absorption band) reaches the molecule of interest, i.e., for narrow source line excitation, E_v of the laser source must exceed $2E^S/\pi\delta\nu_{\text{laser}}$ and for broad band excitation solutions, the requirement for saturation is that E_v of the laser source must exceed E_v^S , the saturation spectral irradiance equal to $2E^S/\pi\delta\nu_{\text{abs}}$;
- (x) assuming saturation is reached, direct excitation of the triplet state is nearly as efficient as conventional excitation of the first excited singlet state with intersystem crossing to the first triplet state; therefore, visible cw Ar ion dye lasers, assuming they can be focused down to $\sim 10 \mu\text{m}$ to achieve $\sim \text{MW}/\text{cm}^2$, can be used to excite many molecules with no need for doubling; if $\sim \text{MW}/\text{cm}^2$ can not be achieved and if the phosphorescence quantum efficiency is considerably less than unity, then saturation of the triplet level (essentially a 2-level case) by direct excitation is not possible;
- (xi) if the source irradiance exceeds the saturation irradiance, the steady state condition is reached in a shorter time;
- (xii) the steady state concentration of n_3 (singlet) may be exceeded under pulsed excitation conditions. The optimum measurement

system for fluorescence is a pulsed laser where the high peak power may be utilized to increase the fluorescence signal;

(xiii) due to the relatively long time required to reach steady state in level 2 (triplet), saturation of the triplet level using pulsed lasers will not be possible without focusing the laser to small areas to increase the irradiance to a level of $(5\tau_p/t_o)E^S$ where τ_p is the phosphorescence lifetime, t_o is the pulse width, and E^S is the saturation irradiance; this term is obtained from $1 - \exp(-t_o/\tau_p) = t_o/\tau_p$ for $t_o/\tau_p \ll 1$ and the factor of 5 from the fact approximately five lifetimes (rise-times) are required to reach steady state.

CHAPTER IV

PULSED LASER TIME RESOLVED PHOSPHORIMETRY

Introduction

Time resolved phosphorimetry was first demonstrated as a means of chemical analysis by Keirs et al. (47). They resolved a mixture of acetophenone ($\tau_p = 0.008$ s) and benzophenone ($\tau_p = 0.006$ s) at concentrations in the range of 10^{-3} to 10^{-6} M. O'Haver and Winefordner (48) discussed the influence of phosphoroscope design on detected phosphorescence signals. St. John and Winefordner (49) used a rotating can phosphoroscope system to determine simultaneously two component mixtures. O'Haver and Winefordner (50) later extended the phosphoroscope equations to apply to pulsed light sources and pulsed photomultiplier tubes. The expression for the duty factor (50) applies to a d.c. measurement system. The expression for the duty factor using a gated detector (boxcar integrator) is given in Table VI.

Winefordner (51) has suggested that the independent variability of gate time, t_g , delay time, t_d , and repetition rate, f , of a pulsed source-gated detector along with the spectral shift toward the ultraviolet (52) when using pulsed xenon flashlamps should make such a system optimal for phosphorescence spectrometry.

Fisher and Winefordner (53) constructed a pulsed source time resolved phosphorimeter and demonstrated the analysis of mixtures via time resolution. This system was modified to use a higher power xenon

flashlamp with which O'Donnell et al. (54) time resolved mixtures of halogenated biphenyls and Harbaugh et al. (55) measured phosphorescence lifetimes and quantitated drug mixtures (56). Strambini and Galley (57) have described a similar instrument for phosphorescence lifetime measurements.

The emphasis in pulsed source time resolved phosphorimetry has been on selectivity rather than sensitivity or precision. Johnson, Plankey, and Winefordner (58) compared pulsed versus continuous wave xenon lamps in atomic fluorescence flame spectrometry and found the continuous wave xenon lamp to give 10-fold better detection limits. The pulsed xenon lamp had been predicted to give better detection limits (15). The continuous wave source had an 85-fold larger solid angle. The linear flashlamp used was 2 in long, making it difficult to transfer the radiant flux to a small area. This is a critical problem in phosphorimetry because the sample height is less than 1 cm. Johnson et al. (59) attempted to overcome this problem by pulsing a 300 W Eimac lamp (Eimac, Division of Varian, San Carlos, Calif. 94070). The improvement in S/N failed to materialize due to instability of the pulsed lamp and due to the high d.c. current required to maintain the discharge between pulses, which reduced the fluorescence modulation depth. In phosphorimetry, such a source would give extremely high stray light levels caused by the cylindrical sample cells. A point source flashlamp is now available (Model 722, Xenon Corp., Medford, Mass. 02155) and would appear to offer the best compromise as a pulsed continuum source for phosphorimetry. The point source should allow an increase in the useable radiant flux transferred to the sample.

A second major consideration to signal levels when using pulsed sources is the pulse repetition rate, f ; at constant peak power, f controls the average power of the lamp. Previous investigators (54-56,60) have operated xenon flashlamps at a maximum f of 0.2 Hz. From the equations in Table VI, it can be seen that the term, $[1 - \exp(-1/f\tau_p)]$, in the denominator decreases as $f\tau_p$ becomes greater than unity. If all else is constant and $\tau_p = 1$ s, the signal level is 20-fold higher at 20 Hz than at 0.2 Hz. This is the major reason for low signal levels observed with pulsed source phosphorimetry when compared to conventional phosphorimetry.

One of the fundamental limitations with continuum sources, whether continuous wave or pulsed, is that only a small fraction of spectral output is useful for excitation of phosphorescence. Even assuming fast collection optics and wide-band interference filters, the useful radiant flux transferred to the sample is still only a small fraction of the total spectral output. Using higher power sources is difficult due to stray light problems. The ideal case would be a source of high intensity, tunable, monochromatic radiation. Such a source is the tunable dye laser.

The dye laser is the finest available excitation source for both atomic and molecular luminescence spectrometry due to its high spectral irradiance, small beam diameter and divergence, and wavelength tunability. The theory of laser operation is given in many texts (61-63). Allkins (64) and Steinfeld (65) have reviewed many uses of lasers in analytical spectrometry. Both continuous wave (66) and pulsed (67) dye lasers have been utilized to obtain excellent detection limits in atomic fluorescence flame spectrometry. Dye lasers have been applied to molecular

fluorescence spectrometry (68-70), photoacoustic spectrometry (71), Raman spectrometry (72), and Coherent anti-Stokes Raman spectrometry (73). Fixed frequency lasers such as the nitrogen laser (74), the He-Cd laser (75), and the argon ion laser (76) have also been utilized in molecular fluorescence spectrometry.

Although dye lasers have been used extensively in studying electronic and vibrational parameters of the triplet state (77-79), no analytical applications of dye lasers in phosphorescence spectrometry have been reported. Wilson and Miller (80) used a nitrogen laser to time resolve the spectra of a mixture of benzophenone and anthrone, but reported no analytical figures of merit. This work reports analytical figures of merit for laser excited time resolved phosphorimetry of drugs and compares the use of two different lasers (pulsed nitrogen laser and flashlamp pumped dye laser) as excitation sources.

External Heavy Atom Effect

Analytical Applications

The first suggestion of the analytical utility of the external heavy atom effect was from McGlynn et al. (81). Hood and Winefordner (82) and Zander (83) found improved detection limits for several aromatic hydrocarbons using glasses of ethanol and ethyl iodide. The use of quartz capillary sample cells with solutions of ethanol or methanol water mixtures permitted the use of large concentrations of halide salts in the solvent matrix (84). Lukasiewicz et al. (16,17) reported improved detection limits in 10% w/w sodium iodide solutions. Other investigators (85,86) have reported on the analytical utility of sodium iodide

in 10/90 v/v methanol/water at 77 K and at room temperature (87-89) on filter paper.

Rahn and Landry (90) found a 20-fold enhancement in the phosphorescence of DNA when silver ion was added and attributed the effect to silver ion acting as an internally bound heavy atom perturber. Boutilier et al. (18) studied the effect of silver and iodide ions on the phosphorescence of nucleosides and found silver ion to improve detection limits 20 to 50-fold. Other metal ions (Cd(II), Hg(II), Zn(II), and Cu(II)) have been studied as heavy atom perturbers (91-92) at 77 K and Ag(I) and Tl(I) at room temperature on filter paper (19,93-94).

Theory

The external heavy atom effect was first observed in 1952 by Kasha (95) when the mixing of 1-chloronaphthalene and ethyl iodide, both colorless liquids, gave a yellow solution. The color was attributed to an increase in the singlet-triplet transition probability from increased spin-orbit coupling due to an external heavy atom effect. The increase in spin-orbit coupling was later proved by McGlynn et al. (96).

A spin-orbit coupling increase was the reason given by McClure (97) and Gilmore et al. (98) for the internal heavy atom effect. Transitions between states of different multiplicities are forbidden due to the selection rule requiring conservation of spin angular momentum. It is never really possible to have pure spin states because the spinning electron has a magnetic moment which can interact with the magnetic field associated with orbital angular momentum (an electron moving in the electric field of the nucleus generates a magnetic field). Because

of the interaction of these two magnetic fields, it is only possible to conserve total angular momentum rather than spin or orbital angular momentum independently. The mixing of states of different multiplicities (singlet and triplet) is proportional to the spin-orbit interaction energy and inversely proportional to the energy difference between the states being mixed (99). The spin-orbit interaction energy for a hydrogen-like atom is proportional to Z^4 , where Z is the atomic number. This Z^4 dependence is the origin of the term "heavy atom effect" (100).

A major point of discussion is the nature of the state mixed with the emitting triplet. Three types of states have been proposed to mix with the lowest triplet to increase the transition probability, which are

- (i) the transition from the triplet to the ground state in molecule, M , mixes with a charge-transfer transition in a charge-transfer complex, MP , where M is an electron donor and P , the perturber, is a heavy atom containing electron acceptor (101);
- (ii) the triplet-singlet transition in molecule M may mix with an "atomic like" transition in the heavy atom containing perturber, P (102);
- (iii) the triplet-singlet transition in molecule M mixes more strongly with an allowed transition in molecule M caused by the perturbing species, P (103).

There seems to be fairly good agreement that the charge-transfer mechanism (i) or exchange mechanism (ii) is the most important. Some investigators (100,104-106) favor a charge-transfer mechanism while others support the exchange mechanism (89,107-112). There is excellent

evidence in favor of the charge-transfer mechanism in the case of planar aromatic molecules perturbed by heavy atom containing aromatics such as tetrabromobenzene (104,105).

This study reports phosphorescence lifetimes and spectra of carbazole, phenanthrene, quinine, 7,8-benzoflavone, and thiopropazate at 77 K in 10% v/v ethanol/water with different concentrations of iodide, silver, and thallous ions. Also reported is the effect of these heavy atom perturbers on the detection limits of several drugs.

Experimental

Instrumentation

A block diagram of the equipment used in the pulsed laser time resolved phosphorimeter is shown in Figure 7. Table VII lists the model numbers and manufacturers of this equipment.

The two lasers used for excitation sources were the Avco nitrogen laser and the Chromatix CMX-4 flashlamp pumped dye laser. The nitrogen laser is a super-radiant discharge giving a peak output power of 100 kW, and a pulse width measured to be 7.7 ns at 337.1 nm with an output spectral bandwidth of less than 0.1 nm. This laser was operated at 17 kV with an operating gas pressure of 17.2 torr of prepurified nitrogen in the laser channel. When a high voltage, high current pulse is rapidly applied to channel, which consists of two electrodes running the length of the channel separated by dielectric sidewalls, a transient population inversion is created by electron impact. Laser operation is achieved for a time on the order of the radiative lifetime of the upper level of the lasing transition. The laser will then radiate from both

Figure 7. Block Diagram of Pulsed Laser Time Resolved Phosphorimeter

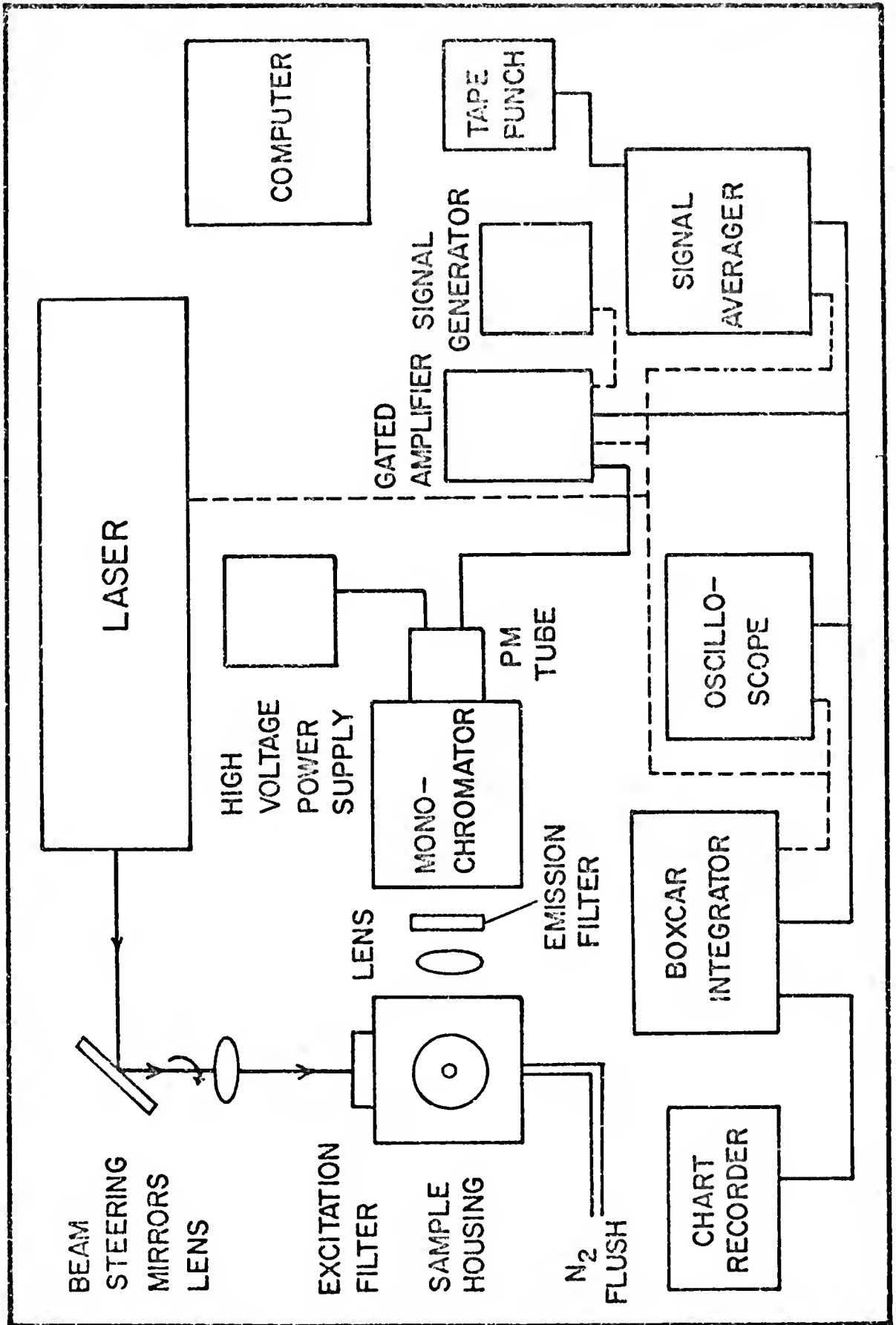


Table VII. Experimental Equipment and Manufacturers

Item	Model Number (Description)	Source
Laser		
Nitrogen	C950	Avco Everett Research Laboratories, Everett, Mass.
Flashlamp	CMX-4	Chromatix, Sunnyvale, Calif. 94086
Sample Housing	--	Laboratory Constructed
Monochromator	H-10	American ISA, Inc., Metuchen, N.J. 08840
Photomultiplier Tube	4837	RCA Corp., Lancaster, Pa. 17604
Photomultiplier Housing	180	PAR Corp., Princeton, N.J. 08540
High Voltage Power Supply	EU-42A	Heath Co., Benton Harbor, Mich. 49022
Gated Amplifier	--	Laboratory Constructed
Signal Generator	110	Wavetek, Inc., San Diego, Calif. 92123
Oscilloscope	122AR	Hewlett-Packard, Palo Alto, Calif. 94306
Boxcar Integrator	CW-1	PAR Corp., Princeton, N.J. 08540
Chart Recorder	SRG	Sargent-Welch, Skokie, Ill. 60076
Signal Averager	BIOMAC 1000	Data Laboratories Ltd., Mitcham, Surrey, U.K.
Tape Punch	2	Friden, Inc., Rochester, N.Y.
Computer	PDP 11/20	DEC, Maynard, Mass. 01754

ends of the channel. Maximum output power is obtained using a plane mirror on one end of the channel. The divergence angle is given by the output dimension of the channel divided by twice the channel length. The output beam is two lines occurring close to each electrode wall of the channel, approximately 2.5 in wide separated by 1/8 in.

The flashlamp pumped dye laser was operated at 270 nm by frequency-doubling the output of laser dye coumarin 504 at 540 nm. A linear flashlamp in an elliptical cavity is used to pump the laser dye. A dye laser is a four level system. The dye is optically pumped to a higher vibrational level in the excited singlet from which it very rapidly relaxes to the lowest vibrational level in the first excited singlet. A population inversion relative to a higher vibrational level in the ground state results and laser action occurs. A tuning element, in this case a birefringent filter, is used to select the wavelength at which laser action occurs. Second harmonic generation, or frequency-doubling, is accomplished using a nonlinear crystal within the laser cavity to make use of the high circulating fundamental power within the laser cavity. The peak power at 270 nm is listed as 200 W with a pulse width of 1 μ s. Repetition rate was restricted to 15 Hz after the destruction of a SCR in the lamp trigger circuit.

As previously mentioned, the nitrogen laser output consists of two lines. It was found that the two lines would focus together into one line quite well, but along the 2.5 in length would only focus to about 5 mm. This is reasonable because the divergence along this dimension is approximately fifteen times greater than the divergence in the perpendicular direction due to the dimensions of the laser channel. The sample width is 2 mm and the long dimension of the beam is

perpendicular to the sample. In order to transfer the maximum laser irradiance to the sample, the beam was rotated 90° with two front surface mirrors shown in Figure 8. The two mirrors were mounted on beam steering units which allow two coplanar rotations. The two units were mounted on a 0.5 in steel rod giving a common vertical rotation axis. The entire assembly is held in position on a steel plate with a magnetic mount. The output beam from the CMX-4 is 3 mm diameter with a divergence of less than 1 mr, so although no special optical train is required, the beam steering mirrors were used for convenience to place the CMX-4 at the same location as the nitrogen laser.

The laser beam was focused on the sample by a 3 in diameter 8 in focal length lens. With the CMX-4 laser, a Corning CS7-54 filter was used to transmit the 270 nm second harmonic, but block the 540 nm fundamental. The transmittance of the output mirror used for frequency-doubling is only 1% at the fundamental wavelength. This is still a substantial amount of light, and will cause a significant interference for phosphorescence in the 540 nm range if not attenuated by a filter. When using the nitrogen laser, an interference filter with a peak transmittance of 42% at 340 nm and a bandwidth of 10 nm was used to block the nonlasing nitrogen emission lines at wavelengths greater than 360 nm.

Figure 9 shows a scan of the output of the nitrogen laser from 340 to 401 nm. The beam was reflected off of an aluminum block positioned to give just full-scale at 340 nm. Figure 10 shows a scan of the output of the nitrogen laser from 360 to 540 nm using a Corning CS3-75 sharp cut yellow glass filter to block the 337.1 nm lasing line.

The sample compartment is constructed from aluminum painted optical-flat black and consists of two sections. The lower section has

Figure 8. Front Surface Beam Rotator

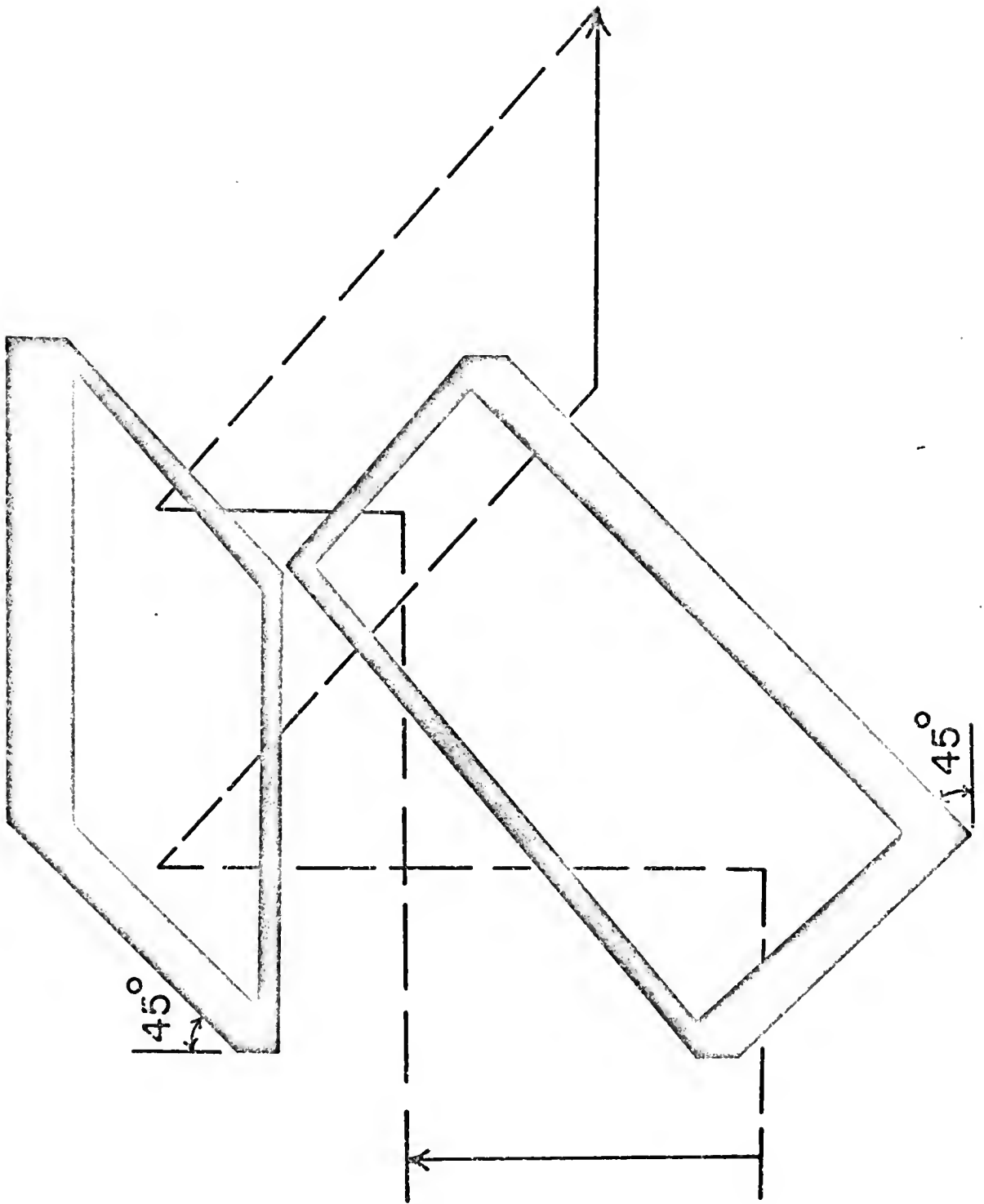


Figure 9. Spectrum of Nitrogen Laser Output from 340 to 401 nm

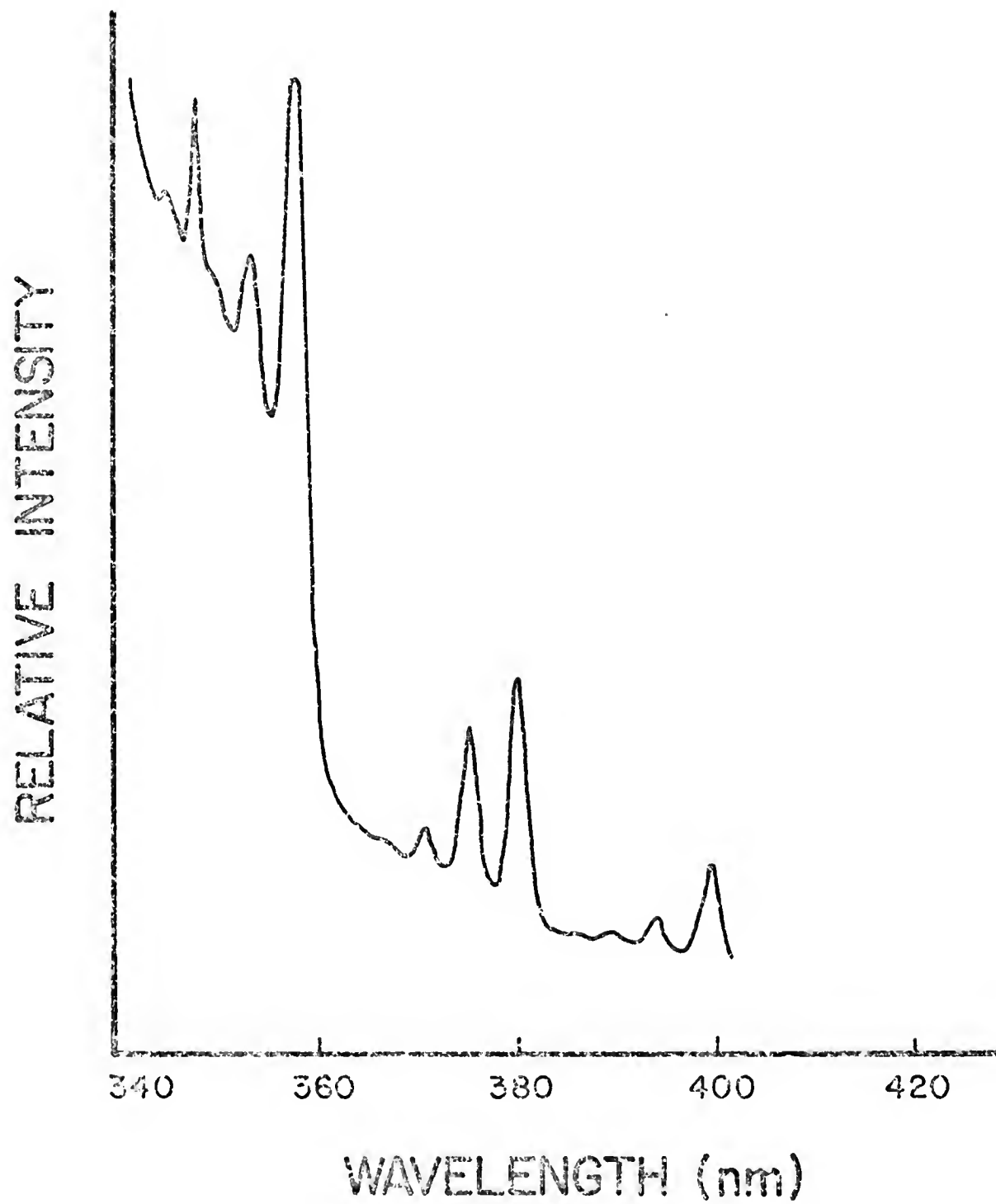
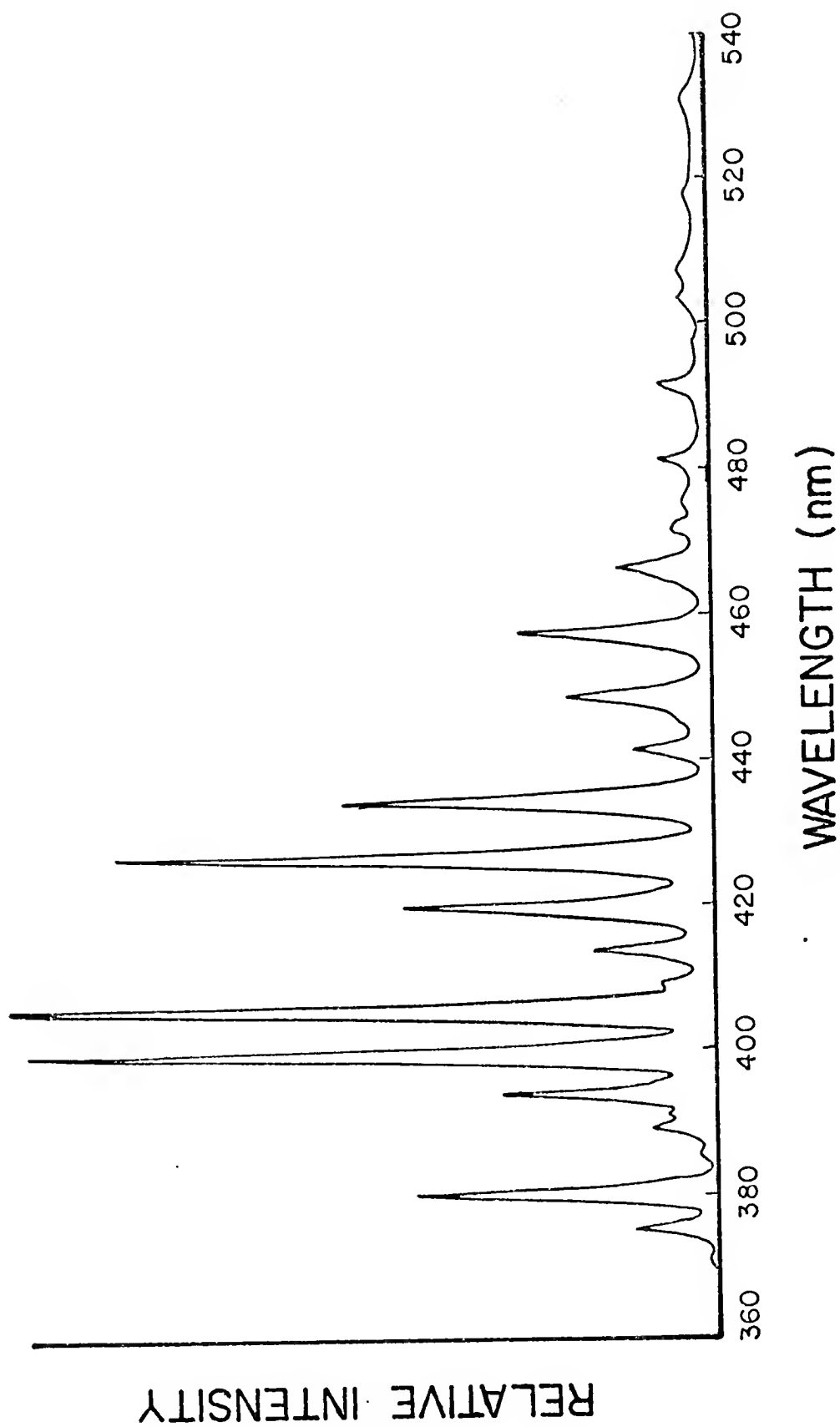


Figure 10. Spectrum of Nitrogen Laser Output from 360 to 540 nm

A Corning CS3-75 filter was used to block the 337.1 nm lasing line.
Full scale is 0.1 times Figure 9.



a circular opening at the top to accomodate a Dewar flask with a quartz optical tail. The Dewar flask is held in place with a Teflon ring slip-fit to the compartment opening. Nitrogen gas is flushed through the lower section to prevent condensation on the optical tail of the Dewar. A cylindrical cover fits over the Dewar and slip-fits to the lower portion of the sample compartment. On top of this cylinder an nmr spinner (84) is mounted to position the sample cell. A sample cell is a 30 cm length of synthetic fused quartz (Thermal American Fused Quartz Co., Montville, N.J. 07045) of 2 mm inner diameter and 4 mm outer diameter. The cell is fit into a Teflon cylinder using Teflon tape. The Teflon cylinder slip-fits into the nmr spinner assembly.

A 15 mm diameter 25 mm focal length quartz lens is used to form an image of the sample cell on the entrance slit of the monochromator. The monochromator is a f/3.5 0.1 m focal length equipped with a concave holographic grating having reciprocal linear dispersion of 8 nm/mm. Phosphorescence selected by the monochromator is detected by a photomultiplier tube in a light-tight compartment. Conventional wiring designs providing voltage to the dynodes cannot supply sufficient current to maintain linear response for the large pulses encountered using pulsed sources. They also lack the ability to keep from distorting very short (<100 ns) pulses. Lytle (113,114) has discussed photomultiplier base wiring designs to obtain fast response from photomultiplier tubes. For phosphorescence signals, the response time is easily adequate to avoid distortion, but one would like to insure that the response time is such that fluorescence or stray light does not distort the response characteristics for a long time after the light pulse has terminated. Using a linear chain of 100 k Ω resistors, as was originally supplied by

the manufacturer, with a 1 kV supply voltage, the maximum current that can be drawn is 10 μ A (assuming drawing 1% of the current flowing through the resistors does not result in nonlinearity). Using the scheme shown in Figure 11, charge can be supplied on a transient basis from the capacitors to keep the interdynode voltage from dropping. Drawing 1% of the charge in the final capacitor for a 1 ms phosphorescence lifetime allows a peak current of 81 μ A. For shorter lifetimes, the permitted peak current is higher, while for longer lifetimes the peak current is lower. It is still necessary to keep the average current 1% or less of the current flowing through the dynode resistors.

Both the signal averager and boxcar integrator used require a voltage input. The input impedance of the boxcar integrator is 10 k Ω and that of the signal averager is 100 k Ω . Assuming a 1% loading error, the minimum current measureable at the boxcar would be 2×10^{-5} A, and the minimum peak current required to measure a lifetime would be 5×10^{-4} A. A block diagram of the gated current-to-voltage (I-V) amplifier is shown in Figure 12 and a complete schematic diagram in Figure 13. In order to avoid driving the front end amplifier to saturation on stray light or fluorescence, from which recovery was slow, the front end was gated using a 4016 quad analog switch. One switch is in series with the input and a second shunts the input while the other two are not used. Control voltage to the switches comes from a 4047 monostable multivibrator with complementary outputs. When the monostable is triggered, the outputs change state for a time variable from 80 to 500 μ s. The shunt switch then conducts and gives a 300 Ω path to ground while the series switch is turned off which isolates the amplifier input by >1 G Ω . When the monostable outputs return to their original state, the two switches

Figure 11. Wiring Diagram of Photomultiplier Dynode Chain

$R = 100\text{ k}$

$C = 0.002$

All resistance values in ohms.

All capacitance values in microfarads.

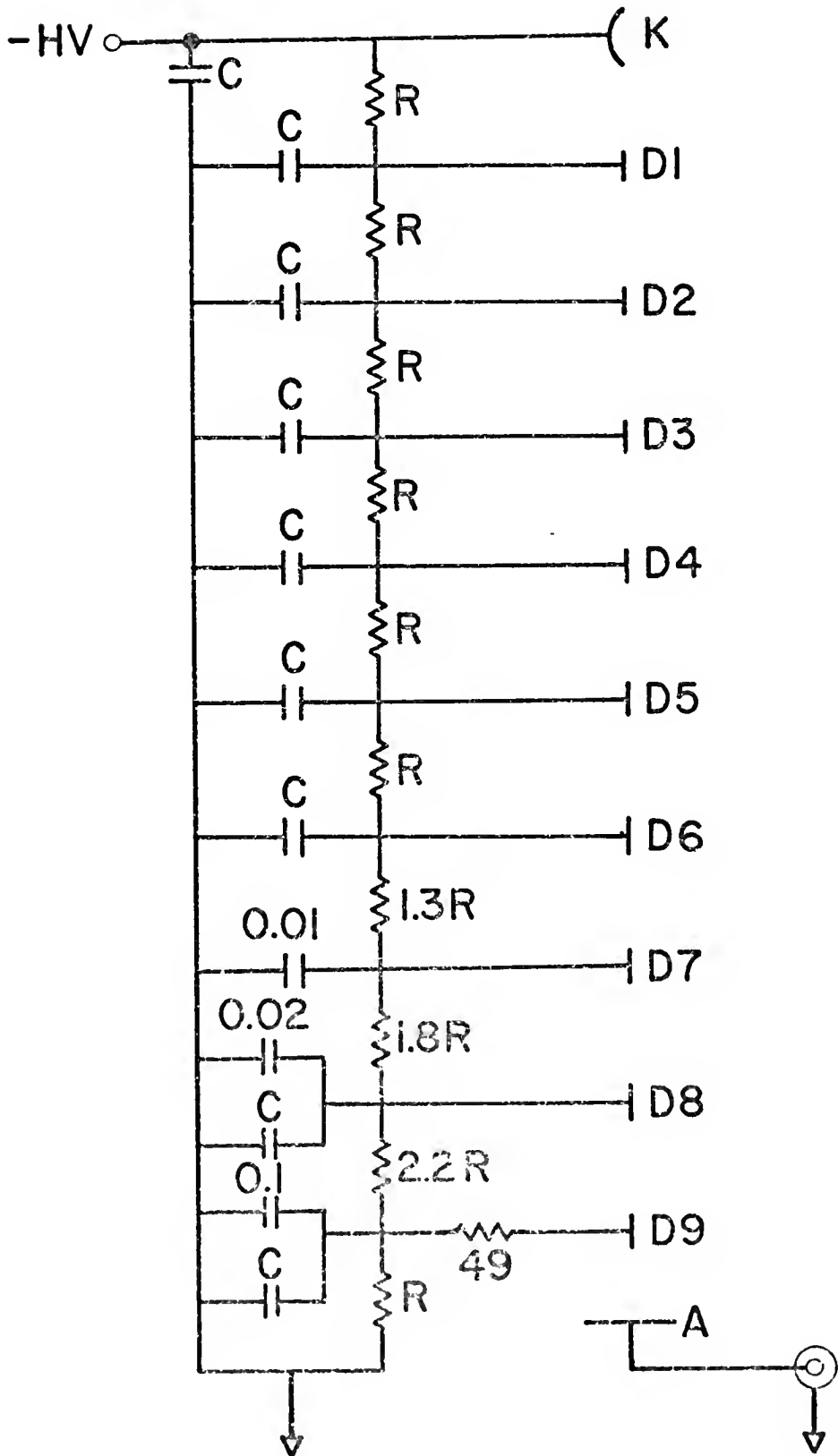


Figure 12. Block Diagram of Current-to-Voltage Gated Amplifier

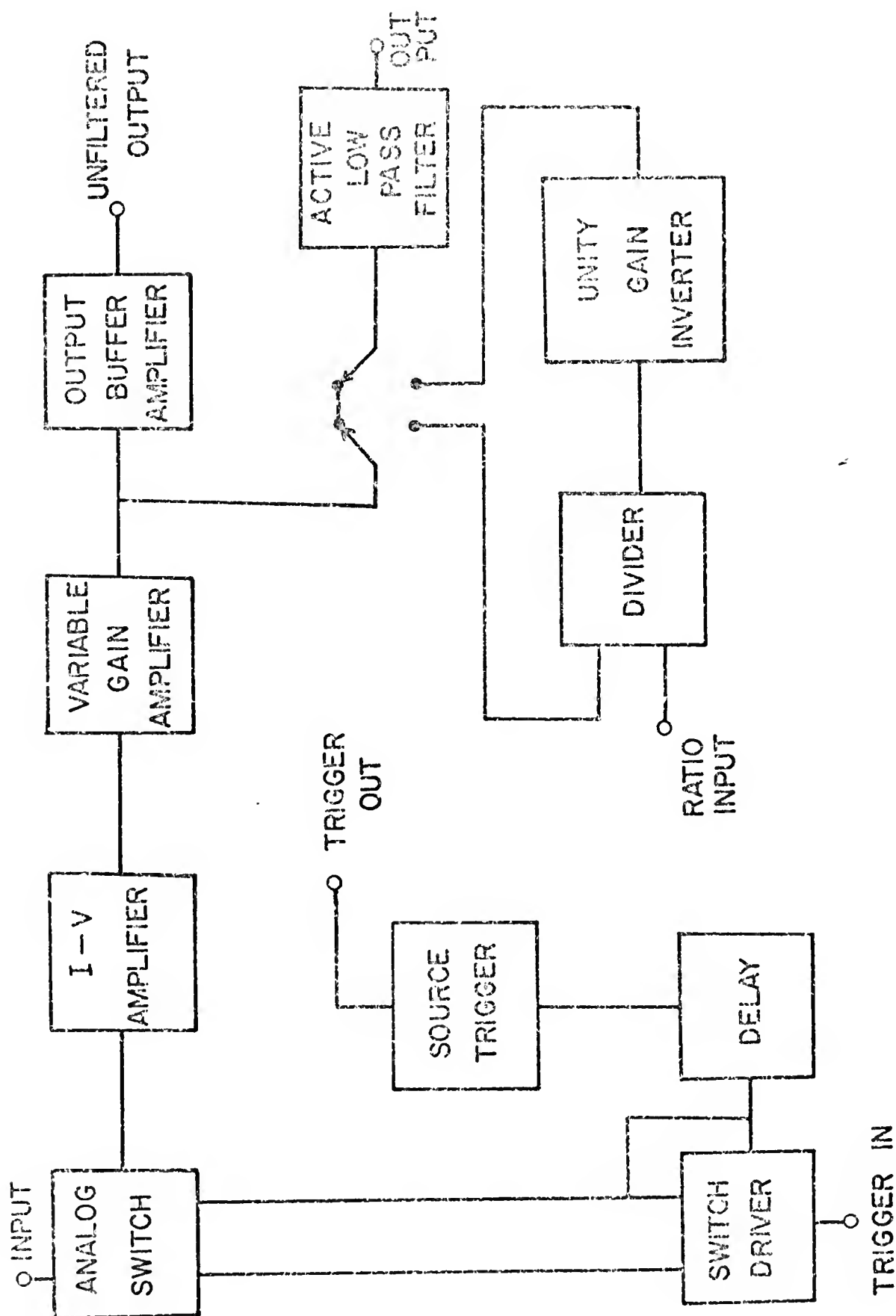


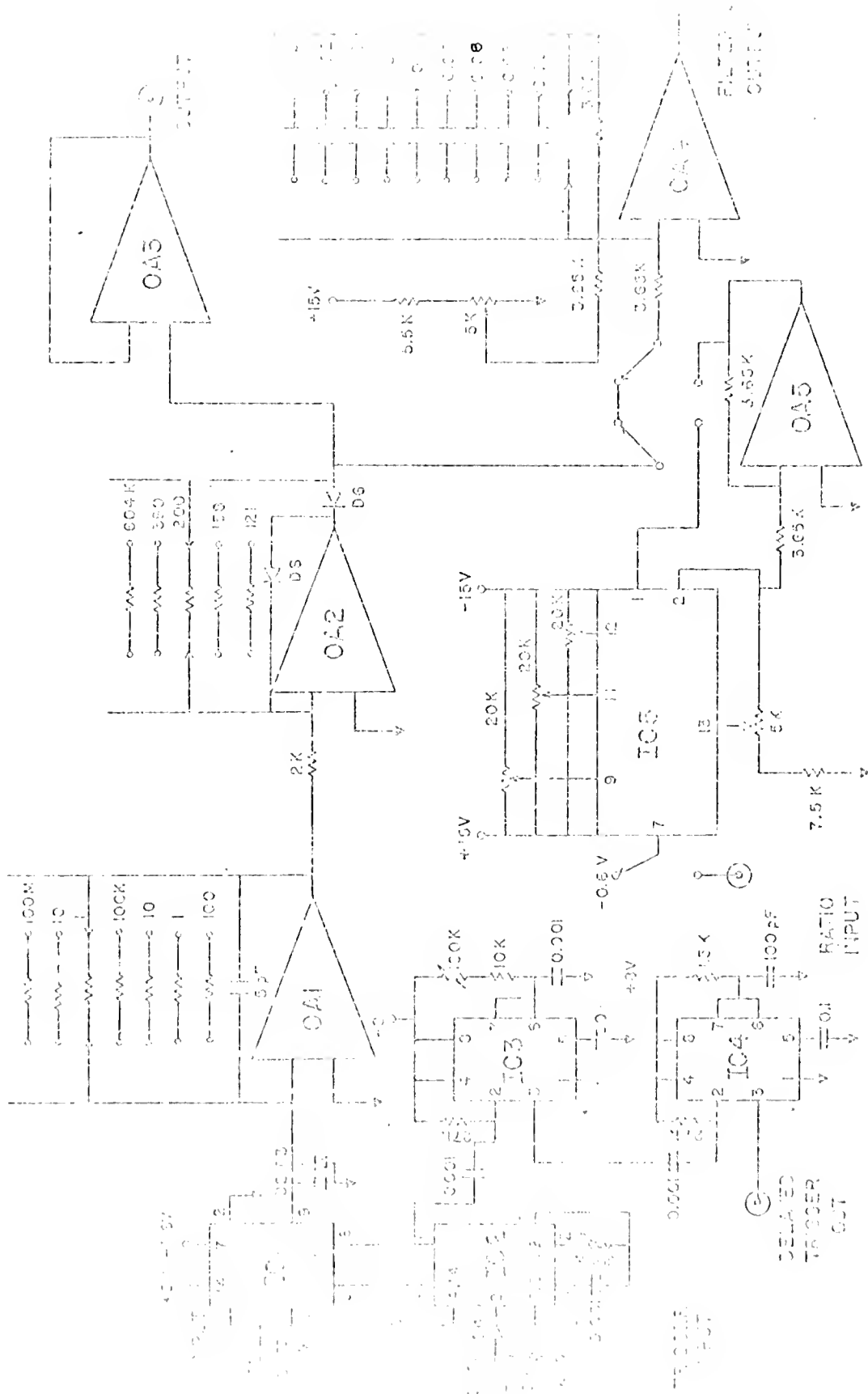
Figure 13. Schematic Diagram of Current-to-Voltage Gated Amplifier

KEY TO COMPONENTS:

IC1	CD4016AE
IC2	CD4047AE
IC3, IC4	NE555
IC5	AD533K
OA1	40J
OA2-OA5	741
D1-D6	1N914

All resistance in ohms.

All capacitance in microfarads unless otherwise specified.



reverse condition and essentially all the current is allowed to reach the input of the first amplifier. The 4016 was found to give smaller switching transients than any of the FET's or MOSFET's tested in this circuit. To ensure that the excitation source did not trigger while the switches were changing state, a 555 timer was triggered from the monostable output and set for a $40\ \mu\text{s}$ delay before triggering a second 555 timer. The $3\ \mu\text{s}$ output pulse from the second 555 timer was used to trigger the excitation source.

The first amplifier is a 40J which gives a voltage output equal to minus the input current times the feedback resistance. The second amplifier is a 741 with variable gain and is clamped to respond only to positive input voltages. The output of the variable gain amplifier is output through a buffer amplifier and through an active low pass filter with time constants varying from 0.03 ms to 340 ms. The output of the active filter is offset by -3.00 V for use with the signal averager. The boxcar integrator input was connected to the unfiltered output. If a voltage proportional to the excitation source output is available, an analog divider may be switched in to ratio the signal to the source intensity. Such a system will compensate for source output variation.

A Wavetek signal generator was used to trigger the monostable in the amplifier and control the laser repetition rate when using the nitrogen laser. The CMX-4 is externally triggerable only in phase with line frequency. A 10 V square wave output in phase with line frequency is provided from the CMX-4. This output was level shifted with a 4050 buffer and divided down to the desired frequency using one or two $4018 \div N$ counters depending on the desired frequency. This signal was used to trigger the amplifier monostable.

For lifetime measurements, the filtered amplifier output was connected to the signal averager. This signal averager has sweep times variable in factors of 2 from 5 ms to 81.92 s and delay before the start of the sweep in factors of 2 from 0.32 ms to 5.12 s. The delay before may also be zero. The input analog-to-digital converter (A/D) operates in the range of -3.15 to 3.20 V. The conversion factor is one count per 50 mV. The -3.00 offset on the amplifier allowed maximum use of the available A/D dynamic range. The signal averager acquires 1000 points during each sweep and sums the value acquired at each point into memory. To select the proper repetition rate, sweep time, and amplifier gain, the signal was first displayed on an oscilloscope. After the desired number of sweeps have been averaged, the contents of the signal averager memory are output to the paper tape punch in the form of 16 bit words. Paper tapes were read into a PDP 11/20 minicomputer at a later time for calculation of lifetimes.

For quantitative analysis, a PAR CW-1 boxcar integrator is used. Despite the term integrator in the name, a more appropriate name would be boxcar averager because the output is proportional to the average value of the input signal during the gate width. The boxcar and signal averager are both triggered from the same pulse used to trigger the laser. The delay before and gate width are continuously variable from 1 μ s to 1 s. The output from the boxcar integrator is displayed on a strip chart recorder.

Instrumental Procedure

For all intensity measurements and lifetime measurements, the monochromator slit width was 2.0 mm (giving a spectral bandwidth of 16 nm).

For scanning the phosphorescence spectra, the slit width was decreased to 0.5 mm for a spectral bandwidth of 4 nm. All spectra are uncorrected for variation in response with wavelength. The photomultiplier voltage was -800 V and the amplifier was gated off for 200 μ s in all experiments.

In all lifetime determinations, the sweep time was set to four or five times the lifetime estimated from the oscilloscope trace. For lifetimes of 1 s or less, 128, 256, or 512 sweeps were averaged. For lifetimes longer than 1 s, the nitrogen laser was run at 20 Hz (CMX-4 at 15 Hz) until the phosphorescence signal reached steady state; the laser trigger was turned off and the phosphorescence decay for one sweep was stored in the signal averager. For determining the short component in a two component or nonexponential decay, the sweep time was set long enough to allow the short component to decay completely and establish a baseline of the long component. To determine the long component, a delay before the sweep time was set long enough to allow the short component to decay completely.

Although a long enough delay to allow an intense short component to decay completely is possible, the amplifier still has a finite dynamic range. Recovery time for amplifiers driven to saturation is dependent on how long the amplifier has been saturated. Increasing the time constant will prevent saturation and will result in the short component decay having a lifetime equal to the time constant (assuming a time constant greater than the short component lifetime). This in turn increases the required delay time. These effects make the measurement of a long lifetime less precise if an intense short component is present.

For studies of the external heavy atom effect, the nitrogen laser was operated at 20 Hz, the boxcar integrator delay time set to 0.2 ms, and the gate width to 1 ms. This was done to maintain a roughly constant detection duty cycle as the lifetimes changed. The observed time constant (OTC) of the boxcar integrator is given by

$$\text{Observed Time Constant} = \frac{\text{Time Constant}}{\text{Gate Width} \times \text{Repetition Rate}}$$

With a 20 Hz repetition gate and 1 ms gate width, a 30 ms time constant to give an OTC of 1.5 s was used. For limits of detection, the delay time and gate width were varied to maximize the S/N ratio, and the OTC set as close to 3 s as possible.

Data Reduction

Fisher (115) and Harbaugh (60) have described methods of data reduction for single and multicomponent decays. The basic theme of all involves reading decays off of a chart recorder and either plotting the data on semi-log paper or taking the natural log of the relative intensity and using a linear least squares to fit the decay curve. It is impractical to try and read 1000 points from a chart recorder tracing of the decay curve, so most of the data is wasted. Digital data are already available from the signal averager, so the effort expended in re-digitizing the data by eye is not justified.

To utilize the maximum amount of data available in the most reasonable amount of time, programs were written in BASIC for a PDP 11/20 minicomputer. Data are read into the computer from paper tape and stored on floppy disks in a virtual file as 16 bit binary words. Lifetimes

were calculated from the least squares slope of the natural log of the phosphorescence signal versus time after subtracting the blank. The short component of a two component decay was calculated after extrapolating back the long component using a previously calculated lifetime of the long component. Programs used are listed in the Appendix.

Reagents

All chemicals used in this study were reagent-grade and used as received. Controlled substances were ordered and used in accordance with BNDD regulations. Chemicals and drugs used in this study were obtained from the following sources:

carbazole, K & K Laboratories Inc., Plainview, N.Y.;

7,8-benzoflavone, phenanthrene, Eastman Kodak Co., Rochester, N.Y.;

benzophenone, sodium iodide, Fisher Scientific Co., Fairlawn, N.J.;

silver nitrate, potassium iodide, Mallinckrodt Chemical Co., St. Louis, Mo.;

thiopropazate, Searle Co., San Juan, Puerto Rico;

phencyclidine, Phillips Roxane, Inc., St. Joseph, Mo.;

2,5-dimethoxy-4-methylamphetamine (STP or DOM), NIMH, Center for Studies of Narcotics and Drug Abuse, Rockville, Md.;

vinblastine sulfate, Eli Lilly and Co., Indianapolis, In.;

phenylbutazone (butazolidin), sulfinpyrazone (anturane), oxyphenbutazone (tandearil), Ciba-Beigy, Summit, N.J.;

quinine, morphine, ethylmorphine, codeine, procaine, phenobarbitol, cocaine, Applied Science Laboratories, State College, Pa.;

ethyl alcohol, U.S. Industrial Chemicals Co., New York, N.Y.;

deionized water from a Barnstead Nanopure water system, Barnstead, Boston, Mass.

Structures of drugs have been previously given (60,94).

Stock solutions of phosphors were prepared in ethanol and stock solutions of sodium iodide, potassium iodide, and silver nitrate in water. Solutions for analysis were prepared by diluting 1 ml of the ethanol stock solution and the appropriate volume of other reagent solution and filling to the mark in a 10 ml volumetric flask. In all studies, a 10/90 v/v ethanol/water solvent was used. The concentration of heavy atom perturber given is that at room temperature in the mixed ethanol-water solvent.

Results and Discussion

External Heavy Atom Effect of Iodide, Silver, and Thallous Ions

Silver nitrate (18,93), sodium iodide and potassium iodide (85,88), and thallous nitrate (19,116) were chosen for investigation as heavy atom perturbers based on previous reports of analytical utility. No difference was found between sodium and potassium iodide with respect to the heavy atom effect, but potassium iodide was found to give lower phosphorescence background. Carbazole (93), phenanthrene (94,112), quinine, 7,8-benzoflavone, and thiopropazate were chosen for study from previous reports of interaction with heavy atom perturbers and to represent several different classes of molecules. Lifetimes, correlation coefficients, intensity ratios for the long and short components of the phosphorescence, and the ratios of the phosphorescence signal with and without heavy atom perturbers are given for the molecules studied in Tables VIII through XII. The ratio of shorter lived component to the longer component is dependent on the lifetimes, laser pulse width, and repetition rate of the laser when using the signal averager. The

excitation duty cycle, d_{ex} , is given by (see Table VI, time resolution section)

$$d_{ex} = \frac{t_p}{\tau_p [1 - \exp(-1/f\tau_p)]} \quad (IV.1)$$

assuming $t_p \ll \tau_p$ (10 ns \ll 1 ms), where τ_p is the phosphorescence lifetime. As the phosphorescence lifetime decreases, this term increases. For $f = 20$ Hz and $t_p = 10^{-8}$ s, d_{ex} increases from 2×10^{-7} to 1×10^{-5} as τ_p decreases from 1 s to 1 ms. The ratio I_S/I_L is defined as the ratio of the initial intensity of the short component to the initial intensity of the long component at the listed repetition rate. Also, I_S^o/I_L^o is defined as the ratio of the initial intensity of the short component to the initial intensity of the long component after dividing each by its respective d_{ex} . In equation form, this is

$$\frac{d_{ex}(\text{short})I_S^o}{d_{ex}(\text{long})I_L^o} = \frac{I_S}{I_L} \quad (IV.2)$$

The ratio I_S^o/I_L^o would be observed for continuous wave excitation.

The ratio I/I_o is defined as the ratio of the phosphorescence signal with heavy atom perturber to the phosphorescence signal without heavy atom perturber where both signals have been measured using the boxcar integrator with $f = 20$ Hz, $t_g = 1.0$ ms, and $t_d = 0.2$ ms. This reflects the increase (decrease) in phosphorescence signal using the heavy atom effect in pulsed laser time resolved phosphorimetry. The portion of the duty cycle (Table VI, time resolution case) associated with gated detection, d_{gd} , is given by

$$d_{gd} = \frac{\tau_p [1 - \exp(-t_g/\tau)] \exp(-t_d/\tau)}{t_g} \quad (IV.3)$$

Under these conditions ($f = 20$ Hz, $t_g = 1.0$ ms, and $t_d = 0.2$ ms), if the lifetime changes from 10 s to 1 ms, d_{gd} changes from 1.0 to 0.52.

Because the gated detector averages over the gate time, using a gate time much shorter than the lifetime does not decrease the signal at the boxcar output. Using a gate time longer than the lifetime does decrease the signal at the boxcar output. This does not mean that the conditions used give the optimum S/N ratio, but it does eliminate the need to change the gate time unless the lifetime gets below 1 ms. The ratio I_L/I_L^0 is still influenced by the excitation duty cycle.

The normalized heavy atom enhancement factors listed in Table XIII are the ratios of the phosphorescence signals with and without the heavy atom perturber, after each signal has been divided by its respective excitation and detection duty cycle (or divided by d_{AM} , time resolution case, in Table VI). This value now reflects the ratio of the phosphorescence signal with heavy atom perturber to the phosphorescence signal without heavy atom perturber with continuous wave detection and emission. It is an approximation of the change in phosphorescence quantum efficiency, but it is only an approximation because the entire phosphorescence spectrum has not been integrated (only measured at the given wavelength with a 16 nm spectral bandwidth).

Due to the nonexponential decay of phosphorescence enhanced by the external heavy atom effect, calculation of lifetimes presents a problem. McGlynn et al. (100) have reported first observable half lives, which are the half lives of the earliest portion of the decays measurable. Lifetimes of room temperature phosphorescence have also been reported in this way (117). This lifetime is dependent on the delay between the termination of excitation and the first observation of phosphorescence

Table VIII. Carbazole (1.7 $\mu\text{g/ml}$) Lifetimes and Relative Intensities at 440 nm with NaI, TlNO₃, and AgNO₃

Concentration (M)	Lifetime (s) ^a Long Component	Lifetime (ms) ^a Short Component	I_S/I_L^b (10 Hz)	$I_S^0/I_L^0^c$	I/I_0^d
NaI					
0	6.7 (0.995)	--	--	--	1
1.0×10^{-3}	6.0 (0.994)	--	--	--	1.1
3.0×10^{-3}	6.1 (0.995)	21 (0.949)	2×10^{-3}	4×10^{-4}	1.1
1.0×10^{-2}	5.9 (0.995)	17 (0.985)	5×10^{-2}	9.6×10^{-3}	1.4
3.0×10^{-2}	4.8 (0.995)	17 (0.988)	0.11	1.9×10^{-2}	1.8
2.0×10^{-1}	0.32 (0.994)	18 (0.973)	0.17	3.5×10^{-2}	6.8
4.0×10^{-1}	0.30 (0.993)	20 (0.978)	0.33	7.1×10^{-2}	10
6.0×10^{-1}	0.24 (0.996)	17 (0.957)	0.38	0.11	11
8.0×10^{-1}	0.23 (0.995)	17 (0.955)	0.71	0.14	13
TlNO ₃					
1.0×10^{-5}	6.8 (0.996)	--	(20 Hz)	--	1.0
3.3×10^{-5}	6.7 (0.995)	--	--	--	1.0
1.0×10^{-4}	6.6 (0.995)	--	--	--	1.1
3.3×10^{-4}	6.7 (0.995)	--	--	--	1.2
1.0×10^{-3}	6.7 (0.995)	--	--	--	1.0
3.3×10^{-3}	6.3 (0.995)	1.1 (0.992)	0.77	0.017	1.2
1.0×10^{-2}	6.3 (0.995)	1.4 (0.992)	0.84	0.024	1.4
3.3×10^{-2}	6.8 (0.995)	1.1 (0.993)	0.74	0.016	1.5
1.0×10^{-1}	6.3 (0.994)	0.90 (0.993)	0.80	0.014	1.5

Table VIII. (continued)

Concentration (M)	Lifetime (s) ^a Long Component	Lifetime (ms) ^a Short Component	I_S/I_L^b (20 Hz)	$I_S^0/I_L^0{}^c$	I/I_0^d
AgNO ₃					
1.0 x 10 ⁻⁵	6.5 (0.994)	--	--	--	1.0
3.3 x 10 ⁻⁵	6.4 (0.995)	--	--	--	1.1
1.0 x 10 ⁻⁴	5.9 (0.993)	2.1 (0.9996)	3.9	0.16	2.3
3.3 x 10 ⁻⁴	6.1 (0.988)	2.1 (0.9997)	29	1.2	6.4
1.0 x 10 ⁻³	5.8 (0.989)	2.1 (0.9997)	41	1.7	21
3.3 x 10 ⁻³	6.8 (0.977)	1.9 (0.9996)	208	7.9	48
1.0 x 10 ⁻²	5.2 (0.974)	1.9 (0.998)	1400	53	91
3.3 x 10 ⁻²	--	1.5 (0.9987)	>1400	>53	74
1.0 x 10 ⁻¹	--	0.93 (0.997)	>1400	>53	49

^aCorrelation coefficient in parentheses.

^bRatio of intensity of short component to long component at t = 0 at given repetition rate.

^cRatio of intensity of short component to long component at t = 0 corrected for excitation duty cycle.

^dRatio of phosphorescence signal with heavy atom perturber to signal without heavy atom perturber at 20 Hz, 0.2 ms delay, and 1 ms gate.

Table IX. Phenanthrene (1.9 $\mu\text{g/ml}$) Lifetimes and Relative Intensities at 500 nm with NaI and AgNO_3

Concentration (M)	Lifetime (s) ^a Long Component	Lifetime (MS) Short Component	I_S/I_L^b (20 Hz)	I_S^c/I_L^c	I/I_O^d
NaI					
0	3.4 (0.998)	--	--	--	--
1.0×10^{-3}	3.2 (0.997)	6.0 (0.989)	0.20	0.024	1.0
3.0×10^{-3}	2.9 (0.995)	3.6 (0.967)	0.21	0.015	1.0
1.0×10^{-2}	2.7 (0.995)	5.1 (0.944)	0.15	0.015	1.1
3.0×10^{-2}	2.1 (0.997)	5.3 (0.987)	0.15	0.016	1.2
2.0×10^{-1}	1.1 (0.994)	3.0 (0.984)	0.13	0.097	2.4
4.0×10^{-1}	0.78 (0.996)	5.0 (0.975)	0.43	0.044	3.5
6.0×10^{-1}	0.68 (0.992)	5.0 (0.987)	0.79	0.082	5.0
8.0×10^{-1}	0.57 (0.994)	5.0 (0.988)	1.1	0.11	5.3
AgNO_3					
1.0×10^{-4}	3.4 (0.997)	--	--	--	1.0
3.3×10^{-4}	3.3 (0.996)	--	--	--	1.1
1.0×10^{-3}	3.2 (0.995)	3.2 (0.989)	0.54	0.035	1.5
3.3×10^{-3}	3.0 (0.995)	3.0 (0.995)	1.1	0.067	1.8
1.0×10^{-2}	3.0 (0.995)	3.0 (0.995)	3.5	0.21	3.5
3.3×10^{-2}	2.7 (0.991)	2.4 (0.996)	67	3.26	16
1.0×10^{-1}	2.6 (0.963)	2.0 (0.998)	520	21	41

a,b,c,d See Table VIII.

Table X. Quinine (4.3 $\mu\text{g/ml}$) Lifetimes and Relative Intensities at 515 nm with NaI and AgNO_3

Concentration (M)	Lifetime (s) ^a Long Component	Lifetime (ms) ^a Short Component	I_S/I_L^b (10 Hz)	$I_S^0/I_L^0^c$	I/I_0^d
NaI					
0	1.1 (0.997)	--	--	--	--
1.0×10^{-5}	1.1 (0.996)	5.6 (0.937)	0.07	5×10^{-3}	1
1.0×10^{-4}	1.1 (0.996)	8.0 (0.981)	1.4	0.14	2.6
1.0×10^{-3}	1.1 (0.993)	15 (0.976)	6.6	1.2	7.2
3.0×10^{-3}	1.0 (0.989)	15 (0.970)	11	2.0	16
1.0×10^{-2}	0.92 (0.986)	14.3 (0.977)	33	9.1	26
3.0×10^{-2}	0.75 (0.991)	13 (0.971)	77	20	40
1.0×10^{-1}	0.38 (0.987)	9.5 (0.978)	180	37	56
3.0×10^{-1}	0.16 (0.983)	8.3 (0.985)	180	35	64
5.0×10^{-1}	0.14 (0.967)	8.1 (0.988)	500	83	72
7.0×10^{-1}	0.12 (0.982)	7.9 (0.988)	240	47	70
AgNO_3			(20 Hz)		
1.0×10^{-5}	1.1 (0.996)	--	--	--	1.0
3.3×10^{-5}	0.066 (0.999)	--	--	--	4.9
1.0×10^{-4}	0.064 (0.998)	--	--	--	7.5
3.3×10^{-4}	0.063 (0.998)	--	--	--	7.7
1.0×10^{-3}	0.060 (0.998)	--	--	--	8.2
3.3×10^{-3}	0.061 (0.999)	--	--	--	8.7
1.0×10^{-2}	0.057 (0.996)	--	--	--	13
3.3×10^{-2}	0.049 (0.996)	6.2 (0.993)	3.7	0.73	19
1.0×10^{-1}	0.046 (0.997)	6.4 (0.992)	8.9	1.8	32

a,b,c,d See Table VIII.

Table XI. 7,8-Benzoflavone (2.7 $\mu\text{g/ml}$) Lifetimes and Relative Intensities at 500 nm with KI and AgNO_3

Concentration (M)	Lifetime (s) ^a Long Component	Lifetime (ms) ^a Short Component	I_S/I_L^b	$I_S^o/I_L^o^c$	I/I_o^d
KI			(3 Hz)		
0	2.6 (0.997)	--	--	--	--
3.0×10^{-3}	2.5 (0.982)	79 (0.969)	0.38	0.094	1.1
1.0×10^{-2}	2.2 (0.995)	74 (0.942)	1.1	0.26	1.4
3.0×10^{-2}	0.84 (0.993)	71 (0.959)	1.9	0.48	2.0
1.0×10^{-1}	0.38 (0.994)	62 (0.966)	2.3	0.64	5.0
3.0×10^{-1}	0.42 (0.994)	61 (0.957)	7.2	1.9	4.7
AgNO_3			(20 Hz)		
1.0×10^{-5}	2.6 (0.996)	--	--	--	1.0
1.0×10^{-4}	2.6 (0.996)	--	--	--	1.0
1.0×10^{-3}	2.6 (0.996)	--	--	--	1.3
1.0×10^{-2}	2.5 (0.996)	6.8 (0.983)	0.24	0.033	1.6
1.0×10^{-1}	2.2 (0.996)	6.6 (0.980)	6.4	0.85	11

a, b, c, d See Table VIII.

Table XII. Thiopropazate (5.2 $\mu\text{g/ml}$) Lifetimes and Relative Intensities with KI and AgNO_3

Concentration (M)	Lifetime (s) ^a Long Component	Lifetime (ms) ^a Short Component	I_S/I_L^b (20 Hz)	I_S^c/I_L^c	I/I_O^d
KI					
0	0.067 (0.999)	--	(20 Hz)	--	--
1.0×10^{-3}	0.066 (0.999)	--	--	--	1.0
3.0×10^{-3}	0.067 (0.999)	2.7 (0.967)	0.16	1.3×10^{-2}	1.2
1.0×10^{-2}	0.065 (0.999)	4.1 (0.959)	0.17	2.0×10^{-2}	1.4
3.0×10^{-2}	0.063 (0.999)	2.6 (0.956)	0.26	2.0×10^{-2}	1.4
1.0×10^{-1}	0.059 (0.998)	2.6 (0.951)	0.61	3.1×10^{-2}	0.65
3.0×10^{-1}	0.058 (0.995)	4.0 (0.982)	0.51	7.8×10^{-2}	1.9
5.0×10^{-1}	0.057 (0.998)	5.2 (0.981)	0.50	7.5×10^{-2}	2.2
7.5×10^{-1}	0.064 (0.998)	3.5 (0.96)	0.43	7.0×10^{-2}	1.7
AgNO ₃					
1.0×10^{-5}	0.067 (0.998)	--	(20 Hz)	--	1.0
1.0×10^{-4}	0.057 (0.997)	16.6 (0.983)	0.51	0.18	0.49
1.0×10^{-3}	0.029 (0.997)	4.2 (0.977)	1.0	0.15	0.45
1.0×10^{-2}	--	13.3 (0.999)	--	--	1.5
1.0×10^{-1}	--	6.5 (0.997)	--	--	4.5

a,b,c,d See Table VIII.

Table XIII. Normalized Heavy Atom Enhancement Factors

		Enhancement Factor ^a
Carbazole	0.8 M NaI	9.6
	0.01 M AgNO ₃	5.0
Phenanthrene	0.8 M NaI	5.1
	0.1 M AgNO ₃	2.3
Quinine	0.7 M NaI	12
	0.1 M AgNO ₃	6.2
7,8-Benzoflavone	0.3 M KI	3.4
	0.1 M AgNO ₃	2.7
Thiopropazate	0.75 M KI	1.2
	0.1 M AgNO ₃	0.91

^aRatio of signal with and without heavy atom perturber after correcting each by dividing by d_{AM} from Table VI. See text for discussion.

which will vary for different experimental systems. Najbar and Chadhowka (111) have observed for triphenylene in the presence of KI in an ethanol glass at 77 K that the lifetime becomes exponential with the same lifetime as unperturbed triphenylene after approximately two lifetimes. The long component reported here is the longest lifetime measurable subject to the dynamic range considerations of the amplifier and signal averager. Short component lifetimes were all calculated after subtraction of the long-lived component. Results for individual molecules will be discussed first.

Carbazole shows a substantial reduction in phosphorescence lifetime for NaI and AgNO_3 perturbers, but little effect for TlNO_3 . The long component lifetimes with added NaI are reduced, and the correlation coefficients are as good as those for unperturbed carbazole. The short-lived component is certainly nonexponential. Using silver nitrate as the perturber gives the opposite case. The short component appearing at 1.0×10^{-4} M grows in intensity until 1.0×10^{-2} M AgNO_3 after which it begins to decrease. The lifetime of the long-lived component shortens much less than with NaI while the intensity is much smaller than the short-lived component. The poorer correlation coefficients of the long lived component may reflect nonexponential character, but it is more likely that they reflect the difficulty in measuring a long-lived species in the presence of a much more intense shorter component. The normalized enhancement of phosphorescence of 9.6 for 0.8 M NaI and 5.0 for 0.01 M AgNO_3 reflects a difference between the two heavy atom perturbers. The intersystem crossing efficiency (Eq. III.34) for carbazole is reported as 0.36 (118); so regardless of how large the intersystem crossing rate constant (k_{32} or k_{ISC} , s^{-1}) becomes, the

phosphorescence quantum efficiency can increase at most by a factor of 2.8 due to intersystem crossing. The phosphorescence quantum efficiency (Eq. III.33) may also increase if the phosphorescence transition probability, A_{21} , increases relative to the radiationless rate constant, k_{21} . The phosphorescence lifetime is $(A_{21} + k_{21})^{-1}$. From the ratio of the lifetimes in 0.75 M KI (0.23 s) and without KI (6.8 s), the sum $(A_{21} + k_{21})$ has increased a factor of 30 in 0.75 M KI. Because there is more increase in the normalized enhancement than can be accounted for by increase in intersystem crossing efficiency, A_{21} has increased more than k_{21} . Studies of the internal heavy atom effect and the external heavy atom effect have indicated (100) that A_{21} is affected more than k_{21} . In 0.01 M AgNO_3 , the phosphorescence lifetime has decreased more than a factor of 3000, but the normalized enhancement factor is only 5.0 which is less than that found for iodide. If it is true that k_{ISC} is the parameter most sensitive to the external heavy atom effect (100), then silver ion must have a greater affect on k_{21} than does iodide or the normalized enhancement would be the same. Silver ion certainly affects the sum $(A_{21} + k_{21})$ to a greater extent than does iodide ion. The decrease in phosphorescence signals for silver nitrate concentrations above 0.01 M could be due to an increase in k_{21} , but the signal levels are approaching the point of nonlinear photomultiplier response.

The phosphorescence spectra of carbazole, carbazole in 0.75 M KI, and carbazole in 0.1 M AgNO_3 are shown in Figure 14. All of the bands resolvable without NaI appear to be present in 0.75 M NaI with the intensities of the bands at 422, 438, and 453 nm increased in intensity relative to the 409 nm band with the band at 422 nm enhanced to the

largest degree. In 0.1 M AgNO_3 , only two broad bands centered at 426 and 447 nm are resolved.

The interaction of phenanthrene with AgNO_3 and NaI perturbers is very similar to that of carbazole. The interaction of phenanthrene with KI in ethanol glass at 77 K (112), fluorescence quenching at room temperature by KI in acetonitrile (119) and in bromobenzene (120), and phenanthrene phosphorescence with ethyl iodide and iodonaphthalene as heavy atom perturbers have all been reported. The lifetimes measured for phenanthrene perturbed by NaI are qualitatively in good agreement with the results of Najbar et al. (112). Lifetimes of the long component reported here are somewhat shorter than theirs for the same iodide concentration. The results in a snowed-matrix which is mainly aqueous are not likely to be directly transferrable to results in an ethanol glass for the same iodide concentration. The concentration of phenanthrene studied by Najbar et al. (70) is not stated, but results for naphthalene are given at 10^{-3} M, or 100-fold higher than the concentrations studied here. Becker (44) tabulates the intersystem crossing efficiency for phenanthrene as 0.88 and 0.76 and the phosphorescence quantum efficiency as 0.20, 0.11, and 0.09 depending on how the measurements were made. Little increase in the intersystem crossing efficiency is possible, so the majority of the increase in phosphorescence efficiency must come from an increase in the phosphorescence transition probability. The normalized enhancement factor of 5.1 in 0.8 M KI corresponds to a 6-fold decrease in lifetime, so radiationless deactivation of the triplet seems enhanced only to a small extent. Results with AgNO_3 perturbing phenanthrene are also similar to carbazole. The normalized enhancement factor is smaller probably due to the already high intersystem crossing efficiency in phenanthrene.

Phosphorescence spectra of phenanthrene without heavy atom perturbors, with 0.75 M KI, and with 0.1 M AgNO_3 are shown in Figure 15. Broadening of bands by silver nitrate is again observed, and no change of relative band intensities in 0.75 M KI is observed. At this point, it should be mentioned that 0.1 M TlNO_3 was also investigated as a heavy atom perturber on phenanthrene with results very similar to those obtained for carbazole. Equally insignificant phosphorescence enhancement was observed for quinine, at which point, investigations using TlNO_3 were discontinued.

The effect of iodide and silver ions on quinine phosphorescence is markedly different than the effect on carbazole or phenanthrene. Quinine fluorescence is known to be sensitive to quenching by halide ions (121). The trends in the values of the lifetimes with iodide as the heavy atom perturber are consistent with the data for phenanthrene and carbazole, but the intensities are not. The short component is observable at 100-fold lower iodide concentrations and is 100-fold more intense relative to the long component. Adams et al. (80) observed complete quenching of quinine fluorescence at 10^{-3} M Cl^- and a 1.7-fold increase in the photoacoustic signal. The fluorescence quantum efficiency measured was 0.52. It would seem that most of the fluorescence quenching goes through the quinine triplet and a 2-fold upper limit on the increase in intersystem crossing efficiency seems reasonable. Extrapolating from information obtained with 0.1 M HCl and 0.1 M H_2SO_4 should be treated with caution. The point to be made is that it is again unlikely that all of the increase of the normalized enhancement factor can be attributed to an increase in intersystem crossing efficiency.

Silver ion also has a markedly different effect on the lifetime and intensity. A gradual decrease in the lifetime of the long component is not observed, but rather a sharp decrease in the lifetime at 3.3×10^{-5} M AgNO_3 . A shorter component is observed starting at 3.3×10^{-2} M AgNO_3 of lower intensity relative to the long lifetime than previously discussed cases. Quenching of quinine fluorescence at room temperature by AgNO_3 was investigated using an Aminco-Bowman spectrofluorimeter. Fluorescence is quenched less rapidly than the phosphorescence is enhanced as is shown by comparison of the results in Figure 16 with the tabulated increase in phosphorescence. Nitrate ion has been observed to quench the room temperature fluorescence of aromatic hydrocarbons (122), so it is possible that some of the quenching is due to nitrate ion. The lack of change in the phosphorescence of quinine by 0.1 M TlNO_3 would serve to confirm that the effect on phosphorescence is due to silver ion rather than nitrate. The conclusion is that the sharp drop in phosphorescence lifetime at 3.3×10^{-5} M AgNO_3 is not accompanied by any major increase in intersystem crossing efficiency and that the phosphorescence transition probability is more sensitive to perturbation by silver ion than the intersystem crossing rate constant. The phosphorescence spectra of quinine perturbed by NaI and AgNO_3 are shown in Figure 17. The bands at 474 and 509 nm in 0.7 M NaI have the same intensity ratio as the bands at 474 and 497 nm of unperturbed quinine, while the 463 nm band in unperturbed quinine is a shoulder in the NaI perturbed spectrum. The 509 nm band may correspond to the 509 nm shoulder in unperturbed quinine, and the similar intensity ratio may be coincidence. The spectrum of quinine perturbed by AgNO_3 has two bands at 477 and 509 nm which could correspond to the 474 and 509 nm

bands or red shifted and enhanced 463 and 497 nm bands from unperturbed quinine.

Results obtained for 7,8-benzoflavone (BF) are intermediate to the previously discussed cases. The lifetimes of the short component of the decay in KI perturbed BF are longer than those obtained for quinine, while the majority of the intensity starting at 1.0×10^{-2} M KI is in the short component. The normalized enhancement factor in KI is lower, but the phosphorescence quantum efficiency has been reported as 0.45 (122). This would make the enhancement of 3.4 in 0.3 M KI seem too high. The reported quantum efficiency may be high and the factor of 3.4 is not a true quantum efficiency as the phosphorescence spectrum has not been integrated. There is no observed fluorescence for BF due to highly efficient intersystem crossing from the n, π^* lowest singlet to the π, π^* triplet (123,124). At concentrations of KI higher than 0.3 M, solutions turned yellow due to formation of I_3^- . After standing for several hours, a blue-green precipitate was observed. To avoid complications, only freshly prepared solutions were used and 0.3 M was the maximum KI concentration studied. Instability of BF in solution has been reported (123). Lifetimes with silver ion as a perturber are consistent with carbazole and phenanthrene data with smaller interaction in terms of the short component lifetimes and the ratios of the short and long component intensities. The spectra of perturbed and unperturbed BF are shown in Figure 18. The 459 and 493 nm bands have been enhanced in 0.3 M KI relative to the band at 471 nm. The spectrum in 0.1 M $AgNO_3$ appears as a broadened and slightly red shifted version of the unperturbed spectrum.

Thiopropazate perturbed by KI shows essentially no change in lifetime and a weak nonexponential short component. The presence of a chlorine and sulfur in thiopropazate will give an internal heavy atom effect resulting in the short lifetime of the unperturbed molecule. The normalized enhancement factor of 1.2 in 0.75 M KI is also consistent with this. The spectra of externally perturbed and unperturbed thiopropazate is shown in Figure 19. The spectra of thiopropazate with and without KI is a broad structureless band centered at 500 nm. The lifetime data for thiopropazate perturbed by AgNO_3 is not consistent with any of the other cases, nor is the 25 nm blue shift observed in the phosphorescence spectrum. The decrease for 1×10^{-4} and 1×10^{-3} M AgNO_3 of the phosphorescence intensity is due to the fact that the band is shifting.

An interesting application of the external heavy atom effect is to study the triplet states of molecules that fluoresce, but do not phosphoresce. At 77 K, riboflavin has intense green fluorescence, but in 0.75 M KI, riboflavin has no fluorescence and bright orange phosphorescence.

The work by Azumi (104) and Yamauchi et al. (105) clearly explains the nature of the heavy atom effect assuming a planar molecule and an external heavy atom perturber. Treating the three triplet spin subcomponents separately, the x, y, and z subcomponents transform as rotations about the x, y, and z axes. One-center integrals mix the y and z subcomponents with σ, π^* or π, σ^* singlets and three-center integrals mix the x subcomponent, so the y and z subcomponents should contribute the majority of the intensity found in the triplet. For the molecule-perturber pair, a charge transfer state from a π orbital of the molecule to a σ^* orbital of the perturber will mix two-center terms with the x, y, and z subcomponents. The new two-center terms are larger than the

Figure 14. Phosphorescence Spectra of Carbazole

Carbazole concentration $0.95 \mu\text{g/ml}$.

(—) Carbazole in 10/90 v/v E/W
 $f = 20 \text{ Hz}$, $t_d = 9 \text{ ms}$, $t_g = 10 \text{ ms}$, 10^{-7} A Full Scale.

(- - -) Carbazole in 10/90 v/v E/W, 0.75 M KI
 $f = 20 \text{ Hz}$, $t_d = 9 \text{ ms}$, $t_g = 10 \text{ ms}$, $2 \times 10^{-7} \text{ A}$ Full Scale.

(. . .) Carbazole in 10/90 v/v E/W, 0.1 M AgNO_3
 $f = 20 \text{ Hz}$, $t_d = 0.2 \text{ ms}$, $t_g = 1 \text{ ms}$, $5 \times 10^{-6} \text{ A}$ Full Scale.

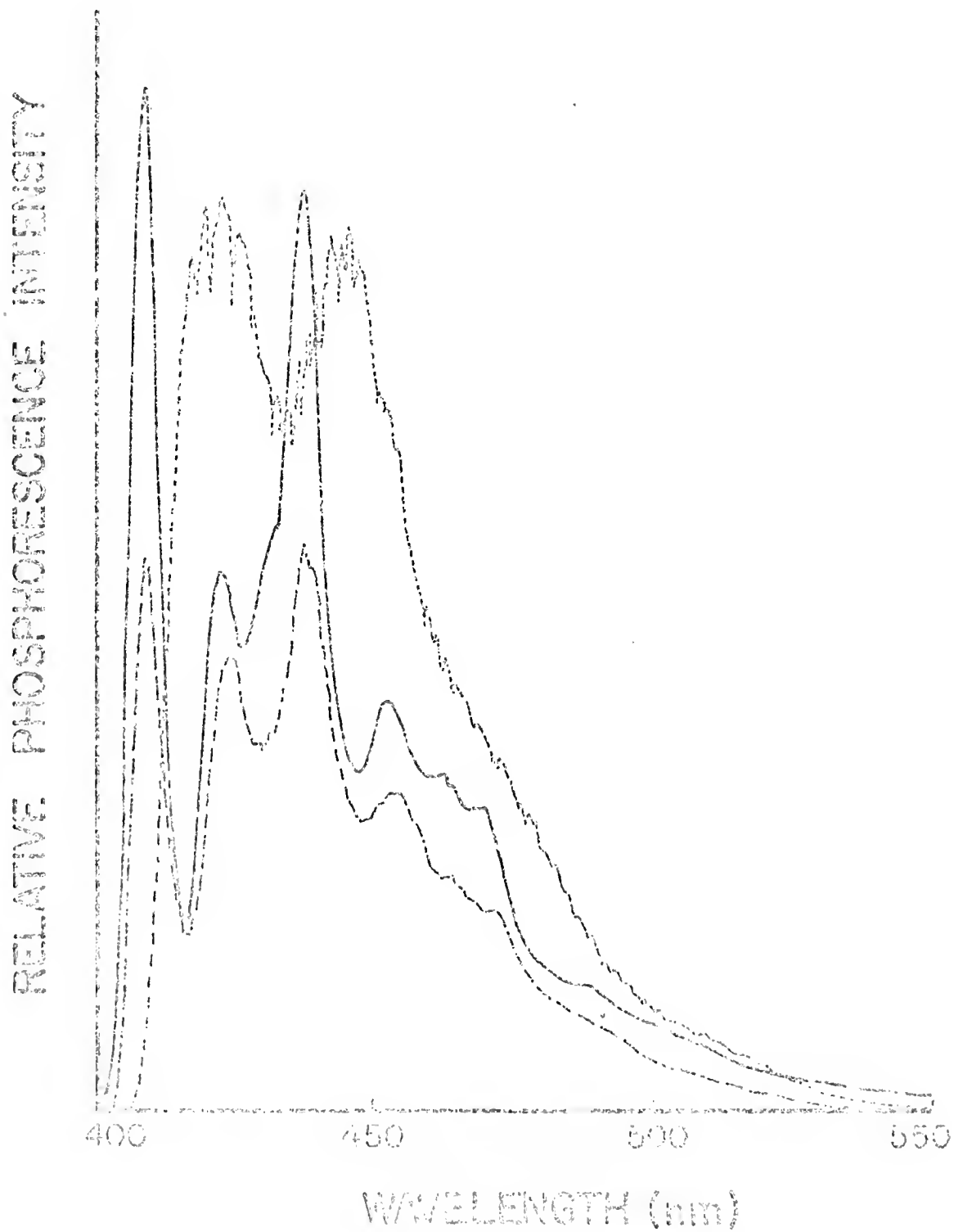
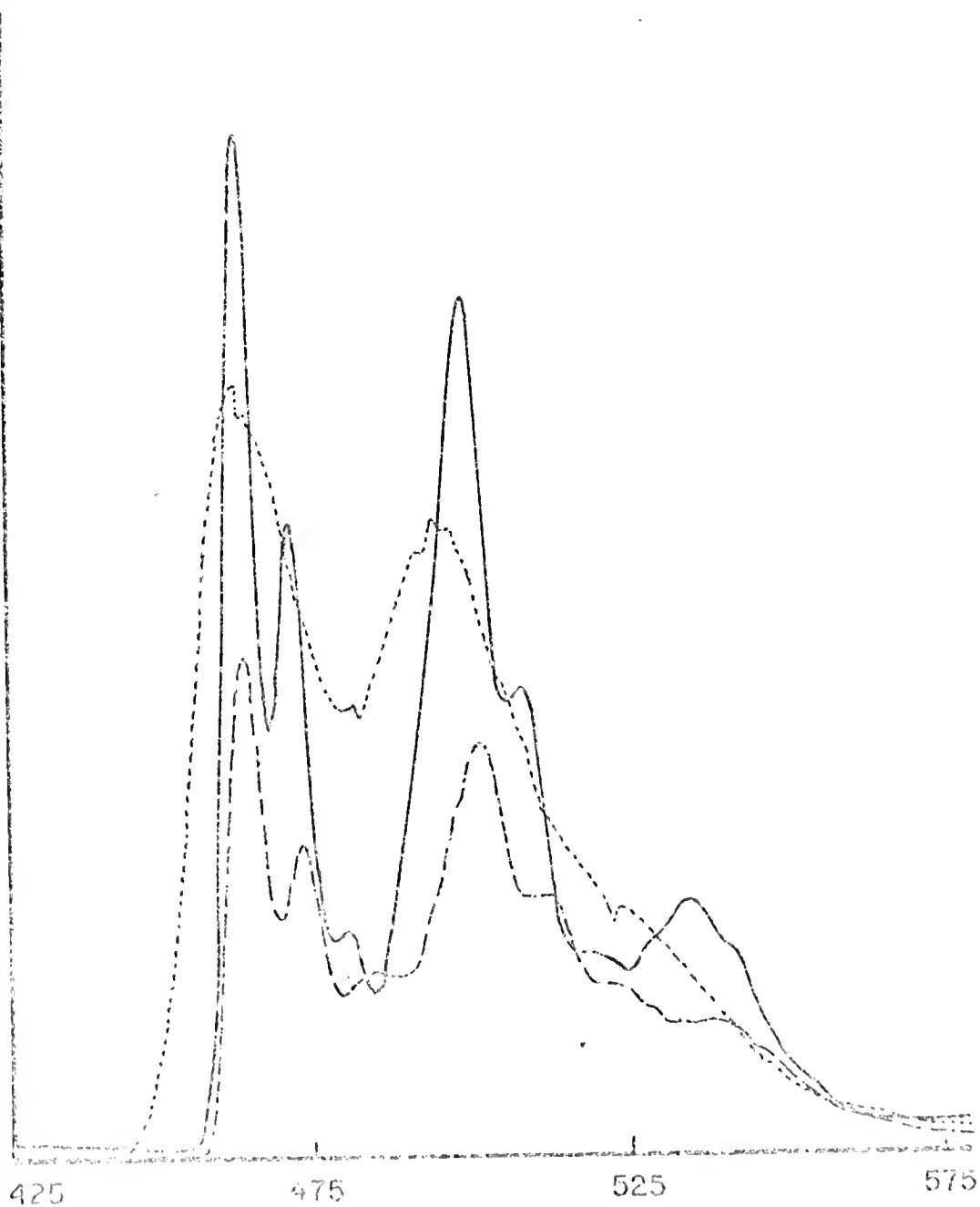


Figure 15. Phosphorescence Spectra of Phenanthrene

Phenanthrene concentration $1.5 \mu\text{g/ml}$.

- (—) Phenanthrene in 10/90 v/v E/W
 $f = 30 \text{ Hz}$, $t_d = 4 \text{ ms}$, $t_g = 15 \text{ ms}$, $2 \times 10^{-8} \text{ A}$ Full Scale.
- (- - -) Phenanthrene in 10/90 v/v E/W, 0.75 M KI
 $f = 30 \text{ Hz}$, $t_d = 4 \text{ ms}$, $t_g = 15 \text{ ms}$, $5 \times 10^{-8} \text{ A}$ Full Scale.
- (· · ·) Phenanthrene in 10/90 v/v E/W, 0.1 M AgNO_3
 $f = 30 \text{ Hz}$, $t_d = 0.2 \text{ ms}$, $t_g = 1.0 \text{ ms}$, $5 \times 10^{-7} \text{ A}$ Full Scale.

RELATIVE PHOSPHORESCENCE INTENSITY



WAVELENGTH (nm)

Figure 16. Quenching of Quinine Room Temperature Fluorescence by AgNO_3

Quinine concentration, 4.3 $\mu\text{g/ml}$;
Excitation wavelength, 310 nm;
Emission wavelength, 382 nm.

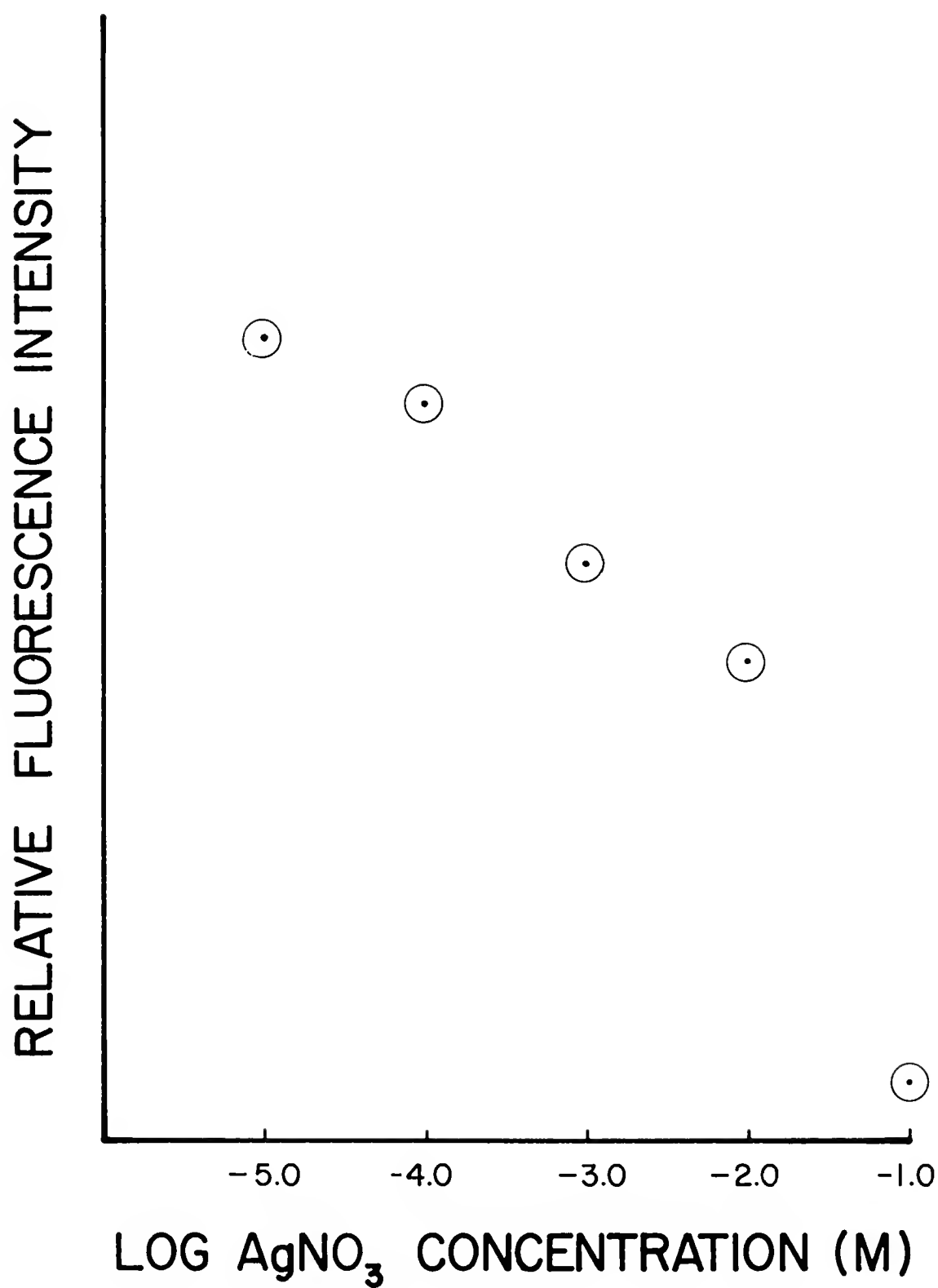


Figure 17. Phosphorescence Spectra of Quinine

Quinine concentration 4.3 $\mu\text{g/ml}$.

- (—) Quinine in 10/90 v/v E/W
 $f = 20 \text{ Hz}$, $t_d = 0.4 \text{ ms}$, $t_g = 10 \text{ ms}$, $5 \times 10^{-8} \text{ A}$ Full Scale.
- (- - -) Quinine in 10/90 v/v E/W, 0.75 M KI
 $f = 20 \text{ Hz}$, $t_d = 0.2 \text{ ms}$, $t_g = 2.0 \text{ ms}$, $5 \times 10^{-6} \text{ A}$ Full Scale.
- (· · ·) Quinine in 10/90 v/v E/W, 0.1 M AgNO_3
 $f = 20 \text{ Hz}$, $t_d = 0.2 \text{ ms}$, $t_g = 2.0 \text{ ms}$, $2 \times 10^{-6} \text{ A}$ Full Scale.

RELATIVE PHOSPHORESCENCE INTENSITY

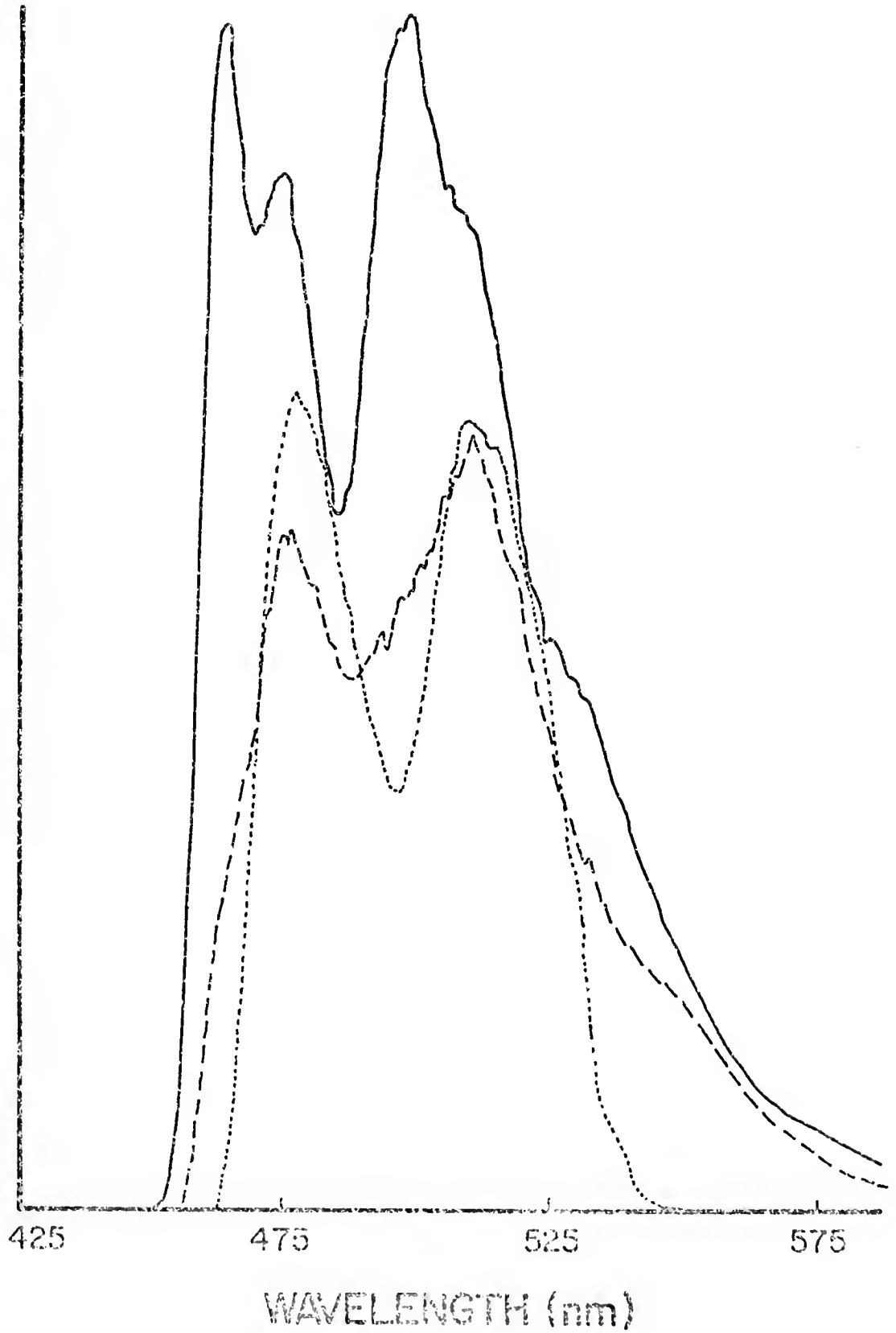


Figure 18. Phosphorescence Spectra of 7,8-Benzoflavone

BF concentration $2.7 \mu\text{g/ml}$.

(—) BF in 10/90 v/v E/W

$f = 20 \text{ Hz}$, $t_d = 1 \text{ ms}$, $t_g = 9 \text{ ms}$, 10^{-7} A Full Scale.

(- - -) BF in 10/90 v/v E/W, 0.3 M KI

$f = 20 \text{ Hz}$, $t_d = 0.2 \text{ ms}$, $t_g = 1 \text{ ms}$, 10^{-6} A Full Scale.

(. . .) BF in 10/90 v/v E/W, 0.1 M AgNO_3

$f = 20 \text{ Hz}$, $t_d = 0.2 \text{ ms}$, $t_g = 2.0 \text{ ms}$, 10^{-6} A Full Scale.

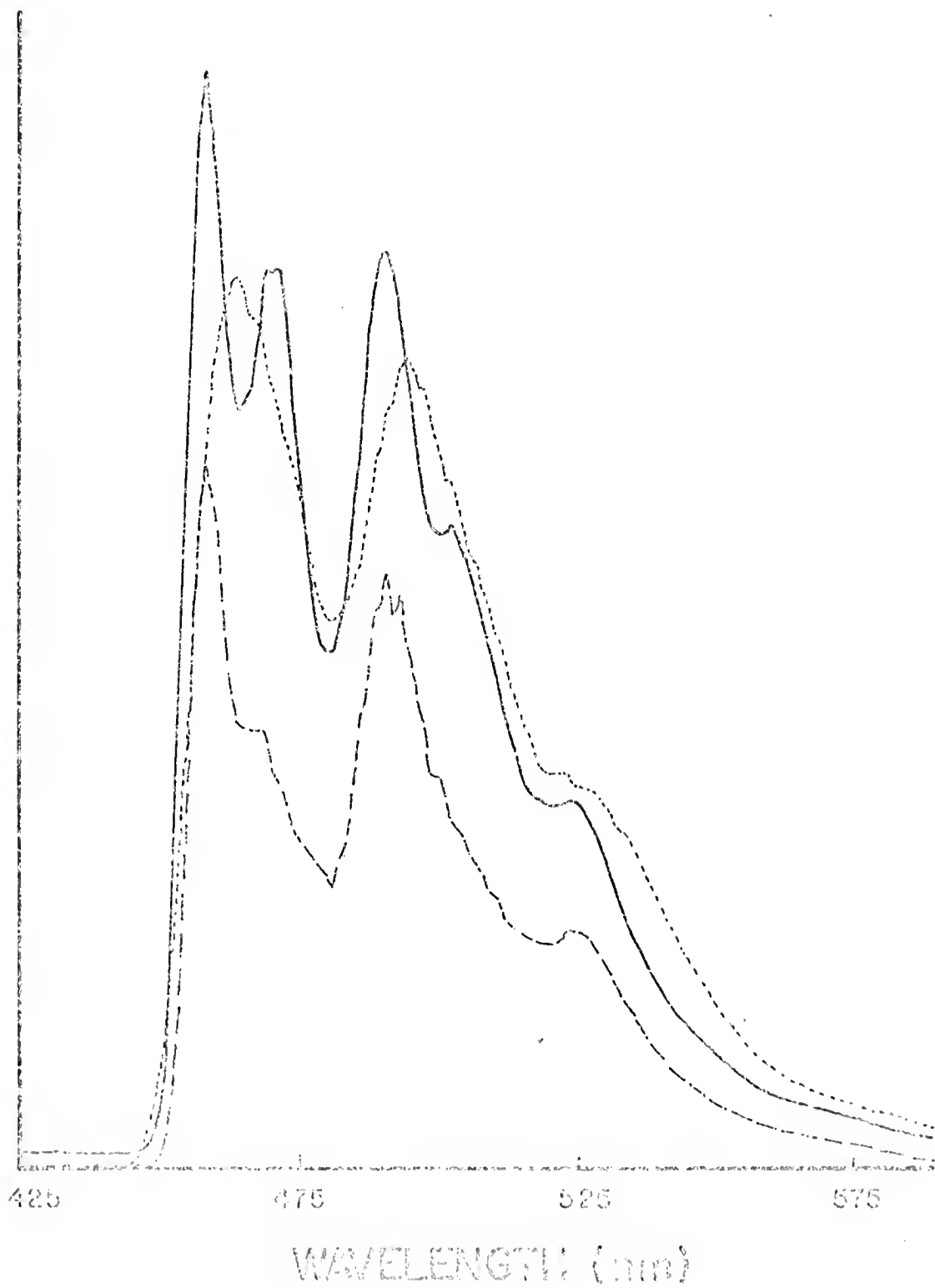


Figure 19. Phosphorescence Spectra of Thiopropazate

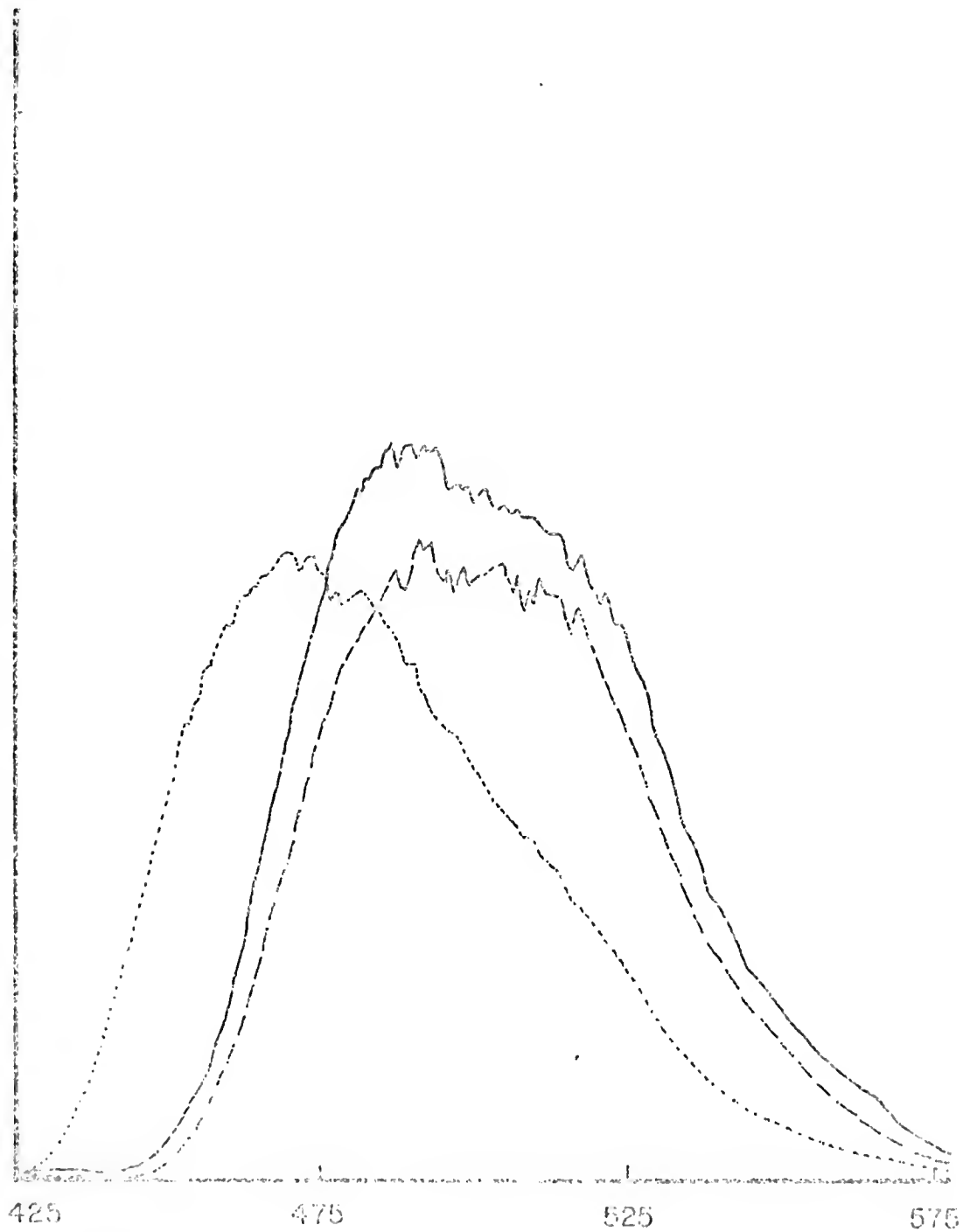
Thiopropazate concentration 5.2 $\mu\text{g/ml}$.

(—) Thiopropazate in 10/90 v/v E/W
 $f = 20 \text{ Hz}$, $t_d = 0.2 \text{ ms}$, $t_g = 6.0 \text{ ms}$, $2 \times 10^{-7} \text{ A}$ Full Scale.

(- - -) Thiopropazate in 10/90 v/v E/W, 0.75 M KI
 $f = 20 \text{ Hz}$, $t_d = 0.2 \text{ ms}$, $t_g = 4.0 \text{ ms}$, $2 \times 10^{-7} \text{ A}$ Full Scale.

(. . .) Thiopropazate in 10/90 v/v E/W, 0.1 M AgNO_3
 $f = 30 \text{ Hz}$, $t_d = 0.2 \text{ ms}$, $t_g = 2.0 \text{ ms}$, $1 \times 10^{-6} \text{ A}$ Full Scale.

RELATIVE PHOSPHORESCENCE INTENSITY



WAVELENGTH (nm)

three-center terms mixing with the x subcomponent, but are not likely to be larger than the original one center terms. Experimental results for quinoxaline confirm this treatment. Extension to include vibronic coupling indicates that those vibronic bands which originally gain intensity in the triplet manifold are enhanced by an external heavy atom perturber while those vibronic bands which gain intensity by vibronic coupling in the singlet are not perturbed. In summary, the external heavy atom perturber opens new spin-orbit coupling channels and which vibronic bands are enhanced depends upon the manifold from which intensity is gained.

It is difficult to visualize a charge-transfer complex with iodide ion acting as an electron acceptor, but it might be expected to act as a donor. No charge-transfer absorption bands in the room temperature spectra of naphthalene and phenanthrene in the presence of KI have been observed (112). Azumi (104) proposes that the charge-transfer complex need not be stable, while Najbar et al. (112) state that a stable charge-transfer complex is a requirement. They report that in 0.125 M KI, the phenanthrene spectrum has three components. One is unperturbed phenanthrene, one is heavy atom enhanced phosphorescence, and the third is due to asymmetric CH vibrational mode. In 0.7 M NaI with a lower concentration of phenanthrene, the unperturbed component is likely to be much smaller due to the heavy atom perturbed component, and the component due to the asymmetric vibrational mode is also of lower intensity. The spectra of carbazole, quinine, and BF perturbed by iodide, along with the lifetime data are consistent with a picture of the external heavy atom effect enhancing different vibrational modes to a different extent depending on the way in which the bands gain intensity in the unperturbed molecule.

The data for thiopropazate with iodide are consistent with a small effect expected on a molecule already containing an internal heavy atom. Substitution of a chlorine on naphthalene decreases the phosphorescence lifetime from 2.3 s to 0.29 s, and the lifetime of the sulfur containing analog of carbazole, dibenzothiophene, is 1.3 s (100). An unperturbed lifetime of 67 ms seems reasonable for a molecule containing both a sulfur and chlorine, but an n, π^* triplet would also be unperturbed by an external heavy atom. For example, no decrease in the lifetime of benzophenone was observed in 0.75 M KI. Najbar et al. (112) have assigned the heavy atom enhanced component of aromatic hydrocarbons to the purely electronic exchange mechanism based on observations of Giachino and Kearns (108,109) that the phosphorescence spectrum should appear unchanged and include only symmetric vibrational modes. They attribute the enhanced asymmetric vibrations to a third order perturbation involving electron exchange, spin-orbit coupling, and vibronic coupling. Azumi (104) has pointed out that for purely electronic exchange, the locally excited states of the perturber contribute to the transition moment proportional to the fourth power of the intermolecular overlap while charge-transfer states contribute terms approximately proportional to the second power of the overlap. Azumi (104) also noted that this formalism may require modification in cases where the charge-transfer configuration is not easily conceived of.

In the case of silver ion, complexes with olefins and aromatic compounds are well-known (125). The crystal structure of $[C_6H_6 \cdot Ag]^+ ClO_4^-$ has been determined, and the silver ion is located asymmetrically with respect to the ring (126). The bonding is normally considered to consist

of one component involving overlap of the π electron density of the aromatic with a σ -type acceptor orbital on silver ion and a "back bond" from filled d_{xz} or $d\pi$ - $p\pi$ hybrid orbitals into antibonding orbitals on the carbon atoms. The donation of π electron density to the metal σ orbital is considered the larger effect, so the interaction may be thought of in terms of an aromatic donor and metal ion acceptor charge-transfer complex. For carbazole, phenanthrene, quinine, and BF, the phosphorescence spectra in 0.1 M AgNO_3 have the same components enhanced as those enhanced by iodide ion with substantial broadening in the silver nitrate case. The absorption spectrum of toluene complexed with silver ion is slightly red shifted and broadened compared to the absorption spectrum of toluene (127). The anomaly of the quinine lifetimes perturbed by AgNO_3 may be explained by the binding of silver ion at the ring nitrogen. This is consistent with the fact that silver ion binds at both the double bond and ring nitrogen in 2-allylpyridine (125). Similar effects have been observed on the phosphorescence of purine nucleosides (18). The ring nitrogen binding occurs at lower concentration of silver ion than the complex with the aromatic portion of the molecule. The blue shift of the phosphorescence and behavior of the lifetimes of thiopropazate does not seem to fit in. Silver ion has been shown to interact strongly with sulfhydryl proteins (128,129) so binding of silver at the sulfide is possible. The energy level of the lowest triplet has certainly increased, so the relative positions of the singlet and triplet π, π^* and n, π^* levels may change. A mixed π, π^* and n, π^* triplet may also account for the short phosphorescence lifetime of thiopropazate. Orbital inversion and vibronic coupling have been observed to be important for a number of aza aromatics and aryl ketones

(130). A systematic study of phenothiazine and phenoxanthin along with the respective halo substituted compounds is required to resolve this question.

Certain aspects of the heavy atom effect on room temperature phosphorescence can be discussed based on these studies. Iodide has been observed to be a more effective heavy atom perturber on carbazole than is silver ion (93). This is consistent with the results reported here and the fact that in strong bases (1 M NaOH) carbazole is ionic. Phenanthrene is the opposite case, with silver ion more effective than iodide. To further compare results, the room temperature phosphorescence lifetime of phenanthrene in 0.1 M AgNO_3 was measured and found to be 12 ms, which is longer than the lifetime at 77 K. Thallous ion has been observed to be a more effective heavy atom perturber on phenanthrene and other aromatic hydrocarbons than silver ion (19). In view of the small effect of thallium ion at 77 K it would appear that some other factors, such as the way the molecule is held on the paper at room temperature, are also of major importance. Caution should be applied in interpreting room temperature phosphorescence using thallium and silver ions strictly in terms of the heavy atom effect.

The comparison of results for iodide and silver ion as heavy atom perturbers indicate that a stable charge-transfer complex with an aromatic molecule acting as the donor is not required for the external heavy atom effect to operate. The lack of effect for thallium ion relative to silver ion indicates that something besides a heavy atom in the vicinity is required. For inorganic ions, the energy difference between levels suitable for mixing is likely to be as important as the atomic number. The formalism of Azumi (104) is impressive for cases

where the charge-transfer configuration is accessible, but it can not in its present form explain the iodide results as a heavy atom perturber. The exchange mechanism does predict broadening (108,109), so it would appear to offer the best explanation for the results of iodide ion in the heavy atom effect at the present time. Silver has a lower atomic number than iodine, so a smaller heavy atom effect would be predicted. In all cases studied here, silver ion had a larger effect on the phosphorescence lifetime than iodide. This could indicate that a "charge-transfer complex" heavy atom effect is a stronger perturber than an "exchange" heavy atom effect.

Lifetimes and Limits of Detection for Several Drugs

The lifetimes of the drugs investigated in this study are given in Table XIV along with other pertinent information on the experimental conditions. In cases where a single exponential decay was found, the lifetime is arbitrarily placed under the Long Component heading. For several of the drugs present as hydrochlorides, it was not possible to use 0.1 M AgNO_3 due to precipitation of AgCl .

Morphine, ethyl morphine, and codeine all have relatively short phosphorescence lifetimes and showed weak phosphorescence. The observed increase in the lifetime of morphine in 0.75 M KI is likely an error due to the weak signal. Morphine gave the poorest signal of all the drugs studied. The lifetimes of all three were reduced in 0.1 M AgNO_3 along with an increase in phosphorescence signal. All other drugs, except the phenylbutazone derivatives anturane, butazolidin, and tandearil, have decreased lifetimes and nonexponential decays in 0.75 M KI. Anturane,

Table XIV. Phosphorescence Lifetimes of Drugs at 77 K in 10/90 v/v Ethanol/Water with 0.1 M AgNO₃ or 0.75 M KI Excited at 270 nm with CMX-4 Laser

Compound	Concentration ($\mu\text{g/ml}$)	Emission Wavelength (nm)	Solvent ^a	Long Component			Short Component		
				Lifetime (s)	Correlation Coefficient	Number of Points	Lifetime (s)	Correlation Coefficient	Number of Points
Morphine	10.8	515	E/W KI AgNO ₃	0.028	0.967	989			
				0.036	0.926	989			
				0.0021	0.991	989			
Ethyl Morphine	10.4	515	E/W KI AgNO ₃	0.022	0.997	854			
				0.0065	0.995	245			
				0.0024	0.985	989			
Codeine	10.8	515	E/W KI AgNO ₃	0.021	0.959	718			
				0.0095	0.972	764			
				0.0021	0.991	989			
Phenobarbital	10	385	E/W KI AgNO ₃ ^b	2.0	0.994	918	--	--	--
				1.8	0.997	989	19	0.967	967
				--	--	--	--	--	--
Procaine	9.6	445	E/W KI AgNO ₃ ^b	2.4	0.987	933	--	--	--
				0.13	0.998	479	8.2	519	0.991
				--	--	--	--	--	--
Phencyclidine	10	385	E/W KI AgNO ₃ ^b	4.8	0.992	809	--	--	--
				0.046	0.998	571	2.5	0.976	287
				--	--	--	--	--	--
Cocaine	10	415	E/W KI AgNO ₃ ^b	2.3	0.997	813	--	--	--
				0.089	0.990	954	0.22	0.900	22
				--	--	--	--	--	--

Table XIV. (continued)

Compound	Concentration ($\mu\text{g/ml}$)	Emission Wavelength (nm)	Solvent ^a	Long Component			Short Component		
				Lifetime (s)	Correlation Coefficient	Number of Points	Lifetime (s)	Correlation Coefficient	Number of Points
STP (DOM)	10.8	411	E/W KI AgNO ₃ ^c	2.8	0.998	989	--	--	--
				0.68	0.992	934	44	0.970	943
				--	--	--	--	--	--
Anturane	9.7	428	E/W KI AgNO ₃ ^c	0.015	0.999	963			
				0.024	0.976	989			
				--	--	--			
Butazolidin	10	390	E/W KI AgNO ₃	0.069	0.960	907			
				0.023	0.955	989			
				0.0045	0.986	760			
Tandearil	10.4	420	E/W KI ^d AgNO ₃	0.18	0.994				
				--	--				
				0.0053	0.997				
Vinblastine Sulfate	10	450	E/W KI AgNO ₃	6.0	0.999	989	--	--	--
				1.48	0.988	863	125	0.985	970
				0.0012	0.999	462	--	--	--

^aE/W is 10/90 v/v Ethanol/Water, KI is 0.75 M KI, AgNO₃ is 0.1 M AgNO₃.

^bPrecipitate formed.

^cNo phosphorescence signal.

^dReaction with iodide ion.

like morphine, gave an increased lifetime in 0.75 M KI. The reason, in this case, is most likely due to a photochemical reaction. Under laser excitation, most other compounds gave slowly decreasing signals with time, but the phosphorescence of anturane increases with time. The rate of increase qualitatively appeared to be greater in 0.75 M KI. Butazolidin phosphorescence decreased in 0.75 M KI, and tandearil solutions rapidly turned yellow from triiodide formation. Phencyclidine and cocaine showed the largest increase in phosphorescence signal and the greatest decrease in lifetime. The "short" component of cocaine's phosphorescence decay having a 0.22 ms lifetime was the most intense of all the "short" components of nonexponential decays.

Vinblastine sulfate is an antitumor alkaloid isolated from Vinca Rosea. It is the only drug studied which showed any vibrational structure in the phosphorescence spectrum, shown in Figure 20. Also shown in Figure 20 is the phosphorescence spectrum of vinblastine sulfate in 0.1 M AgNO_3 . The broadening of the phosphorescence spectrum and sharp decrease in lifetime in 0.1 M AgNO_3 are consistent with results discussed in the previous section.

O'Donnell and Winefordner (131) have reviewed the potential application of phosphorescence spectrometry in clinical chemistry, and a number of the drugs studied here have been previously studied by conventional phosphorimetry (132-135). Limits of detection for laser excited time resolved phosphorimetry are given in Table XV. With the exception of morphine and codeine, the detection limits using pulsed laser excitation and gated detection are 2 to 45-fold better than those previously reported. All limits of detection were calculated on the basis of S/N ratio of 3; the noise on the blank was taken as the standard deviation

of 16 blank measurements. It is not likely that the noise was calculated in this manner in the literature data for morphine and codeine (132), and so previous detection limits should be treated with caution when compared with those determined in this study.

With the exception of phencyclidine and anturane, the limits of detection in 0.75 M KI are not improved even though the phosphorescence signal has increased. The phosphorescence background with 0.75 M KI is larger than that of 10/90 v/v ethanol/water without 0.75 M KI, and the increase in signal does not offset the increase in background. The background luminescence is a broad structureless band centered about 500 nm. Phencyclidine is the exception because it has the largest increase in phosphorescence signal, and the background at 385 nm increases the least in 0.75 M KI. Phenobarbital has a smaller increase in phosphorescence signal than phencyclidine when perturbed by iodide, so the detection limit does not improve. Tandearil and vinblastine are the only drugs which show a notable improvement in detection limit in 0.1 M AgNO_3 .

For the currently available dyes for use in the CMX-4, the lowest wavelength which can be obtained by frequency-doubling is 265 nm. Using coumarin 504 as the laser dye, the peak output is at 270 nm. Changing the dye to sodium fluorescein or rhodamine 575 and tuning to higher wavelength gives less power than at 270 nm. For these reasons, no attempt was made to tune the laser as it was unlikely to give any improvement. The possible exception to this is vinblastine, but only 2-fold more power is available at any wavelength up to 365 nm than is available at 270 nm.

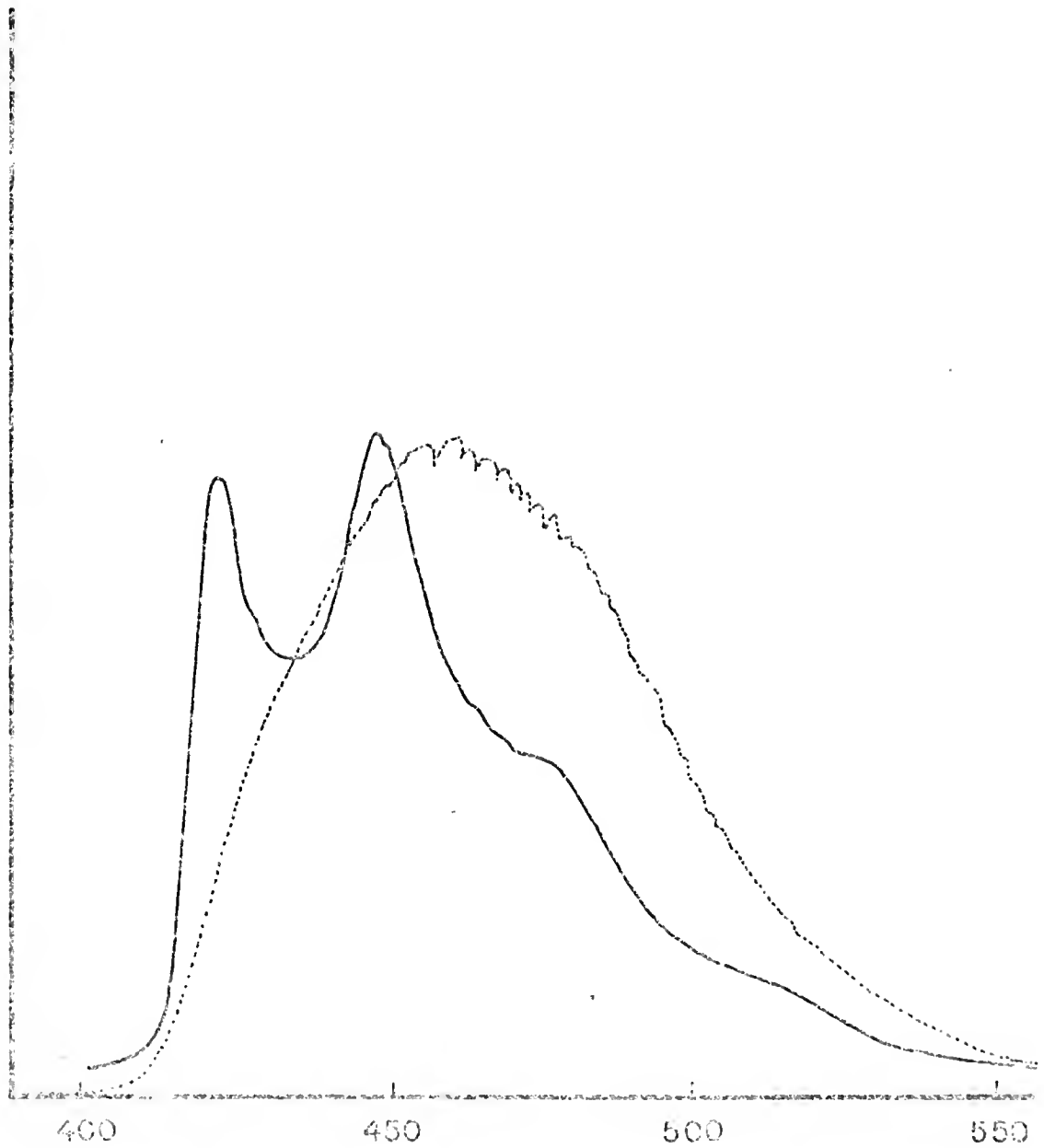
Figure 20. Phosphorescence Spectra of Vinblastine

Vinblastine concentration of $10\ \mu\text{g/ml}$.

(—) Vinblastine in 10/90 v/v E/W
 $f = 15\ \text{Hz}$, $t_d = 0.5\ \text{ms}$, $t_g = 10.0\ \text{ms}$, $1 \times 10^{-7}\ \text{A}$
Full Scale.

(. . .) Vinblastine in 10/90 v/v E/W, $0.1\ \text{M}\ \text{AgNO}_3$
Recorded on Aminco-Bowman spectrofluorimeter
with an Aminco-Keirs phosphoroscope attachment.

RELATIVE PHOSPHORESCENCE INTENSITY



WAVELENGTH (nm)

Table XV. Limits of Detection for Several Drugs by Laser Excited Time Resolved Phosphorimetry

Compound ^a	Emission Wavelength (nm)	Limits of Detection ^b ($\mu\text{g/ml}$) in		
		10/90 v/v	Ethanol/Water with 0.75 M KI	0.1 M AgNO_3
Morphine	515	1.3 (0.1) ^c	3.6	1.2
Ethyl Morphine	515	0.76 (6.0) ^d	2.2	0.63
Codeine	515	0.22 (0.01) ^c	0.93	0.17
Phenobarbital	385	0.0072 (0.1) ^e	0.011	--
Procaine	445	0.0025 (0.01) ^e	0.014	--
Phencyclidine	385	0.091	0.039 (0.32) ^f	--
Cocaine	415	0.028 (1.3) ^d	0.064	--
STP (DOM)	411	0.0080 (0.02) ^d	0.044 (0.03) ^f	--
Anturane	428	0.034	0.024	--
Butazolidin	390	0.043	0.18	0.19
Tandearil	420	0.12	--	0.046
Vinblastine	450	0.027	0.074	0.0057
Thiopropazate	488	0.0016	0.0017	0.0024

^aAll drugs excited at 270 nm with CMX-4, 15 Hz, except Thiopropazate, excited at 337 nm with Avco Laser, 15 Hz.

^bBased on Signal-to-Noise of 3, Observed Time Constant ~ 3 s.

^cValues taken from reference (132).

^dValues taken from reference (133).

^eValues taken from reference (134).

^fValues taken from reference (135).

Comparison of Excitation Sources

In order to make a comparison of the nitrogen laser and flashlamp pumped dye laser, it is necessary to first discuss some of the differences pertinent to use in time resolved phosphorimetry. The CMX-4 has a longer pulse width ($\sim 1 \mu s$) than does the nitrogen laser ($\sim 7 ns$); the CMX-4 should do better in exciting phosphors due to their long lifetimes. On the other hand, the nitrogen laser has much larger peak power, but the power is only at 337.1 nm. Combining these factors, using Eq. IV.1, and assuming:

- (i) the repetition rate of the lasers and complete detection system are the same;
- (ii) the comparison is based on a sample phosphor with a concentration low enough that the phosphorescence signal is directly proportional to the peak irradiance of the laser, P , and the molar absorptivity, $\epsilon(40)$;
- (iii) the phosphorescence lifetime is greater than $100 \mu s$.

The ratio of the phosphorescence signal predicted for the nitrogen laser (S_N) to the signal predicted for the CMX-4 (S_C) is given by

$$\frac{S_N}{S_C} = \frac{P_N(337) t_N \epsilon_N(337)}{P_C(\lambda) t_C \epsilon_C(\lambda)} \quad (IV.4)$$

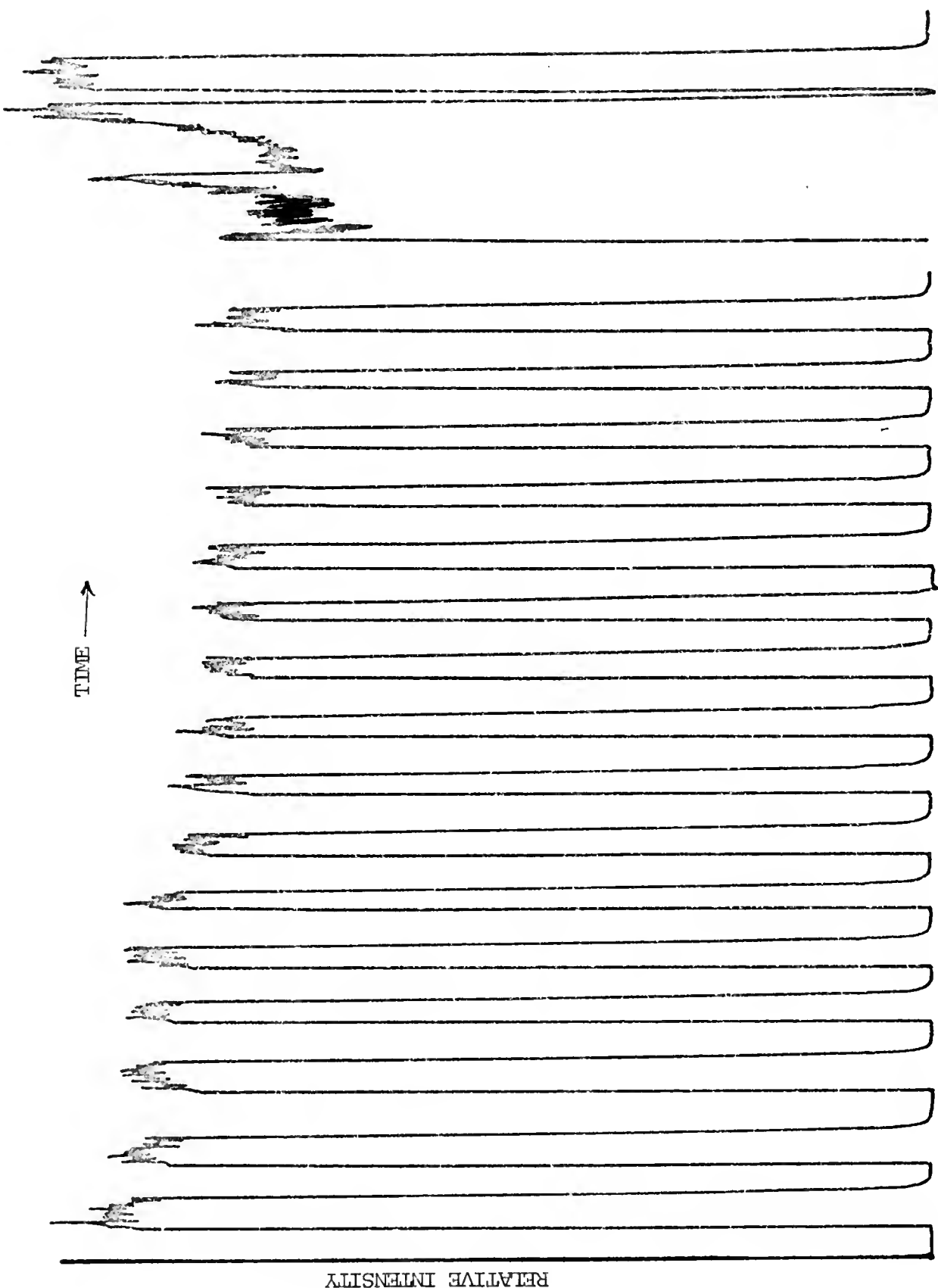
Because $\epsilon(\lambda)$ is a function of wavelength, it is necessary to specify a wavelength. At 337 nm for both assuming $P_N = 40 kW$ (100 kW attenuated 40% by a filter), $P_C = 300 W$, and both are focused to the same area, the ratio is 0.93. If the CMX-4 is tuned to a different wavelength, the ratio will depend on $P_C(\lambda)$ and $\epsilon_C(\lambda)$. Assuming 270 nm for the CMX-4 ($P_C = 200 W$), the ratio is $1.4 \epsilon(337)/\epsilon(270)$. The molar absorptivity

must increase by more than a factor of 1.4 going from 337 to 270 nm for the CMX-4 to give a larger signal. For many molecules (for example, most of the drugs previously discussed), the first excited singlet is at higher energy than the energy at 337 nm and use of a nitrogen laser is not possible. For any molecule with a first excited singlet below this energy, either laser could be used to excite phosphorescence.

The S/N ratio is of more interest than the signal alone, and so it is necessary to discuss the noise sources. To measure the noise due to variation in laser output, a short length of uranyl glass rod was placed in a sample cell and excited with each laser. The intense, short-lived, yellow-green luminescence was measured at 500 nm with a delay time of 0.2 ms, a gate width of 0.1 ms, and an OTC of 2 s. The luminescence of the uranyl glass was much more intense when excited by the nitrogen laser than when using the CMX-4, and so slit width and slit height were adjusted to give approximately the same detector photocurrent ($\sim 5 \mu\text{A}$). The results for sixteen consecutive measurements are shown for the CMX-4 in Figure 21 and for the nitrogen laser in Figure 22. The detection system noise is negligible at these signal levels. It is readily apparent that the nitrogen laser is more stable in terms of pulse-to-pulse reproducibility indicated by the noise on the sixteen individual measurements. The long-term stability (time for each measurement was 1 minute) is also better for the nitrogen laser. The last measurement shown in Figure 21 is the signal obtained by re-peaking the frequency-doubling crystal. The fact that signals returned to approximately the signal of the first measurement would indicate that this is the source of the slowly decreasing signal observed. This was a continuing problem in all experiments using the CMX-4.

Figure 21. Noise on CMX-4 Laser

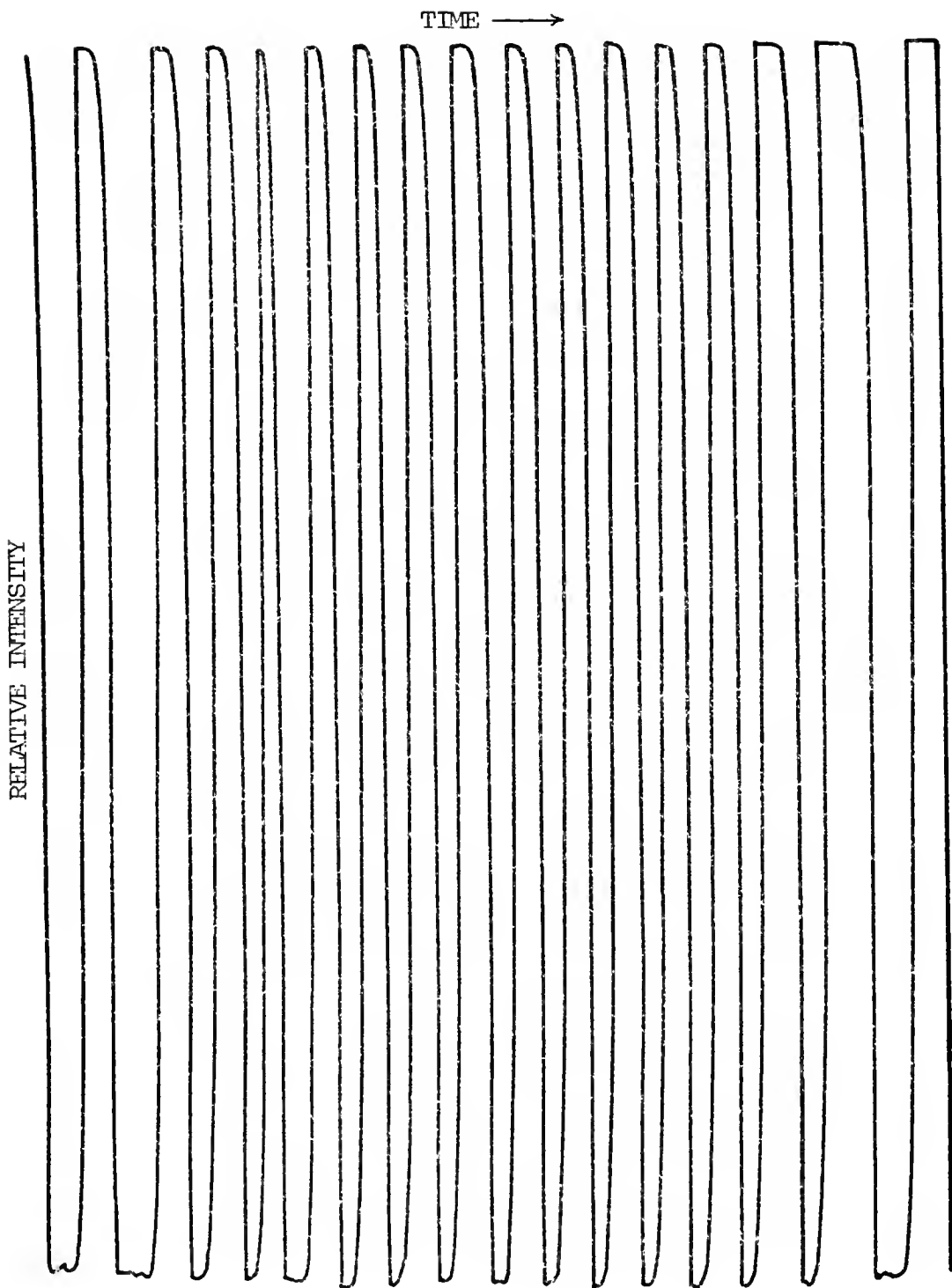
$f = 15 \text{ Hz}$, $t_d = 0.2 \text{ ms}$, $t_g = 0.1 \text{ ms}$, $5 \times 10^{-6} \text{ A}$ Full Scale.
Uranyl glass luminescence at 500 nm.



RELATIVE INTENSITY

Figure 22. Noise on Nitrogen Laser

$f = 15 \text{ Hz}$, $t_d = 0.2 \text{ ms}$, $t_g = 0.1 \text{ ms}$, $5 \times 10^{-6} \text{ A}$ Full Scale.
Uranyl glass luminescence at 500 nm.



Sample cell positioning has been a long standing problem in phosphorimetry. Hollifield and Winefordner (136) used an nmr spinner to rotate the sample cell and randomize positioning errors. This device works very well in conventional phosphorimetry, but can not be used with pulsed excitation sources. Quartz capillary tubing is never straight enough to spin without wobbling even if the spinner itself does not wobble. Because the pulsed source is not on all the time by its very nature, it is possible for the sample cell because of sample wobble to be completely out of the optical path every time the source is triggered. The sleeve of the spinner assembly was used with a slip-fit Teflon^R cylinder that could be reproducibly positioned. The relative standard deviation, rsd, of 0.009 in the present studies is equivalent to rsd values for rotating sample cells.

The different noise sources of importance are given in Table XVI. It is immediately evident that background variation from the solvent blank is the noise source of major importance. It is also the most difficult to reduce. Background variation is dependent on how the sample is cooled to liquid nitrogen temperature, along with nitrogen bubbling and ice crystals in the dewar. The optimum method was found to be cooling the sample for 20 s just above the liquid nitrogen and slowly lowering the sample tube into the liquid nitrogen.

Limits of detection for benzophenone, quinine, phenanthrene, and carbazole are given in Table XVII. Benzophenone, phenanthrene, and quinine were chosen for the comparison of the CMX-4 and the nitrogen laser sources. The benzophenone signal and lifetime are unaffected by the heavy atom effect as its lowest triplet is n, π^* . The signal is 12-fold larger with the CMX-4, but the detection limits are only ~5 times

Table XVI. Noise Sources in Pulsed Laser Time Resolved Phosphorimetry

Noise Origin	Relative Standard Deviation ^a	
	CMX-4	Avco
Source Induced	0.064	0.005
Sample Cell Holder Positioning	0.009	0.009
Sample Compartment Top Positioning	0.023	0.023
<u>Solvent Background</u>		
10/90 v/v Ethanol/Water ($\tau = 5.2$ ms)	0.14	0.15
10/90 v/v Ethanol/Water, 0.75 M KI ($\tau = 6.6$ ms)	0.20	0.13
10/90 v/v Ethanol/Water, 0.1 M AgNO ₃ ($\tau = 2.9$ ms)	0.075	0.067

^aRelative Standard Deviation determined from standard deviation and mean of sixteen measurements.

Table XVII. Comparison of Limits of Detection Using Avco Nitrogen Laser and Chromatix CMX-4 Laser

Compound	Delay Time (ms)	Gate Time (ms)	Solvent ^a	Limits of Detection ^b (ng/ml)	
				Avco ^c	CMX-4 ^d
Benzophenone 440 nm	0.2	2.0	E/W	0.92	0.22
	0.2	2.0	KI	2.4	0.41
	4.0	2.0	AgNO ₃	0.62	0.10
Quinine 515 nm	10	20	E/W	1.9	13
	0.2	2.0	KI	0.40	9.2
	4.0	2.0	AgNO ₃	0.21	2.7
Phenanthrene 500 nm	10	20	E/W	5.5	8.6
	10	20	KI	4.3	14
	0.2	2.0	AgNO ₃	1.9	0.26
Carbazole 440 nm	9	10	E/W	0.55	e
	9	10	KI	0.34	e
	0.2	1.0	AgNO ₃	0.038	e

^aE/W is 10/90 v/v Ethanol/Water, KI is 0.75 M KI, AgNO₃ is 0.1 M AgNO₃.^bBased on Signal-to-Noise of 3, observed time constant of 3.3 s.^cAvco Nitrogen Laser, 337.1 nm, 15 Hz, except Carbazole, 20 Hz.^dChromatix CMX-4 Laser, 270 nm, 15 Hz.^eOnly Avco laser used to determine Carbazole detection limits.

better due to an increase in the solvent background when excited at the lower wavelength. The detection limits are best in 0.1 M AgNO_3 due to the smaller standard deviation of the background.

Quinine is more efficiently excited at 337 nm, and so detection limits with the nitrogen laser are better. Due to the long lifetime of quinine, it is possible to gate off of the short-lived background in the ethanol/water. In 0.75 M KI, the background is smaller when excited at 337.1 nm than when excited at 270 nm which also makes the detection limits better using the nitrogen laser. In 0.1 M AgNO_3 quinine gives a smaller signal using either laser than the phosphorescence signal from quinine in 0.75 M KI. The background and the background noise are also smaller in 0.1 M AgNO_3 by a large enough factor to improve the detection limits. Going from the CMX-4 to the nitrogen laser increases the signal by a factor of 15, but only increases the background noise by a factor of 2. Time resolution is useful in 0.1 M AgNO_3 as the quinine lifetime is longer than the background lifetime, but less useful in 0.75 M KI because the background lifetime and the quinine lifetime are close to the same value.

Phenanthrene, like benzophenone, should give larger signals with the CMX-4 as $\epsilon(337) = 225$ and $\epsilon(270) = 13000$. Rather than a 40-fold increase in signal, only a 2-fold increase in signal was observed with the CMX-4 for phenanthrene in 10/90 v/v ethanol/water or 0.75 M KI and a 7-fold increase in signal for 0.1 M AgNO_3 , all relative to excitation with the nitrogen laser. This discrepancy is due to the difficulty in maintaining the frequency-doubling crystal at the optimum angle due to thermal drift, dye decomposition, and large variation in output energy from pulse-to-pulse. The value of 200 W for the peak power of the CMX-4

is only an estimate based on manufacturers literature. A detector calibrated at 270 nm was not available to measure the actual laser output power.

The detection limits for carbazole (carbazole was not used for a comparison compound) excited at 337 nm with the nitrogen laser are also listed in Table XVII. Less than 2-fold improvement in detection limit is found using 0.75 M KI, while nearly 15-fold improvement in detection limit is found for 0.1 M AgNO_3 .

The initial intent of this work was to compare laser excitation with point source xenon flashlamp excitation. No results have been presented here using flashlamp excitation because of the experimental difficulties associated with reproducibly triggering the flashlamp. Even at repetition rates as low as 1 Hz, it was not possible to trigger the flashlamp 100 consecutive times without missing several flashes. This severely limited the analytical utility of these particular lamps. The cost (\$125), lifetime (10^6 shots), and radio frequency noise associated with these sources does not make them particularly attractive in comparison to the Avco nitrogen laser.

Conclusions

Based on this study, the following conclusions regarding the external heavy atom effect and laser excited time resolved phosphorimetry may be reached:

- (i) Iodide and silver ions affect phosphorescence in a manner consistent with the external heavy atom effect;
- (ii) iodide and silver ions will increase the sensitivity of phosphorescence spectrometry for many molecules;

- (iii) iodide and silver ions may improve limits of detection in phosphorescence spectrometry depending on the magnitude of the increase of the background phosphorescence;
- (iv) the decrease in phosphorescence lifetime using silver ion in pulsed laser excited phosphorimetry makes more efficient use of the high peak power available from pulsed lasers, which may greatly improve both sensitivity and limits of detection;
- (v) the pulsed nitrogen laser is an excellent excitation source for phosphors having molar absorptivities as small as 10 at 337 nm due to its high peak power and excellent pulse-to-pulse reproducibility;
- (vi) the Chromatix CMX-4 flashlamp pumped dye laser requires the use of a ratio system to compensate for pulse-to-pulse variation, dye decomposition, and frequency-doubling crystal drift in order for it to be of great analytical use in phosphorimetry;
- (vii) the major noise sources in this study were found to be associated with immersion cooling in liquid nitrogen, so it is possible that the noise from these sources could be reduced by using conduction cooling.

APPENDIX

COMPUTER PROGRAMS USED FOR LIFETIME CALCULATIONS

Two computer programs, written in BASIC, were used to calculate phosphorescence lifetimes on a PDP 11/20 minicomputer. The program FOS was used to calculate lifetimes from the slope of the least-squares line of the natural logarithm of the phosphorescence decay versus time. The program SLFOS calculates lifetimes by the same procedure after subtracting the signal due to a long-lived component.

PROGRAM NAME - 125

```

1 DATA V(1000)
3 PRINT "IF BLANK AND ANALYTE HAVE SAME SWEEP, DELAY, & # OF SWEEPS, INPUT 0"
4 PRINT "IF YOU JUST HAVE 1 ANALYTE, GIVE THEM BLANK, BUT NOT INPUT 1"
5 PRINT "IF BLANK AND ANALYTE ARE TEMPORARILY DIFFERENT, INPUT 2"
6 INPUT B1
7 PRINT "IF YOU HAVE SEVERAL RUNS WITH SAME BLANK, INPUT Y" INPUT Y$
14 Z=0
16 OPEN "332.1\NW1" (800)
18 PRINT "DATE RUN" INPUT A$
20 PRINT "SAMPLE" INPUT B$
22 PRINT "RECORD" INPUT Q$
24 PRINT "CORRELATION" INPUT D$
26 PRINT "SOLVENT" INPUT C$
28 PRINT "TEMP NUMBER" INPUT X$
50 IF Y$=Y1$ THEN Z=1
52 PRINT "BLANK FULL NAME" INPUT E$
54 PRINT "SWEEP TIME IN SECONDS" INPUT S(1)
56 PRINT "DELAY TIME IN SECONDS (BLANK)" INPUT D(1)
60 PRINT "# OF SWEEPS (BLANK)" INPUT C(1)
70 PRINT "GATE OF AMP (BLANK)" INPUT G1
71 IF G1=1 THEN G=0
72 PRINT "ANALYTE FULL NAME" INPUT F$
74 PRINT "SWEEP TIME IN SECONDS" INPUT S(2)
76 PRINT "DELAY TIME IN SECONDS (ANALYTE)" INPUT D(2)
78 PRINT "NUMBER OF SWEEPS (ANALYTE)" INPUT C(2)
80 PRINT "GATE OF AMP (ANALYTE)" INPUT G
82 IF Y1$=Y$ THEN B1=1
86 OPEN "1" FOR INPUT AS FILE #12(1000)
87 M=0:ND=0:Z=0
88 FOR I=200 TO 800
89 Q(I)=VAL(LEFT$(Q$,129)
90 IF Q(I)=0 THEN B1=0
91 RE DEFEND(ND)=ND+Q(I)*2
92 IF Z=Z1+ND/4 THEN
94 B1=B1+(B1+ND/Z1)
95 B1=INT(B1/(25.1))
96 B1=B1+0.1405/G1
97 B1=B1/Z1
98 B1=DEFEND(.05*B1)
99 CORR=170
100 B1=B1*(S(1)/1000)
101 FOR I=11 TO 810
102 B1=Q(I)*VAL(C(1)/C(1))
103 B1=B1*Q(I)*Q(I)*2
104 B1=B1*Q(I)*Q(I)*B1
105 B1=B1*Y9/Y9+Q(I)
106 B1=B1*Q(I)*1.0000001*(C1 THEN 13/
107 B1=B1*Q(I)*100(Q(I))
110 B1=B1*Y1/Y1+Q(I)
111 B1=B1*Y2/Y2+Q(I)*2
112 B1=B1*(B1+Q(I)*Q(I)*.5047)
113 B1=B1*24.8111
114 B1=B1*2*(Y1/Y1+Q(I))
115 B1=B1*2*(B1)
116 B1=B1*(B1+Q(I)*Q(I))
117 B1=B1*2*(Y2/Y2+Q(I))
118 B1=B1*2*(B1)
119 B1=B1*2*(Y1/Y1+Q(I))
120 B1=B1*2*(B1)
121 B1=B1*2*(Y2/Y2+Q(I))
122 B1=B1*2*(B1)

```

```

142 I11 Z0 INCRINC "Z 3"
143 GO TO 154
145 I11 G1 G1
146 GO SUB 360
147 Z(1) ZNG(1)-CXY9(1)*Y9*G1(1)*.0541/G1
148 A(1) ANS3(1)-SANS(1)-BNS1(1)=S1
149 I(1) INSG(1)-SANS(1)-PONS(1)=S5
151 I1 01-1 THEN 162 NEXT G2 G
155 OPEN 14 FOR INPUT AS FILE VIZZ(1000)
156 GO SUB 170
157 GO SUB 240
158 GO SUB 260
159 Z(2) ZNG(2)-CXY9(2)=Y9*G1(2)*.0541/G
160 A(2) ANS3(2)-SANS(2)-BNS1(2)=S1
161 I(2) INSG(2)-SANS(2)-PONS(2)=S5
162 GO TO 586
170 I11 X1=0
180 I11 X2=0
190 I11 Y1=0
200 I11 Z1=0
205 I11 Y9=0
210 I11 W=0
220 I11 Z=0
231 RETURN
240 I11 I=S(2)/1000
241 FOR K=11 TO 999
245 IF G1(2)=1 THEN 246 NF9=.1N60 TO 250
246 F9=1
250 I11 T1=B(2)+((K-.5)*I)
251 IF 02<12 THEN 252 N60 TO 254
252 V(K)=(VF2(K)/G1(2))+Z9-(VF1(K)/G1(1))+Z9)*(G/G1)
253 GO TO 260
254 K1=INT(((G1)-B(1))*1000/(5(1))+.5)
255 IF K1 900 THEN 256 N60 TO 258
256 V(K)=(VF2(K)/G1(2))+Z9-(VF1(K1)/G1(1))+Z9)*(G/G1)
257 GO TO 260
258 V(K)=(VF2(K)/G1(2))+Z9-N1*(G/G1)
260 I11 Y9=Y9+V(K)
265 IF V(K)>15 THEN 356
270 I11 V(K)=100(V(K))
280 I11 Z1=Z1+V(K)
290 I11 Y1=Y1+V(K)
300 I11 Y2=Y2+V(K)*2
320 I11 X1=X1+1
330 I11 X2=X2+(I1*11)
340 I11 W=W+(I1*V(K))
350 W=X1+1
352 RETURN
360 I11 H1=X2-(X1*X1/2)
370 I11 B=(W*(X1+Y1/Z))/H1
380 I11 A=(Y1-B*X1)/Z
390 I11 B2=Y2-(X1*Y1/Z)-(B*B*H1)
400 I11 S2=B2/(Z-.1)*H1
410 I11 S1=2*H1*S2
420 I11 S1=H1*(Z-.1)*X1/Z/G*H1
430 I11 S1=2*H1*S4
440 I11 R=B1*Y1/Z*(Y2-(X1*Y1/Z))
450 I11 C=2*H1*V(K)
460 I11 F1=1+B
470 I11 F9=(F1*S1)*.0541/G
480 I11 Z1=Z1+F9
490 I11 S5=I11*Z1
501 RETURN
510 PRINT "Z1=";Z1; "F1=";F1; "F9=";F9; "S5=";S5; "V(1)=";V(1)
521 RETURN

```

```

550 PRINT 12:"TIME (S)",SIG(10),TAP,"TO(CMS)",SIG(10)
555 PRINT 12:10,55(10),55(10),55(10)
557 PRINT 12:
560 PRINT 12:"INTEGRAL COORDINATES",SIG(10)
565 PRINT 12:Y(10),X(10),Y(10)/X(10)
581 RETURN
585 IF 1 THEN 600
600 OPEN "11:" FOR OUTPUT AS FILE #1
605 PRINT CIRCLE(1) FOR K=1 TO 1000:NEXT K
605 GOSUB 700:GOTO 12
610 PRINT 12:1000 COPY 60 STORE ON DISK, -1-CONTINUE, -2-END*PRINT 12
612 IF 2 THEN 800:IF 3 THEN 720:IF 4 THEN 620
614 PRINT 12:NAME OF MESSAGE FILE*PRINT 12
616 OPEN #1 FOR OUTPUT AS FILE #2:GOTO 622 TO 622
620 OPEN "11:" FOR OUTPUT AS FILE #2
622 IF K=1
625 GOSUB 700
630 GO TO 800
700 PRINT 12:DATE,"PULSED SOURCE TIME RESOLVED PHOSPHOROMETRY"
705 PRINT 12:PRINT 12:
710 PRINT 12:"DATE RUN",ANALYTE,"CONCENTRATION",SOLVENT
712 PRINT 12:ANALYTE,ANALYTE,ANALYTE,ANALYTE
714 PRINT 12:"SOURCE",RC(MS),"PM VOLTS",TAP 1
715 PRINT 12:10,10,10,10
716 PRINT 12:PRINT 12:
726 IF K=2 THEN 730
730 GOSUB 700
730 PRINT 12:"" "INFORMATION ON BLANK",E4
735 PRINT 12:PRINT 12:
735 PRINT 12:"SWEEP TIME (S)",DELAY TIME (S),"# SWEEPS",GAIN (BL)
738 PRINT 12:5(10),10(10),10(10),PRINT 12:
735 PRINT 12:"BL BACKGROUND",SIG(10),BACKGROUND
736 PRINT 12:10,10,10,10
738 IF 3 THEN 744
740 PRINT 12:"CAN'T FIND LUMINESCENCE BACKGROUND"
742 PRINT 12:PRINT 12:GOTO 745
744 IF 1 THEN GOSUB 492
745 IF 1 THEN 770
745 IF 2 THEN 750
745 GOSUB 700
750 PRINT 12:"" "INFORMATION ON ANALYTE",E4
752 PRINT 12:PRINT 12:
753 PRINT 12:"SWEEP TIME (S)",DELAY TIME (S),"# SWEEPS",GAIN (AN)
754 PRINT 12:10,10,10,10,10,10,10,10,10,10
755 IF 1 THEN GOSUB 492
756 PRINT 12:
770 RETURN
780 GOTO 12
785 FOR K=1 TO 1000:NEXT K
788 PRINT CIRCLE(1) FOR L=1 TO 1000:NEXT K
790 OPEN "11:" FOR OUTPUT AS FILE #2
792 PRINT 12:PRINT 12:PRINT 12:
795 RETURN
800 OPEN 12:NAME OF 2 1000*PRINT 12
805 IF 1 THEN 805:IF 2 THEN 810
805 Y(10),X(10),Y(10)/X(10) THEN 810
805 GOTO 12
810 GOTO 12
810 IF 1

```


[illegible]


```

450 LET C=SOURCE
451 LET I=-1.0
452 LET TO=(X1(0)*.05)/62
453 LET SS=SS*PO
454 LET SS=SS*SS1
455 RETURN
456 PRINT I2:"      NUMBER OF POINTS","CORRELATION COEFFICIENT"
457 PRINT I2:"      ",Z(1),"      ",X(1)
458 PRINT I2:
459 PRINT I2:"FILE LINE (C)*SIGNAL,TAU","10(CMPS)","SIGNAL, TO"
460 PRINT I2:"(C)*S(1),P(1)*S(1)
461 PRINT I2:
462 PRINT I2:"TRIGGER (COUNTS)","SIGNAL/NOISE"
463 PRINT I2:"Y(1)*S(1)/X(1)/Z(1)
464 RETURN
465 IF Q1=1 THEN Z66
466 OPEN "1:" FOR OUTPUT AS FILE #2
467 PRINT CHER(C1)NEXT K=1 TO 1000NEXT I
468 GOTO 200 NEXT I2
469 PRINT #1 HARD COPY=0=STORE ON DISK,-1=CONTINUE,-2=END"INPUT Z2
470 IF Z2<0 THEN GOTO 462 IF Z2=0 THEN 620
471 PRINT "NAME OF STORAGE FILE"INPUT H#
472 OPEN H# FOR OUTPUT AS FILE #2GOTO 622
473 OPEN "K9," FOR OUTPUT AS FILE #2
474 LET K=2
475 GOTO 200
476 GO TO 800
477 PRINT #C,BAT#,"PULSED SOURCE TIME RESOLVED PHOSPHORIMETRY"
478 PRINT #C:PRINT I2:
479 PRINT I2:"PAIL RUN","ANGLE","CONCENTRATION","SOLVENT"
480 PRINT I2:"S(1),P(1),C(1),G(1):PRINT I2:
481 PRINT I2:"CORREL","RC(1S)","PR VOLTS","TAPE #1"
482 PRINT I2:"U(1),V(1),W(1),X(1)
483 PRINT I2:PRINT I2:
484 IF K=2 THEN 230
485 GOTO 200
486 PRINT I2:" * INFORMATION ON BLANK",E#
487 PRINT I2:PRINT I2:
488 PRINT I2:"SWITCH TIME (S)","DELAY TIME (S)","# SWEEPS","GAIN (RL)"
489 PRINT I2:"S(2),D(2),C(2),G(2):PRINT I2:
490 PRINT I2:"DC BACKGROUND","SIGNAL, BACKGROUND"
491 PRINT I2:"Z2," "VD:PRINT I2:
492 IF Z2=1 THEN 244
493 PRINT I2:"CANNOT FIND LUMINESCENCE BACKGROUND"
494 PRINT I2:PRINT I2:GOTO 245
495 LET I=1:GOTO 492
496 GOTO 1 THEN 250
497 GOTO 250
498 GOTO 250
499 PRINT I2:" * INFORMATION ON ANALYTE",E#
500 PRINT I2:PRINT I2:
501 PRINT I2:"SWITCH TIME (S)","DELAY TIME (S)","#SWEEPS","GAIN (RD)"
502 PRINT I2:"S(2),D(2),C(2),G(2):PRINT I2:
503 LET I=2:GOTO 492
504 PRINT I2:
505 PRINT I2:"1/(10-1000(CMPS)","1/(0.100/1(C)SHUNT"
506 PRINT I2:"I2","S(2)/P(2)
507 RETURN
508 GOTO 1
509 LET I=1 TO 1000:NEXT I
510 PRINT CHER(C1)NEXT K=1 TO 1000:NEXT K
511 OPEN "1:" FOR OUTPUT AS FILE #2
512 PRINT I2:PRINT I2:PRINT I2:
513 RETURN
514 GOTO 471 PRINT #2 END"INPUT Z2
515 IF Z2=1 THEN 1000 GOTO 471
516 LET I=1 THEN 370 NEXT Y=1 TO 10
517 GOTO 471
518 GOTO 10
519 GOTO 10

```

LIST OF REFERENCES

1. N. Omenetto, P. Benetti, L.P. Hart, J.D. Winefordner, and C. Th. J. Alkemade, Spectrochim. Acta, 28B, 289 (1973).
2. J.W. Daily, Appl. Opt., 15, 955 (1976).
3. J.W. Daily, Appl. Opt., 16, 568 (1977).
4. G.D. Boutilier, M.B. Blackburn, J.M. Mermet, S.J. Weeks, H. Haraguchi, J.D. Winefordner, and N. Omenetto, Appl. Opt., 17, 229 (1978).
5. D.R. de Olivares, Ph.D. Thesis, Indiana University, Bloomington, Indiana, 1976.
6. M. Hercher, Appl. Opt., 6, 947 (1967).
7. M. Hercher, W. Chu, and D.L. Stockman, I.E.E.E. J. Quant. Electr., QE4, 954 (1968).
8. F. Gires and F. Combaud, J. Phys., 26, 325 (1965).
9. F. Gires, I.E.E.E. J. Quant. Electr., QE2, 624 (1966).
10. R.W. Keyes, IBM J. Res. Develop., 7, 334 (1963).
11. M. Yamashita, H. Ikeda, and H. Kashiwaga, J. Chem. Phys., 63, 1127 (1975).
12. D.K. Killinger, C.C. Wang, and M. Hanabusha, Phys. Rev. A13, 2145 (1976).
13. R.H. Rantel and H.E. Puntoff, "Fundamentals of Quantum Electronics," John Wiley, New York, N.Y., 1969.
14. J.J. Aaron and J.D. Winefordner, Talanta, 22, 707 (1975).
15. N. Omenetto, L.M. Fraser, and J.D. Winefordner, chapter in "Applied Spectroscopy Reviews," editor, E.G. Brame, Vol. 7, Marcel Dekker, New York, N.Y., 1973.
16. R.J. Lukasiewicz, J.J. Mousa, and J.D. Winefordner, Anal. Chem., 44, 963 (1972).
17. R.J. Lukasiewicz, J.J. Mousa, and J.D. Winefordner, Anal. Chem., 44, 1339 (1972).

18. G.D. Boutilier, C.M. O'Donnell, and R.O. Rahn, Anal. Chem., 46, 1508 (1974).
19. E.L.Y. Bower and J.D. Winefordner, Anal. Chim. Acta, in press.
20. R. King, "Electrical Noise," Chapman and Hall, London, U.K., 1966.
21. B.M. Oliver and J.M. Case, "Electronic Measurements and Instrumentation," McGraw-Hill, New York, N.Y., 1971.
22. A. van der Ziel, "Noise in Measurements," John Wiley, New York, N.Y., 1976.
23. D.K.C. McDonald, "Noise and Fluctuations: An Introduction," John Wiley, New York, N.Y., 1962.
24. C. Th. J. Alkemade, "Fluctuation-Correlation Considerations in Analytical Spectroscopy," paper presented at Fifth Inter. Conf. on Atomic Spectroscopy, Abstracts of Papers, The Australian Academy of Science, Melbourne, Australia, 1975.
25. T.C. O'Haver, chapter in "Trace Analysis," editor, J.D. Winefordner, John Wiley, New York, N.Y., 1976.
26. H. Kaiser and A.C. Menzies, "The Limit of Detection of a Complete Analytical Procedure," Adam Hilger, London, U.K., 1968.
27. R.B. Blackman and J.W. Tukey, "The Measurement of Power Spectra," Dover, New York, N.Y., 1958.
28. C. Th. J. Alkemade, W. Snelleman, G.D. Boutilier, B.D. Pollard, J.D. Winefordner, T.L. Chester, and N. Omenetto, Spectrochim. Acta, Part B, in press.
29. W. Snelleman, Ph.D. Thesis, Rijksuniversiteit Utrecht, Utrecht, The Netherlands, 1965.
30. A Léger, B. Delmas, J. Klein, and S. De Cheveigne, Rev. Phys. Appl., 11, 309 (1976).
31. J.D. Winefordner, R. Avni, T.L. Chester, J.J. Fitzgerald, L.P. Hart, D.J. Johnson, and F.W. Plankey, Spectrochim. Acta, 31B, 1 (1976).
32. G.D. Boutilier, J.D. Bradshaw, S.J. Weeks, and J.D. Winefordner, Appl. Spectrosc., 31, 307 (1977).
33. R.P. Cooney, G.D. Boutilier, and J.D. Winefordner, Anal. Chem., 49, 1048 (1977).
34. M. Marinkovic and T.J. Vickers, Anal. Chem., 42, 1613 (1970).
35. V. Mossotti, F.N. Abercrombie, and J.A. Eakin, Appl. Spectrosc., 25, 331 (1971).

36. B.L. Sharp and A. Goldwasser, Spectrochim. Acta, 31B, 431 (1976).
37. H.H. Jaffe and M. Orchin, "Theory and Application of Ultraviolet Spectroscopy," John Wiley, New York, N.Y., 1967.
38. A.P. Thorne, "Spectrophysics," Chapman and Hall, London, U.K., 1974.
39. S.J. Strickler and R.A. Berg, J. Phys. Chem., 37, 814 (1962).
40. J.D. Winefordner, S.G. Schulman, and T.C. O'Haver, "Luminescence Spectrometry in Analytical Chemistry," John Wiley, New York, N.Y., 1973.
41. N. Omenetto and J.D. Winefordner, chapter in "Analytical Laser Spectroscopy," editor, N. Omenetto, John Wiley, New York, N.Y., in press.
42. F.R. Lipsett, chapter in "Progress in Dielectrics," Vol. 7, Iliffe Books, Ltd., London, U.K., 1968.
43. Th. Förster, "Fluoreszenze organischer Verbindungen," Vanderhoek and Ruprecht, Gottingen, Ger., 1951.
44. R.S. Becker, "Theory and Interpretation of Fluorescence and Phosphorescence," John Wiley, New York, N.Y., 1969.
45. N. Turro, "Molecular Photochemistry," W.A. Benjamin, Inc., New York, N.Y., 1967.
46. M. Yamashita and H. Kashiwagi, J. Phys. Chem., 78, 2006 (1974).
47. R.J. Keirs, R.D. Britt, and W.E. Wentworth, Anal. Chem., 28, 202 (1957).
48. T.C. O'Haver and J.D. Winefordner, Anal. Chem., 38, 602 (1966).
49. P.A. St. John and J.D. Winefordner, Anal. Chem., 39, 500 (1967).
50. T.C. O'Haver and J.D. Winefordner, Anal. Chem., 38, 1258 (1966).
51. J.D. Winefordner, Acc. Chem. Res., 2, 361 (1969).
52. N. Omenetto, Anal. Chem., 48, 75A (1976).
53. R.P. Fisher and J.D. Winefordner, Anal. Chem., 44, 948 (1972).
54. C.M. O'Donnell, K.F. Harbaugh, R.P. Fisher, and J.D. Winefordner, Anal. Chem., 45, 381 (1973).
55. K.F. Harbaugh, C.M. O'Donnell, and J.D. Winefordner, Anal. Chem., 45, 381 (1973).

56. K.F. Harbaugh, C.M. O'Donnell, and J.D. Winefordner, Anal. Chem., 46, 1206 (1974).
57. G.B. Strambini and W.C. Galley, Can. J. Spectrosc., 21, 1 (1976).
58. D.J. Johnson, F.W. Plankey, and J.D. Winefordner, Anal. Chem., 46, 1898 (1974).
59. D.J. Johnson, W.K. Fowler, and J.D. Winefordner, Anal. Chem., Talanta, 24, 227 (1977).
60. K.F. Harbaugh, Ph.D. Dissertation, University of Florida, Gainesville, Fla., 1973.
61. D.C. O'Shea, W.R. Callen, and W.T. Rhodes, "An Introduction to Lasers and Their Applications," Addison-Wesley, Reading, Mass., 1977.
62. M.J. Colles and C.R. Pidgeon, Rep. Prog. Phys., 38, 329 (1975).
63. A.K. Levine and A.J. De Maria, eds., "Lasers," Vol. 3, Marcel Dekker, New York, N.Y., 1971.
64. J.R. Allkins, Anal. Chem., 47, 752A (1975).
65. J.I. Steinfeld, CRC Crit. Rev. Anal. Chem., 5, 225 (1975).
66. B.W. Smith, M.B. Blackburn, and J.D. Winefordner, Can. J. Spectrosc., 22, 57 (1977).
67. S.J. Weeks, H. Haraguchi, and J.D. Winefordner, Anal. Chem., 50, 360 (1978).
68. B.W. Smith, F.W. Plankey, N. Omenetto, L.P. Hart, and J.D. Winefordner, Spectrochim. Acta, 30A, 1459 (1974).
69. J.H. Richardson and M.E. Ando, Anal. Chem., 49, 955 (1977).
70. J.H. Richardson and S.M. George, Anal. Chem., 50, 616 (1978).
71. A.M. Angus, E.E. Maserino, and M.J. Colles, Opt. Commun., 14, 223 (1975).
72. W.H. Woodruff and S. Farquharson, Anal. Chem., 50, 1389 (1978).
73. L.B. Rogers, J.D. Stuart, L.P. Gross, T.B. Mallory, Jr., and L.A. Carreira, Anal. Chem., 49, 959 (1977).
74. T.F. Van Geel and J.D. Winefordner, Anal. Chem., 48, 335 (1976).
75. R.N. Zare, "Laser Fluorimetry," paper presented at 175th National Meeting of the Amer. Chem. Soc., Abstracts of Papers, Amer. Chem. Soc., Anaheim, Calif., 1978.

76. J.C. Brown, M.C. Edelson, and G.J. Small, Anal. Chem., 50, 1394 (1978).
77. E.I. Al'shits, R.I. Personov, and B.M. Kharlamov, Chem. Phys. Lett., 40, 116 (1976).
78. E.I. Al'shits, R.I. Personov, and B.M. Kharlamov, Opt. Spektrosk., 41, 803 (1976).
79. B.M. Kharlamov, E.I. Al'shits, R.I. Personov, V.I. Nizhankovsky, and V.G. Nazin, Opt. Commun., 24, 199 (1978).
80. R.M. Wilson and T.L. Miller, Anal. Chem., 47, 256 (1975).
81. S.P. McGlynn, J. Daigre, and F.J. Smith, J. Chem. Phys., 39, 675 (1963).
82. L.V.S. Hood and J.D. Winefordner, Anal. Chem., 38, 1922 (1966).
83. M. Zander, Z. Anal. Chem., 226, 251 (1967).
84. R.J. Lukasiewicz, P. Rozynes, L.B. Sanders, and J.D. Winefordner, Anal. Chem., 44, 237 (1972).
85. J.J. Aaron, J.J. Mousa, and J.D. Winefordner, Talanta, 20, 279 (1973).
86. J.J. Aaron, W.J. Spann, and J.D. Winefordner, Talanta, 20, 855 (1973).
87. P.G. Seybold and W. White, Anal. Chem., 47, 1199 (1975).
88. T. Vo Dinh, E. Lue Yen, and J.D. Winefordner, Anal. Chim., 48, 1186 (1976).
89. W. White and P.G. Seybold, J. Phys. Chem., 81, 2035 (1977).
90. R.O. Rahn and L.C. Landry, Photochem. Photobiol., 18, 29 (1973).
91. G.D. Boutilier, J.R. Andrew, C.M. O'Donnell, and T.N. Solie, Anal. Chem., 47, 2454 (1975).
92. R.F. Chen, Fluorescence News, 9, 9 (1975).
93. T. Vo Dinh, E. Lue Yen, and J.D. Winefordner, Talanta, 24, 146 (1977).
94. E.L.Y. Bower and J.D. Winefordner, Anal. Chim. Acta, in press.
95. M. Kasha, J. Chem. Phys., 20, 71 (1952).
96. S.P. McGlynn, R. Sunseri, and N.J. Christodouleas, J. Chem. Phys., 37, 1818 (1962).

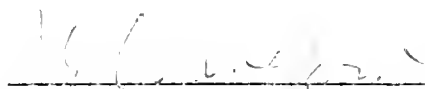
97. D.S. McClure, J. Chem. Phys., 17, 905 (1949).
98. E.H. Gilmore, G.E. Gibson, and D.S. McClure, J. Chem. Phys., 20, 829 (1952).
99. M.A. El-Sayed, Acc. Chem. Res., 1, 8 (1968).
100. S.P. McGlynn, T. Azumi, and M. Kinoshito, "Molecular Spectroscopy of the Triplet State," Prentice-Hall, Englewood Cliffs, N.J., 1969.
101. J.N. Murrell, Mol. Phys., 3, 319 (1960).
102. G.J. Hoijtink, Mol. Phys., 3, 67 (1960).
103. M.K. Chaudhuri and M.A. El-Sayed, J. Chem. Phys., 42, 1947 (1965).
104. T. Azumi, Chem. Phys. Lett., 19, 580 (1973).
105. S. Yamauchi, K. Matsuzaki, and T. Azumi, J. Lumin., 12/13, 369 (1976).
106. C.T. Lin, J. Lumin., 12/13, 375 (1976).
107. G.W. Robinson, J. Phys. Chem., 46, 572 (1967).
108. G.G. Giachino and D.R. Kearns, J. Chem. Phys., 52, 2964 (1970).
109. G.G. Giachino and D.R. Kearns, J. Chem. Phys., 53, 3886 (1970).
110. J. Najbar, J. Lumin., 11, 207 (1975/76).
111. J. Najbar and A. Chodkowska, J. Lumin., 11, 215 (1975/76).
112. J. Najbar, J.B. Birks, and T.D.S. Hamilton, Chem. Phys., 23, 281 (1977).
113. F.E. Lytle, Anal. Chem., 46, 545A (1974).
114. J.M. Harris, F.E. Lytle, and T.C. McCain, Anal. Chem., 48, 2095 (1976).
115. R.P. Fisher, Ph.D. Dissertation, University of Florida, Gainesville, Fla., 1971.
116. I.M. Jakovljevic, Anal. Chem., 50, 1578 (1978).
117. G.J. Niday and P.G. Seybold, Anal. Chem., 50, 1578 (1978).
118. A.A. Lamola and G.S. Hammond, J. Chem. Phys., 43, 2129 (1965).
119. A.R. Watkins, J. Phys. Chem., 78, 2555 (1974).
120. I.B. Berlman, J. Phys. Chem., 77, 562 (1973).

121. M.J. Adams, J.G. Highfield, and G.F. Kirkbright, Anal. Chem., 49, 1850 (1977).
122. T.F. Hunter, Trans. Faraday Soc., 66, 300 (1970).
123. A.A. Efimov, R.N. Nurmhametov, I.L. Belaits, and A.I. Tolmachev, Opt. Spektrosk., 30, 622 (1971).
124. M.A. El-Sayed, J. Chem. Phys., 38, 2834 (1963).
125. F.A. Cotton and G. Wilkinson, "Advanced Inorganic Chemistry," Interscience, New York, N.Y., 1972.
126. E.A.H. Griffith and E.L. Amma, J. Amer. Chem. Soc., 93, 3167 (1971).
127. R.M. Keefer and L.J. Andrews, J. Amer. Chem. Soc., 74, 640 (1952).
128. R.F. Chen, Arch. Biochem. Biophys., 158, 605 (1973).
129. R.F. Chen, Arch. Biochem. Biophys., 144, 552 (1971).
130. C.M. O'Donnell and T.S. Spencer, J. Chem. Educ., 49, 822 (1972).
131. C.M. O'Donnell and J.D. Winefordner, Clin. Chem., 21, 285 (1975).
132. H.C. Hollifield and J.D. Winefordner, Talanta, 12, 860 (1965).
133. E. Lue Yen, G.D. Boutilier, and J.D. Winefordner, Can. J. Spectrosc., 22, 120 (1977).
134. J.D. Winefordner and M. Tin, Anal. Chim. Acta, 31, 239 (1964).
135. D.M. Fabrick and J.D. Winefordner, Talanta, 20, 1220 (1973).
136. H.C. Hollifield and J.D. Winefordner, Anal. Chem., 40, 1759 (1968).

BIOGRAPHICAL SKETCH

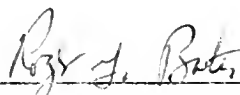
Glenn D. Boutilier was born in Middletown, Connecticut, on February 7, 1953. After attending public schools in Maine, Ohio, and Massachusetts, he graduated from Shrewsbury High School in Shrewsbury, Massachusetts. He obtained a Bachelor of Science degree in chemistry from Colorado State University in June, 1974. Graduate studies at the University of Florida were begun in September, 1974. He is a member of Phi Beta Kappa, the American Chemical Society, the Optical Society of America, and the Society for Applied Spectroscopy.

I certify that I have read this study and that in my opinion it conforms to acceptable standards of scholarly presentation and is fully adequate, in scope and quality, as a dissertation for the degree of Doctor of Philosophy.



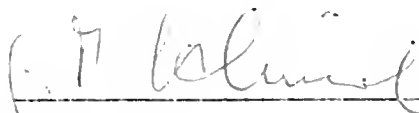
J.D. Winefordner, Chairman
Graduate Research Professor of
Chemistry

I certify that I have read this study and that in my opinion it conforms to acceptable standards of scholarly presentation and is fully adequate, in scope and quality, as a dissertation for the degree of Doctor of Philosophy.



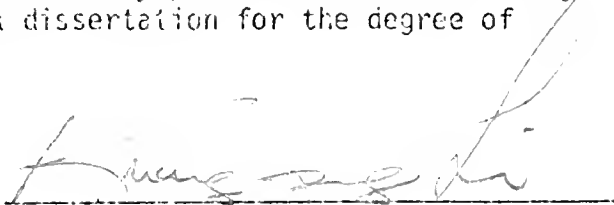
R.G. Bates
Professor of Chemistry

I certify that I have read this study and that in my opinion it conforms to acceptable standards of scholarly presentation and is fully adequate, in scope and quality, as a dissertation for the degree of Doctor of Philosophy.



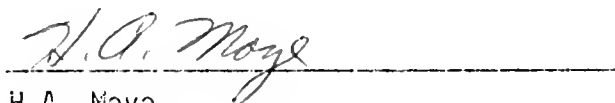
G.M. Schmid
Associate Professor of Chemistry

I certify that I have read this study and that in my opinion it conforms to acceptable standards of scholarly presentation and is fully adequate, in scope and quality, as a dissertation for the degree of Doctor of Philosophy.



K.P. Li
Assistant Professor of Chemistry

I certify that I have read this study and that in my opinion it conforms to acceptable standards of scholarly presentation and is fully adequate, in scope and quality, as a dissertation for the degree of Doctor of Philosophy.



H.A. Moyer
Associate Professor of Food Science

This dissertation was submitted to the Graduate Faculty of the Department of Chemistry in the College of Liberal Arts and Sciences and to the Graduate Council, and was accepted as partial fulfillment of the requirements for the degree of Doctor of Philosophy.

December, 1976

Dean, Graduate School

CVSC 79 0.265
#5992 10-7-11 35
(118)